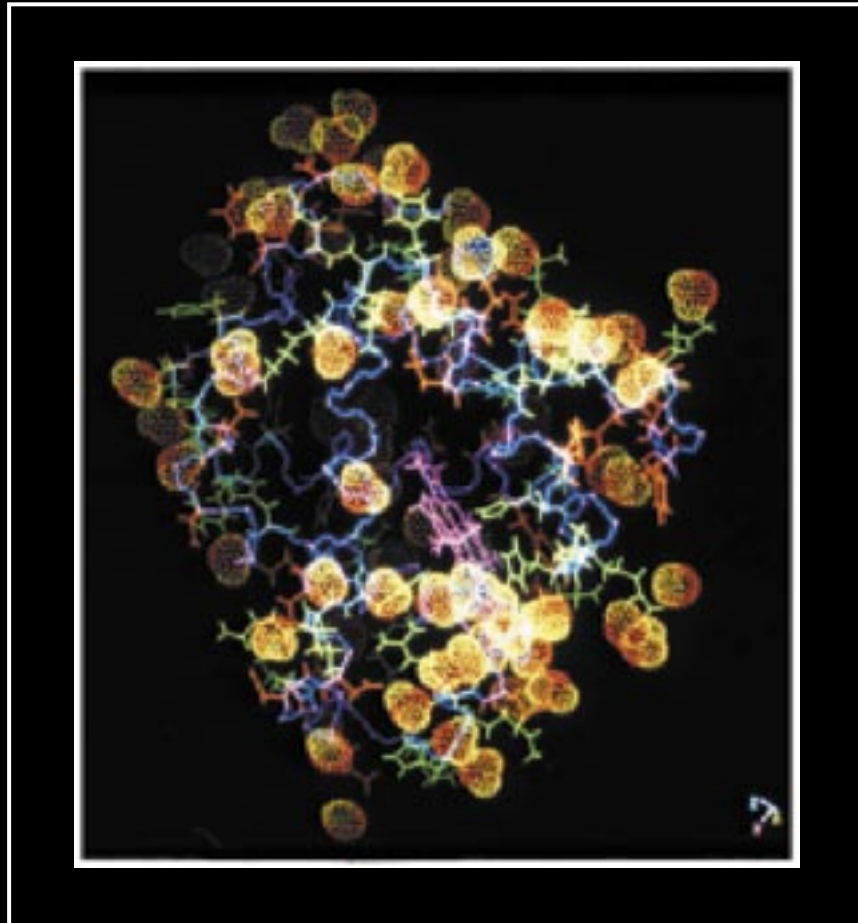


Biological Neutron Diffraction



**TRANSACTIONS OF THE
AMERICAN CRYSTALLOGRAPHIC ASSOCIATION**

Edited by Gerard Bunick and
Leif Hanson

Volume 38, 2003

Proceedings from the Symposium

Biological Neutron Diffraction

ACA TRANSACTIONS
VOLUME 38

Northern Kentucky Convention Center
July 26 – 31, 2003

Editors

Gerard Bunick
Oak Ridge National Lab
Tel: 865-576-2685
Fax: 865-574-1274
bunickgj@ornl.gov

Leif Hanson
Oak Ridge National Lab
Tel: 865-574-1210
Fax: 865-574-1274
hansonl@bio.ornl.gov

TABLE OF CONTENTS

Protein Crystallography With Spallation Neutrons	1
Paul Langan, Xinmin Li, and Benno P. Schoenborn	
Analysis of Neutron Laue Diffraction from Deuterium-Exchanged <i>TRP</i> Repressor	8
Catherine L. Lawson and Alexander S. Chin	
Towards Large Molecule Crystallography at ISIS	14
Chick C. Wilson	
Hydrogen and Hydration in Protein Structural Chemistry	26
Nobuo Niimura, Ichiro Tanaka, Toshiyuki Chatake, Kazuo Kurihara, Mitsuru Maeda and Shigeki Arai	
Evolution and Directions in Macromolecular Neutron Science	40
Benno P. Schoenborn	
Neutron “Small-Angle” Crystallography: Contrast Variation in Single Crystals of Biological Macromolecules	58
P.A. Timmins	
Design and Expected Performance of a High Resolution Macromolecular Neutron Diffraction (MaNDi) at the Spallation Neutron Source	67
P. Thiyagarajan, A.J. Schultz, Ch. Rehm, J.P. Hodges, W.T. Lee and A. Mesecar	

A PRELIMINARY TIME-OF-FLIGHT NEUTRON DIFFRACTION STUDY OF A SITE-SPECIFIC MUTANT (W3Y) OF RUBREDOXIN FROM PYROCOCCLUS FURIOSUS

Xinmin Li,^a Paul Langan^{a,*} Irina Tsyba^b, Robert Bau^b, Michael W. W. Adams^c,
Francis E. Jenney, Jr.^c and Benno P. Schoenborn^a

^aBioscience Division, Los Alamos National Laboratory, Los Alamos NM 87545

^bUniversity of Southern California, Los Angeles CA 90089

^cDept. of Biochemistry, University of Georgia, Athens, GA 30602

*Corresponding Author: M888, Los Alamos National Laboratory, Los Alamos NM 87545

1. ABSTRACT

Rubredoxin from the thermophilic archaeon *Pyrococcus furiosus* maintains its native structure at high temperatures (100°C). In order to investigate the role of hydrogen bonding, hydration and chain dynamics in connection with its thermostability, wavelength-resolved Laue neutron diffraction data have been collected from a mutant form of this protein, PfRd (W3Y) on the spallation neutron protein crystallography station (PCS) at the Los Alamos Neutron Science Center. Room temperature data were collected at 9 crystal settings for 12 hours at each setting, over a period of less than 5 days, to a nominal resolution of 2.1 Å (69% completeness, redundancy factor 2.5), from a crystal that had undergone partial H₂O/D₂O exchange. Preliminary results are described here and compared to those reported previously from studies of the wild-type and a triple mutant from the same protein.

2. INTRODUCTION

Pyrococcus furiosus is a thermophilic archaeon found near geothermal vents on the ocean floor. Rubredoxin from *P. furiosus* (PfRd) maintains its native structure at high temperatures (100°C) unlike rubredoxin from many other organisms, for example that from the mesophile *Clostridium pasteurianum* (CpRd) whose optimal growth temperature is 37°C. Rubredoxin has 53 amino acid residues, some of which are arranged in 3 β -sheets folded around a core of hydrophobic side groups. Four cysteine residues from two opposing β -sheets are involved in binding an iron atom. It has been suggested that the thermostability of PfRd may be related to its eight-residue hydrophobic core. Three of these residues are different between PfRd and CpRd. The difference at position 3 (Trp3 in PfRd and Tyr3 in CpRd) is particularly interesting, because not only is it part of the hydrophobic core, but this residue is also part of the small β -sheet that appears to serve a number of structural roles. These structural roles include binding the iron atom and tying down the C-terminal and N-terminal ends. A mutant of PfRd, in which three residues of the hydrophobic core have been mutated to those of CpRd, has been found to be significantly less stable than the wild-type PfRd at low pH. However, NMR analysis of wild-type PfRd and the triple mutant (Zartler et al, 2001) and high-resolution low temperature X-ray structures for the wild-type PfRd (0.95 Å) and CpRd (1.1 Å) (Bau et al, 1992, Dauter et al, 1996) have revealed no striking differences.

The present study is the latest in a series designed to determine the contribution of hydrogen bonding, hydration and dynamics to the thermostability of PfRd. It has been difficult to directly determine all the positions of H atoms in the high-resolution, low temperature, X-ray structures of rubredoxin. Neutron diffraction has been shown to be a powerful technique for locating H atoms even at medium resolution. What is more, neutron diffraction data can be collected at room temperature, rather than the cryo-temperatures required for high resolution X-ray protein crystallography, because thermal neutrons cause little radiation damage. Hydrogen has a relatively strong, but negative, neutron scattering length. H atoms are therefore located as negative density peaks in neutron Fourier maps. Deuterium (D), an isotope of H, also has a relatively strong and positive neutron scattering length, like those of O, C, N, Fe and S.

By dissolving the target protein in D₂O rather than H₂O prior to crystallization, almost all accessible labile H atoms (i.e., most of those in O-H and N-H groups) have been replaced by D atoms. This increases the overall scattering power of the crystal for neutrons at medium resolution where the negative scattering density of H atoms tends to cancel the positive density of other atoms. The positions of individual D atoms and the orientation of D₂O molecules can be determined even at resolutions of 2.2 Å after H₂O/D₂O exchange. Partial deuteration also reduces the incoherent scattering from hydrogen in the crystal, which tends to contribute to high background scattering and reduces the diffraction signal. Finally, and of particular significance in this study, H₂O/D₂O exchange can be used to probe dynamics. The extent of H/D exchange in the main chain amide groups, as determined in neutron Fourier maps, directly reflects local dynamics

along the rubredoxin backbone chain.

The neutron structures of the wild-type PfRd and a triple mutant (W3Y, I23V, L32I) have already been determined using data collected on BIX-3 at JAERI (Kurihara et al, 2001 Chatake et al, 2002). This preliminary report concerns the neutron structure of the W3Y (Trp3 → Tyr3) single mutant PfRd, determined from data collected at the spallation neutron Protein Crystallography Station (PCS) at Los Alamos Neutron Science Center.

3. MATERIALS AND METHODS

3.1 Protein Production and Purification.

The W3Y mutant of PfRd was prepared as described previously (Jenney & Adams, 2001).

3.2 Crystallization and Deuteration.

Crystallization was carried out at the University of Southern California from a D₂O solution containing 40mg/ml of protein (ca. 6mM PfRd), dissolved in 50mM Tris/Tris-DCl buffer (pH 8.0) and 0.3M NaCl. The sitting drop method was used with 40ml drops, 3.6M Na/K phosphate (pH 6.6) in D₂O as precipitant, and with a sample-to-precipitant volume ratio of 3:1 or 4:1. Crystals were harvested, crushed, and used as seeds. The stock seed solution was successively diluted to the point where only one or two crystals appeared in the subsequent drop (Ducruix & Geige, 1992). If more than one crystal appeared after seeding, a small amount of D₂O was added until all but one of the crystals were redissolved. In about 2 months the crystals reached volumes as large as 4mm³ at room temperature and were stabilized after growth by increasing the phosphate concentration in the reservoir. The crystals were then transported in 3.8-4.0M phosphate solutions to the Bioscience division at Los Alamos National Lab where they were mounted and sealed, along with some mother liquor, in clear fused-quartz capillaries with an inner diameter of 2.0mm. A number of crystals were tested for neutron diffraction quality and one of the crystals with the longest dimension of 1.5mm was used for data collection.

3.3 Data Processing

Diffraction data were collected at the recently-commissioned spallation neutron protein crystallography station (PCS) at Los Alamos Neutron Science Center (Langan, Greene & Schoenborn, 2003a). At the spallation source neutrons are produced in pulses at a rate of 20Hz. The neutrons are time-stamped and travel as a function of their energy down the beam-line. By recording the time-of-flight (TOF) information of a detected neutron, its wavelength can be calculated. The Laue data collected on the PCS are therefore resolved in wavelength. The crystal sample and its deuterated mother-liquor, sealed in a fused-quartz capillary, were mounted on the PCS kappa(50°)-circle goniometer. The omega axis was kept at 90° to allow maximum flexibility in orienting the crystal, while keeping the physical bulk of the omega arm from interfering with the diffraction pattern. In all, wavelength-resolved Laue patterns were collected at room temperature from 9 different crystal orientations with 12hr exposures at each setting, as summarized in table 1. The 9 settings can be grouped in three kappa sets (with kappa increments of 25°), each at three phi settings with $\Delta\phi=30^\circ$. A representation of the data collected at one crystal setting is shown in **Figure 1**.

Table 1
Data Collection Parameters For Rubredoxin Single Mutant

Space Groups	P2 ₁ 2 ₁ 2 ₁
Unit cell dimensions (Å) ^a	a=34.32, b=35.31, c=44.23
Wavelength range (Å)	0.6 - 7
Station	PCS
Temperature (K)	295
Crystal settings	9
Average time per setting	12 hours
Observed reflections	10315
Observed reflections d>2.1Å	5357
Unique reflections d>2.1Å	2184

^a Unit cell parameters are from X-ray diffraction.

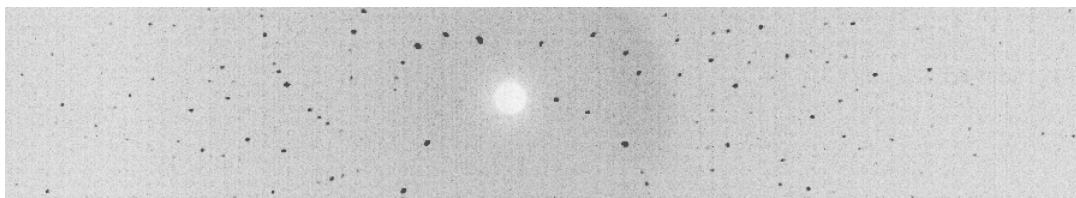


Figure 1. Wavelength-resolved Laue diffraction data collected from PfRd single mutant displayed using d*TREK (Pflugrath, 1998, Langan & Greene 2003b). Although the data is 3-dimensional (2 detector spatial dimensions and a third wavelength (TOF) dimension) a 2-dimensional image has been constructed by displaying at each detector pixel position the maximum value of that pixel over all wavelengths.

In this figure, the data collected at different wavelengths have been projected in the time dimension in order to construct an image similar to a conventional Laue diffraction pattern.

The data over the wavelength range of 0.6-7Å were processed using a version of d*TREK (Pflugrath, 1998) modified for wavelength-resolved neutron Laue protein crystallography (Langan & Greene, 2003b). Out of each setting, a small set of around 150 strong reflections was used by the program for indexing. Before proceeding further, to avoid permuting the indices for a^* and b^* dimension due to the closeness of the a and b cell constants, the indexing was compared (and re-oriented if necessary) to those from other settings for their consistency. This was accomplished by visually examining the relative facings of the distinctive Laue reciprocal space coverage, as would be suggested by the relative kappa and phi settings. Subsequent rounds of refinement of crystal orientation and several other parameters brought the predictions to within 0.7x0.7mm from the spot centers for the chosen set of strong reflections. For all reflections falling within the wavelength and resolution range, the predicted pattern was checked before integration to see how well it matched the observed diffraction pattern. On average for each setting, 1500 reflections were integrated within the wavelength range 0.6Å to 7Å and up to 1.5Å resolution, and typically around 60 reflections around a nodal point would be rejected due to spatial overlap with neighboring reflections.

The processed intensities from all crystal settings were scaled and wavelength normalized using LAUENORM (Campbell & Helliwell et al, 1986). In order to obtain reasonable values for R_{merge} , the wavelength range was narrowed down to 0.8Å-4.5Å and only reflections with $I > 3s$ were used in determining the wavelength scaling normalization curve. The final values are as follows: R_{merge} is 0.131 for all measurements of a reflection, with 2920 reflections; R_{merge} is 0.110 for measurements of a reflection of the same sign, with 2029 reflections; R_{merge} is 0.096 for all measurements of a reflection of the same sign and within $l = 0.1\text{Å}$, with 277 reflections. Reflections in the wavelength range 0.8Å-4.5Å were binned into 10 wavelength intervals and the normalization curve was determined from a Chebyshev polynomial of order 5. The data were output in unmerged form so that SCALA (Evans) could be used for statistical analysis. Table 2 shows the values of R_{merge} and completeness as a function of resolution. The value of I/s flattened off beyond 2.1Å, suggesting that this is about the limit of diffraction. The completeness of the data in the outmost resolution shell (2.1Å -2.2Å) is 63%.

Table 2
Data Processing Statistics for W3Y mutant of PfRd

R_{merge} ($I > 1.5s$) and completeness (%Comp) versus resolution for the rubredoxin single mutant. The cumulative R_{merge} and completeness are also given (Cum R_{merge} , Cum%Comp). The s_a corresponds to the standard deviation in merging reflections as opposed to s , the error involved in measuring individual intensities.

Resolution	Num. Refs.	%Comp	Cum %Comp	R_{merge}	Cum R_{merge}	$\langle I/s_a \rangle$
∞ - 6.64	208	85.2	85.2	0.076	0.076	29.3
- 4.70	426	80.3	82.0	0.093	0.086	22.7
- 3.83	522	79.4	80.8	0.104	0.094	20.9
- 3.32	558	74.5	78.6	0.123	0.102	15.2
- 2.97	587	70.2	76.2	0.156	0.111	10.8
- 2.71	606	69.6	74.6	0.131	0.113	6.2
- 2.51	626	66.8	73.0	0.213	0.118	3.3
- 2.35	607	64.3	71.4	0.192	0.120	2.6
- 2.21	608	65.9	70.6	0.231	0.123	2.0
-2.10	609	62.8	69.4	0.236	0.125	1.4

3.4 Structure Refinement and Water Identification

Structure refinement was carried out using SHELX-97 (Sheldrick, 1997) with scattering factors modified for neutron diffraction and additional geometric restraints involving the H/D atoms of the backbone amide groups and the NH₃ group of the terminal lysine. The low temperature X-ray model of the same W3Y mutant of PfRd (Tsyba, 2002), with all water molecules and hydrogen atoms removed and all thermal parameters set to isotropic values, was subjected to rigid body refinement against the neutron diffraction data. Then tertiary C-Hs, secondary C-H2s and methyl groups were located by examining the difference Fourier maps using the graphics display program O (Jones, Alwyn, 1991), and were added if they led to an improvement in the R-factor. The thermal parameters of these H-atoms are tied to the corresponding C atom by a factor of 1.2. Afterwards, labile H atom positions (those of O-H and N-H bonds) were checked for any indication of deuteration in the protein molecule and the model was modified accordingly. Next, successive rounds of water identification/removal were carried out by careful examination of Fourier difference maps, the local geometry and the consistency between different rounds of refinement. At this stage, 56 water molecules have been included in the model but only as single O atoms. Deuterium atoms will be added in subsequent stages of analysis. Finally, the site occupancy factors for the labile amide H/D atoms, which are telltale parameters for the backbone movement/accessibility, were refined **Figure 3**. The current R-factor ($\Sigma(|F_o|-|F_c|)/\Sigma|F_o|$) for all reflections $>1.5\sigma$ is 30.1%. The medium resolution of the data set makes the data to parameters ratio (2469 reflections and ~800 atoms) precariously low. During every step of the refinement, efforts were made to reduce the number of parameters by using geometric restraints, such as defining the peptide bonds and the aromatic rings as rigid groups.

4. RESULTS AND DISCUSSION

The data collection time of less than 5 days using the PCS instrument is relatively short compared to the weeks, even months, typically required in neutron protein crystallography. This is largely due to the wavelength-resolved Laue technique, which has all of the advantages of the conventional Laue method, including rapid coverage of reciprocal space, but does not suffer to the same extent from reflection overlap and background accumulation, because the spots and the background scattering are resolved in wavelength. The quality of the data and the power of neutron diffraction for locating hydrogen atoms and water molecules at medium resolution are illustrated in **Figures 2, 4 and 5**. **Figure 2** shows a section of a 2.1 Å 2Fo-Fc sigma-A (Read, R., 1986) map in the region of Tyr10 calculated without including the labile H/D atom positions in the phases. The density associated with the hydroxyl group clearly indicates the orientation of this group and also shows that the labile H atom has been replaced by a deuterium atom. A full analysis of this data is revealing a wealth of information on hydration and backbone chain dynamics.

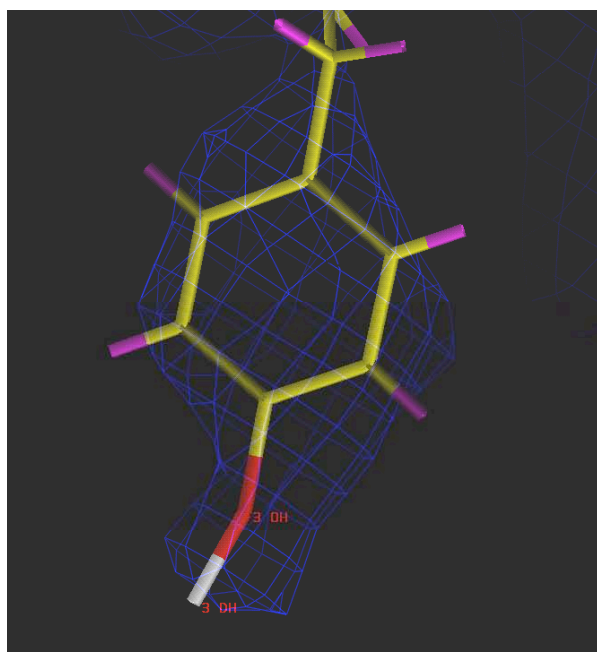


Figure 2. A section of the 2.1 Å 2Fo-Fc sigma-A map in the region of Tyr10 calculated without including the labile H/D atom positions in the phases. Positive density associated with the hydroxyl group clearly indicates the orientation of this group and shows that the labile H atom has been replaced by a D atom.

4.1 H/D Exchange Of The Backbone Amide Hydrogens

At the last step of the refinement, the site occupancies of the labile H/D atoms of the backbone amide groups were refined and compared to other neutron diffraction studies of the wild-type protein (Kurihara, et al.) and one triple mutant of PfRd (Chatake et al.). The preliminary result, shown in **Figure 3**, is quite consistent with the other studies: the amide H/Ds of Tyr12 (**Figure 4**), Cys38 and Ala43 have quite limited deuterium exchange. However slight differences in deuterium exchange in Cys5, Asn21 and Asp34 are observed and will be subjected to further study. In particular, it is intriguing that in all three studies, the exposed amide of residue 34 appears to be partially resistant to deuteration.

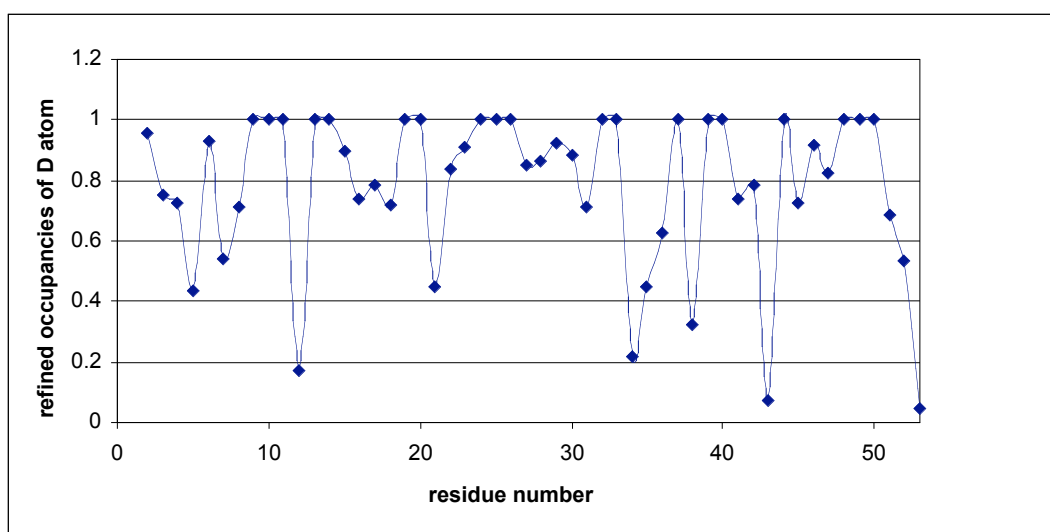


Figure 3. Refined occupancies of D atoms in the amide N-H positions in the W3Y mutant of PfRd. The very low occupancies of amide D atom in residue 12, 38 and 43 are consistent with the neutron studies in the native PfRd and a triple mutant. However, site 21 and 34 have lower values for the W3Y mutant than those from the native and the triple mutant. Note that for five prolines, their non-existent amide H/Ds are assigned with full D occupancies to make the curve continuous.

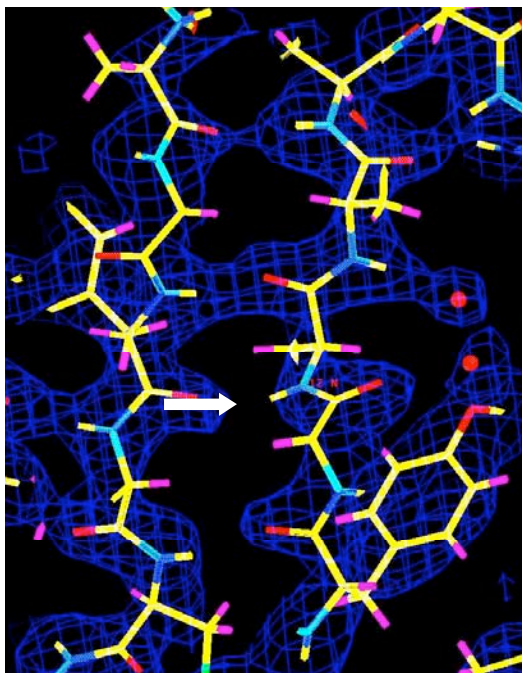


Figure 4. A section of the 2.1Å 2Fo-Fc Sim-weighted electron density map contoured at 1.5σ shows the part of a beta sheet with some partially exchanged backbone amide sites. In the middle part of the map, the lack of density at the H/D site of the amide of Tyr12 clearly shows this site's resistance to H/D exchange.

4.2 Conserved Water Molecules.

Quite a few water molecules are found conserved among the neutron structures of the three proteins: native (Kurihara, et al.), single W3Y mutant (this work), the triple mutant (Chatake, et al.), as well as the X-ray structure of the W3Y mutant. These conserved waters are mostly in the immediate vicinity of the protein backbone, presumably serving important structural roles in the protein's folding and clearly not affected by the mutations that occur some distance away. In particular, the water molecule that pins down the ends of 3 side chains (Tyr3, Glu14 and Glu30), is in a strategic position connecting disparate parts of the protein and serves to pull together the regions near the N and C terminals. Another water molecule, H-bonded to the oxygen of Val37, the H/D ϵ 2 atom of Trp36 and the O δ 2 atom of Asp18, is buried inside the protein fold. Not surprisingly, this water molecule, which appears to be indispensable for protein folding, is also conserved in all four structures. A third water molecule, H-bonding to the amide H/D of Ser24 and situated very close to the I23V mutation site, is also conserved. Another example of a highly conserved water molecule, H-bonded to Lys45's amide H/D, Asp34's O and Trp36's O, is shown in **Figure 5**. But a reliable analysis of the exact role that hydration plays in thermostability has yet to wait until further refinement is completed.

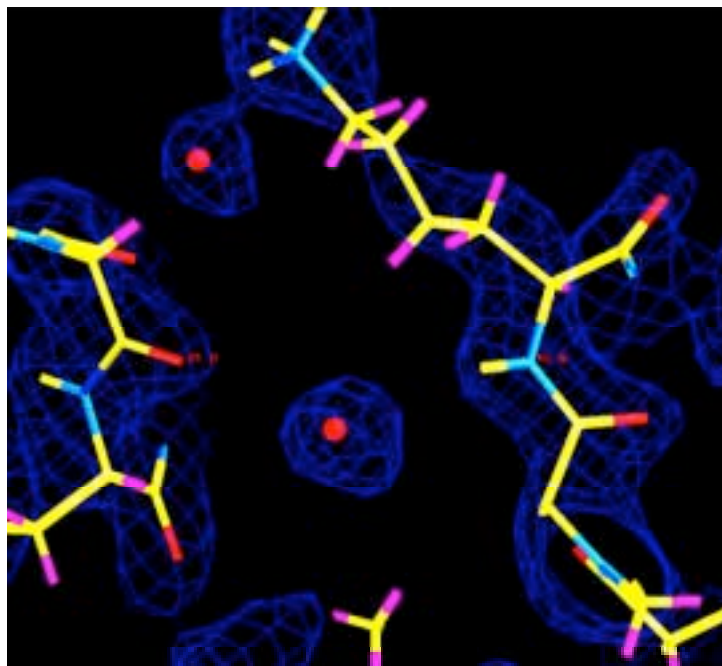


Figure 5. A section of the 2.1Å 2Fo-Fc Sim-weighted electron density map contoured at 1.5 σ showing a water molecule (only the oxygen position is modeled) conserved among the native, single W3Y and a triple mutant structures. This water molecule is H-bonded to Lys45's amide H/D, Asp34's O and Trp36's O (not shown) and plays an important structural role.

5. CATEGORIZATION OF WATER MOLECULES

We can roughly categorize the waters around the protein in three groups. One category directly participates in the folding of the protein, i.e., in fixing the beta-turns, in linking side chains and in sealing the loose ends of the terminal part of the protein. A second category would be water molecules in the immediate surrounding shell of the protein, connected to either the backbone or some important side chains. The third type of water molecules, whose oxygen atoms are observed, can be seen to fill a portion of space between the packed protein molecules.

6. CONCLUSION

The TOF Laue neutron technique using a spallation source has been shown to be an efficient way to collect data in this preliminary study. The medium resolution data described here, collected in a short period of time, offers adequate information for us to examine important deuteration sites and hydration patterns. In this study, similar, though slightly different, backbone accessibility with that of the native and triple mutant of PfRd is observed. In comparisons between

the single, the wildtype and the triple mutant, several water molecules are found to be conserved. This strongly suggests an important structural role played by these water molecules.

The current study is still on going (and the final results will be published elsewhere). Future experiments will involve extending these studies to higher levels of resolution, and exploring in further detail the changes in backbone H/D exchange levels.

7. ACKNOWLEDGEMENTS

The PCS is funded by the Office of Science and the Office of Biological and Environmental Research of the U.S. Department of Energy. This research was supported in part by a grant (GM60329 to MWWA) from the National Institute of Health.

8. REFERENCES

- [1] Bau, R., Rees, D.C., Kurtz, D.M., Scott, R.A., Huang, H.S., Adams, M.W.W., Eidsness, M.K. (1998) *J. Biol. Inorg. Chem.*, **3**, 484-493.
- [2] Chatake, T., Kazuo Kurihara, Ichiro Tanaka, Irina Tsyba, Robert Bau, Francis E. Jenney Jr., Michael W. Adams and Nobuo Niimura *J. Amer. Chem. Soc.*, submitted for publication
- [3] Campbell, J. W., Habash, J., Helliwell, J.R., Moffat, K. (1986) "Determination of the Wavelength Normalisation Curve in the Laue Method", *Information Quarterly for Protein Crystallography*, **18** Daresbury Laboratory, UK.
- [4] Chatake, T., Kurihara, K., Tanaka, I., Adams, M.W.W., Jenney, F.E., Tsyba, I., Bau, R. & Niimura, N. (2002) *Appl. Phys. A*, **74**, [suppl.], S1280-S1282.
- [5] Dauter, Z., Wilson, K.S., Sieker, L.C., Moulis, J.M., Meyer, J. (1996) *Proc. Natl. Acad. Sci U.S.A.*, **93**, 8836-8840.
- [6] A Ducruix, R Giege, eds, *Crystallization of Nucleic Acids and Proteins - A Practical Approach*", IRL Press, Oxford. 1992
- [7] Evans, P. "SCALA", MRC Laboratory of Molecular Biology, Cambridge, UK.
- [8] J. R. Helliwell, J. Habash, D. W. J. Cruickshank, M. M. Harding, T. J. Greenhough, J. W. Campbell, I. J. Clifton, M. Elder, P. A. Machin, M. Z. Papiz and S. Zurek, *J. Appl. Cryst.* (1989). **22**, 483-497
- [9] Jenney, F.E.Jr. & Adams, M.W.W. (2001) *Methods in Enzymol.*, **334**, 45-55.
- [10] Jones, Alwyn, Zou, J. Y., Cowan, S. W., and Kjeldgaard, M. (1991) *Acta Crystallogr.* **A47**, 110-119
- [11] Kurihara, K., Ichiro Tanaka, Toshiyuki Chatake, Michael W. W. Adams, Francis E. Jenney, Jr., Natalia Moiseeva, Robert Bau and Nobuo Niimura, *J. Mol. Biol.*, to be submitted
- [12] Kurihara, K., Tanaka, I., Adams, M.W.W., Jenney, F.E.Jr., Moiseeva, N., Bau, R. & Niimura, N. (2001) *J. Phys. Soc. Jpn. Suppl. Sect. A* **70**.
- [13] Langan, P., Greene, G. & Schoenborn, B.P. (2003a) submitted to *Acta Cryst. D*.
- [14] Langan, P. & Greene, G. (2003b) submitted to *Acta Cryst. D*.
- [15] Pflugrath, J.W. (1998) Molecular Structures Corporation, 3200 Research Forest Drive, The Woodlands, Texas 77381.
- [16] Read, R. (1986) *Acta Cryst.* **A42**, 140-149
- [17] Sheldrick, G. M., and Schneider, T. R. (1997) *Methods Enzymol.* **277B**, 319-343
- [18] Tsyba, I., Ph.D. Dissertation, University of Southern California, 2002
- [19] Zartler, E.R., Jenney, F.E.Jr., Terrell, M., Eidsness, M.K., Adams, M.W.W., Prestegard, J.H. (2001) *Biochemistry*, **40**, 7279-7290.

ANALYSIS OF NEUTRON LAUE DIFFRACTION FROM DEUTERIUM-EXCHANGED *TRP* REPRESSOR

Catherine L. Lawson and Alexander S. Chin
Department of Chemistry and Chemical Biology,
Rutgers University, 610 Taylor Road, Piscataway, NJ 08854, USA
cathy.lawson@rutgers.edu

1. ABSTRACT

Results of preliminary neutron Laue diffraction measurements of wild-type variant Val 58 → Ile of the *E. coli trp* repressor are reported. Limited model refinement alternating between 2.1 Å neutron data and 1.4 Å X-ray data has yielded estimates of H-D exchange along the polypeptide backbone. Protonation of a side-chain carboxyl is also revealed. These results demonstrate the unique ability of neutron diffraction to identify protein hydrogen atom positions at moderate resolution. Improvements in crystal preparation and refinement protocols that would increase the general utility of the neutron diffraction method are discussed.

2. INTRODUCTION

Hydrogen atom positions of crystallized macromolecules and their associated solvent can be identified by measurement of high-resolution neutron diffraction data [1-4]. Widespread application of neutron diffraction to the study of solvent structure in biological systems has historically been hindered by the requirement for well-ordered crystal specimens significantly larger than those needed for X-ray analyses. However, several recent improvements in the method have lowered the minimum crystal volume to about 1 mm³ [5-9]. Employing a neutron source with moderate energy bandpass greatly increases data collection efficiency, since multiwavelength Laue patterns contain many more reflections than corresponding patterns from a monochromatic source [10,11]. This approach has been successfully developed for neutron protein crystallography [12,13] and has now been utilized for neutron measurements in a number of different crystal systems [14-17].

The *E. coli trp* repressor (trpR) is a small, dimeric, ligand-activated DNA-binding protein of the helix-turn-helix motif type (12,500 Da per subunit). Because solvent plays a critical role in the high affinity interaction between trpR and its cognate operator DNA sequences [18-20], a complete description of the interaction chemistry awaits elucidation of hydrogen-atom positions. While it is not currently feasible to prepare large crystals of trpR/operator DNA complexes, X-ray analyses indicate that the solvent structure of trpR crystallized by itself resembles that of trpR bound to DNA [20]. Neutron diffraction studies of trpR by itself can thus provide new insight into the role of solvent in complex formation. A variant trpR bearing the single mutation Val 58 → Ile has structure and activity indistinguishable from wild-type, but fortuitously forms large orthorhombic crystals (up to 0.5 mm³) in hanging-drops [21-23]. We recently reported crystallization and preliminary neutron Laue diffraction to 2.1 Å from a deuterium-exchanged crystal with 1 mm³ volume [24]. Here, we provide an analysis of the preliminary data, aided by complementary X-ray diffraction measurements.

3. METHODS

3.1 Neutron Diffraction

Recombinant expression in *E. coli*, purification, production of orthorhombic crystals in 2.4 M sodium phosphate, pH 5.0, and preliminary neutron diffraction of I58trpR have been reported [24]. To minimize incoherent background scatter of neutrons from ¹H atoms, selected crystals were transferred in conservative steps to fully deuterated solution (2.5 M sodium deuterium phosphate, 0.5 M sodium chloride, 2.0 mM L-tryptophan in D₂O). Approximately 1 month later they were transported from Rutgers University to the EMBL-Grenoble Outstation. Neutron Laue diffraction data were collected at 293 K using the LAue Diffractometer (LADI) neutron sensitive image plate detector at the Institut Laue Langevin (ILL).

3.2 X-ray Diffraction

A second, smaller crystal also exchanged to deuterated solution was mounted in a glass capillary and its X-ray diffraction pattern was measured at room temperature to a resolution limit of 1.4 Å at Beamline X12B of the Brookhaven National Laboratory National Synchrotron Light Source. The incident X-ray beam was monochromatic and tuned to $\lambda=1.1$ Å. Images were collected on an ADSC Quantum IV detector. Reflections were processed using the HKL package [25].

3.3 Refinement

Maximum likelihood model refinement was performed using CNS v. 1.1 [26], with the following modifications. A file containing the neutron scattering lengths for atoms C,H,O,N,S,P, and D was generated and placed in the directory CNS_XRAYLIB. Parameter and topology files for protein and water were modified such that all exchangeable hydrogen atoms were renamed to deuterium (e.g., the main-chain amide "HN" was renamed to "DN"). The complete set of modified files is available from the corresponding author on request.

The 1.3 Å refined X-ray structure of I58trpR (PDB entry 1JHG) [22,23] was the starting point for refinement, with all hydrogen atoms, water and minor side-chain conformers removed from the coordinate set. H and D atom positions were then generated with CNS. Refinement was cycled as follows: (a) positional refinement of all atoms against the X-ray data, (b) isotropic temperature-factor refinement for all atoms against the X-ray data, with strong neighbor restraints to provide reasonable values for H and D atoms, (c) positional refinement of H and D atoms against the neutron data with strong harmonic restraints, and (d) occupancy refinement of deuterium atoms against the neutron data to yield their exchange state. Deuterium occupancy was permitted to vary between -0.57 (the scattering length of hydrogen divided by the scattering length of deuterium) and +1.0. R-free [27] was monitored for each refinement step. The X-ray test set consisted of 5% of measured X-ray reflections. The neutron test set consisted of neutron reflections with *hkl* indices in common with the X-ray test set. Bulk solvent correction was used throughout refinement, with automatic estimation of solvent density level and B-factor.

4. RESULTS AND DISCUSSION

Reflections resulting from neutron Laue diffraction measurements of the deuterium-exchanged crystal were indexed as primitive orthorhombic, with unit cell parameters of $a=53.6$ Å, $b=53.3$ Å, and $c=32.7$ Å, and systematic absences corresponding to space group $P2_12_12$, consistent with prior X-ray studies [23,28,29]. Although measurement redundancy is low, completeness is better than 90% for reflections in the resolution range 50-3.0 Å. The unit cell parameters derived from post-refinement of the monochromatic X-ray diffraction data, $a=53.42$ Å, $b=53.23$ Å, and $c=32.62$ Å, were employed for refinements against both neutron and X-ray data. Summary statistics for both data sets are given in Table 1 (following page).

Structure factors calculated using neutron scattering lengths for non-hydrogen protein atoms of X-ray model 1JHG [22,23] have an initial R-value of 36% against all 4057 unique reflections of the merged neutron data set. Standard crystallographic refinement of 1673 atom positions (H plus non-H), thermal factors and H/D occupancies in the crystal asymmetric unit is not possible; a neutron dataset with at least twice as many reflections would be required. However, the limited model refinement protocol described in Methods produced modest improvements in model statistics against the neutron data (Table I), and provided chemical information useful for design of future neutron diffraction experiments. The most significant improvement to the neutron model statistics (ΔR -free = -0.039) occurred when individual deuterium atom occupancies were refined. At this step, deuterium atom temperature factors were held close to X-ray refined values for heavy-atom neighbors. We therefore anticipated that the neutron refined occupancy values would provide a reasonable estimate of H \leftrightarrow D exchange for all well-predicted hydrogen positions, including the 97 amide protons of the polypeptide main-chain, as shown in **Figure 1**. The plotted occupancy values do appear to be chemically meaningful by the following criteria: (1) there is a strong correspondence with relative exchange rates of trpR backbone protons measured in solution by NMR [30,31], (2) un-exchanged amide protons map without exception to well-ordered regions with poor solvent-accessibility in the crystal lattice, and (3) near-complete exchange within the N-terminus of helix A, all of helix D, and much of helix E is consistent with relative mobility of these regions in both crystal and solution states.

Based on refined D-occupancy values, the average main-chain amide proton exchange is 65% for a crystal soak of 1.5 months. Using a single exponential function as a crude model for the exchange process ($1.0 - e^{-kt}$) leads to the conclusion that a minimum soak period of at least 4 months would be needed to achieve 95% backbone exchange. In contrast, even the slowest backbone amide protons would be fully exchanged within a few weeks in solution, based on

rate constants measured at 45 °C by NMR [31]. Clearly, crystalline trpR has significantly reduced mobility and solvent accessibility.

Historically, the standard protocol for neutron diffraction experiments is to perform deuterium exchange in the crystalline state over long time periods (months to years). To obtain near-complete deuterium exchange needed to optimise signal-to-noise in neutron diffraction, it would be more efficient to perform the exchange in solution prior to crystallization, and then perform crystallization with deuterated solutions. With improvements in the efficiency of neutron facilities leading shorter data collection times [5], parallel reductions in sample preparation time will be essential to maintain a steady flow of projects.

Table 1
Monochromatic X-ray and Neutron Laue Diffraction Statistics, Model Statistics

	Monochromatic X-ray	Neutron Laue
beamline	NSLS X12B	ILL LADI
incident wavelength (Å)	1.1	2.8-3.8
resolution range (high res. shell)	50-1.4 (1.45-1.4)	50-2.1 (2.2-2.1)
reflections measured	149723 (8633)	10102 (527)
unique reflections	18464 (1506)	4057 (280)
$\langle I/\sigma \rangle$	27.5 (8.8)	5.5 (3.5)
Completeness	0.972 (0.808)	0.726 (0.543)
R-merge	0.036 (0.190)	0.114 (0.205)
starting model R-value(R-free)	0.224 (0.243)	0.354 (0.369)
current model R-value (R-free)	0.243 (0.246)	0.304 (0.313)
# model atoms*		1673
D		198
H		647
C,N,O,S		828

*one polypeptide chain (residues 8-108), one L-tryptophan ligand, and one phosphate anion, no waters.

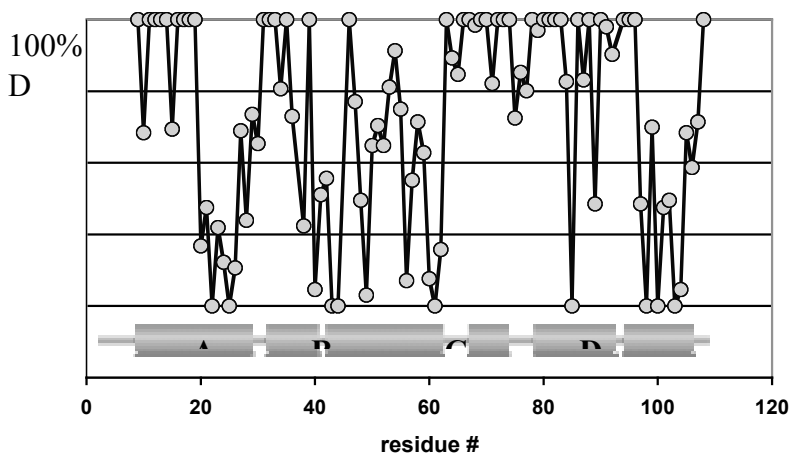


Figure 1. Main-chain amide deuterium exchange in orthorhombic *trp* repressor. Exchange values were obtained by refining deuterium occupancy as described in Methods. The six *trpR* protein helices are indicated (A-F). 100%D corresponds to refined D-occupancy of +10, 100%H corresponds to a refined D-occupancy of -0.57.

Using phases from the limited-refinement model, 2Fo-Fc and Fo-Fc neutron maps were generated and inspected and also compared to corresponding X-ray maps. For deuterium soaked protein crystals, negative scattering by ^1H atoms leads to discontinuities in the neutron map that are particularly prominent in hydrophobic regions of the protein structure. Incomplete data (27% missing over the 50-2.1 Å resolution range), and deficiencies of the phasing model were additional major factors limiting neutron map quality. Despite these limitations, the neutron map provided useful information about side-chain hydrogen positions that were not readily apparent from inspection of the 1.4 Å X-ray map. For instance, the neutron map clearly showed the hydrogen atom positions of side-chain amide groups (Asn, Gln), and in two cases revealed that amide O and N atoms had been incorrectly assigned in the prior 1.3 Å X-ray structure. In addition, as shown in **Figure 2**, protonation of the side-chain carboxyl group of an aspartate residue was evident, a result consistent with the acidic pH of the crystal environment.

Attempts to further improve the quality of the model against the neutron data have not been successful. Positional refinement of all atoms against the neutron data leads to degradation of the model, and in any case is not justified because the data-to-parameter ratio is less than 1. Although there are many oxygen electron density peaks for water molecules strongly bound at the protein surface in the X-ray map, neutron maps phased either with or without bulk solvent correction do not show strong peaks at the X-ray identified sites. Addition of thirty water oxygen atoms with strong density in X-ray maps did not improve the neutron model statistics.

Since there are always nearly twice as many scatterers to account for in neutron diffraction as compared to X-ray diffraction, poor observed data-to-model parameter ratio will always be a concern with moderate-resolution neutron data. Simultaneous (or "joint") model refinement against both neutron and X-ray datasets is therefore highly desirable. This approach was implemented successfully by Wlodawer in the 1980's for three different structures [32-34]. Inclusion of such an option in modern crystallographic refinement packages would tremendously increase the utility of the neutron diffraction technique and would facilitate the routine production of complete-atom models.

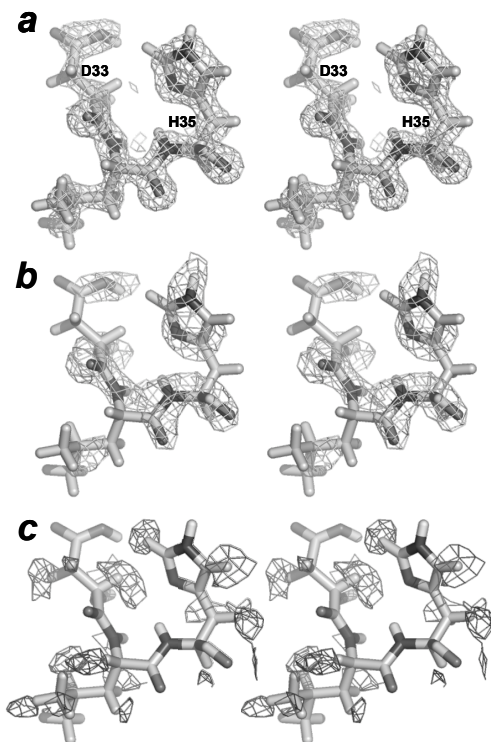


Figure 2. Main-chain amide deuterium exchange in orthorhombic *trp* repressor. Exchange values were obtained by refining deuterium occupancy as described in Methods. The six *trpR* protein helices are indicated (A-F). 100%D corresponds to refined D-occupancy of +1.0, 100%H corresponds to a refined D-occupancy of -0.57.

Additional improvements to data quality, resolution, and map interpretation should be gained by carrying out the neutron diffraction experiment with fully deuterated protein. This procedure removes incoherent scattering from ^1H that contributes to background noise, and results in positive density for all atoms [8,35,36]. Preparation involves growth of the recombinant protein in fully deuterated cell culture media. A final exchange step either before or after crystallization restores full deuteration for the diffraction experiment.

5. ACKNOWLEDGEMENTS

We thank Dean Myles for collecting the neutron diffraction data; Dieter Schneider and Bob Sweet for assistance at NSLS beamline X12B; Benno Schoenborn, Paul Langan and Helen Berman for helpful advice and discussions. This study was supported in part by National Institutes of Health GM21589 to Helen M. Berman (Rutgers University).

6. REFERENCES

- [1] R.B. Knott and B.P. Schoenborn, *Basic Life Sci.* **64** (1996), 1.
- [2] Z.R. Korszun, in C.W. Carter, R.M. Sweet (Editors), *Macromolecular Crystallography*, 1997, p. 218.
- [3] A.A. Kossiakoff, in M.G. Rossmann, E. Arnold (Editors), *International Tables for Crystallography*, Kluwer, Dordrecht, The Netherlands, 2001, p. 419.
- [4] N. Niimura, *Curr. Opin. Struct. Biol.* **9** (1999), 602.
- [5] T. Gutberlet, U. Heinemann and M. Steiner, *Acta Cryst.* **D57** (2001), 349.
- [6] J.R. Helliwell, *Nat Struct Biol* **4** (1997), 874.
- [7] N. Niimura, Y. Minezaki, T. Nonaka, J.C. Castagna, F. Cipriani, P. Hoghoj, M.S. Lehmann and C. Wilkinson, *Nat. Struct. Biol.* **4** (1997), 909.
- [8] F. Shu, V. Ramakrishnan and B.P. Schoenborn, *Proc. Natl. Acad. Sci. USA* **97** (2000), 3872.
- [9] I. Tanaka, Y. Minezaki, K. Harada and N. Niimura, *Physica B* **241** (1997), 227.
- [10] D.W.J. Cruickshank, J.R. Helliwell and K. Moffat *Acta Cryst.* **A43** (1987), 656.
- [11] D.W.J. Cruickshank, J.R. Helliwell and K. Moffat *Acta Cryst.* **A47** (1991), 352.
- [12] F. Cipriani, J.C. Castagna, C. Wilkinson, M.S. Lehmann and G. Buldt, *Basic Life Sci* **64** (1996), 423.
- [13] D.A.A. Myles, C. Bon, P. Langan, F. Cipriani, J.C. Castagna, M.S. Lehmann and C. Wilkinson, *Physica B* **241** (1997), 1122.
- [14] C. Bon, M.S. Lehmann and C. Wilkinson, *Acta Cryst.* **D55** (1999), 978.
- [15] L. Coates, P.T. Erskine, S.P. Wood, D.A.A. Myles and J.B. Cooper, *Biochemistry* **40** (2001), 13149.
- [16] A.J.K. Gilboa, D.A.A. Myles, J. Habash, J. Raftery and J.R. Helliwell, *J. Appl. Cryst.* **34** (2001), 454.
- [17] J. Habash, J. Raftery, S. Weisgerber, A. Cassetta, M.S. Lehmann, P. Hoghoj, C. Wilkinson, J.W. Campbell and J.R. Helliwell, *J. Chem. Soc.-Faraday Trans.* **93** (1997), 4313.
- [18] A. Joachimiak, T.E. Haran and P.B. Sigler, *EMBO J.* **13** (1994), 367.
- [19] C.L. Lawson and J. Carey, *Nature* **366** (1993), 178.
- [20] Z. Otwinowski, R.W. Schevitz, R.G. Zhang, C.L. Lawson, A. Joachimiak, R.Q. Marmorstein, B.F. Luisi and P.B. Sigler, *Nature* **335** (1988), 321.
- [21] D.N. Arvidson, C.G. Arvidson, C.L. Lawson, J. Miner, C. Adams and P. Youderian, *Nucleic Acids Res.* **22** (1994), 1821.
- [22] C.L. Lawson, *Nat. Struct. Biol.* **3** (1996), 986.
- [23] C.L. Lawson, in M.H. Sarma (Editor), *Biological Structure and Dynamics*, Adenine Press, Schenectady, NY, 1996, p. 83.
- [24] B.V. Daniels, D.A.A. Myles, V.T. Forsythe and C.L. Lawson, *Acta Cryst D* **59** (2003), 136.
- [25] Z. Otwinowski and W. Minor, in C.W. Carter, R.M. Sweet (Editors), *Methods in enzymology* ; v. 276, Academic Press, San Diego, 1997, p. 307.
- [26] A.T. Brünger, P.D. Adams, G.M. Clore, W.L. DeLano, P. Gros, R.W. Grosse-Kunstleve, J.S. Jiang, J. Kuszewski, M. Nilges, N.S. Pannu, R.J. Read, L.M. Rice, T. Simonson and G.L. Warren, *Acta*

- Crystallogr D Biol Crystallogr* **54** (1998), 905.
- [27] A.T. Brünger, *Nature* **355** (1992), 472.
- [28] C.L. Lawson and P.B. Sigler, *Nature* **333** (1988), 869.
- [29] C.L. Lawson, R.G. Zhang, R.W. Schevitz, Z. Otwinowski, A. Joachimiak and P.B. Sigler, *Proteins* **3** (1988), 18.
- [30] M.D. Finucane and O. Jardetzky, *J Mol Biol* **253** (1995), 576.
- [31] M.D. Finucane and O. Jardetzky, *Protein Sci* **5** (1996), 653.
- [32] A. Wlodawer, H. Savage and G. Dodson, *Acta Crystallogr B* **45 (Pt 1)** (1989), 99.
- [33] A. Wlodawer and L. Sjölin, *Biochemistry* **22** (1983), 2720.
- [34] A. Wlodawer, J. Walter, R. Huber and L. Sjölin, *J Mol Biol* **180** (1984), 301.
- [35] T.R. Gamble, K.R. Clauser and A.A. Kossiakoff, *Biophys. Chem.* **53** (1994), 15.
- [36] F. Shu, V. Ramakrishnan and B.P. Schoenborn, *Basic Life Sci.* **64** (1996), 309.

TOWARDS LARGE MOLECULE CRYSTALLOGRAPHY AT ISIS

Chick C. Wilson

*Department of Chemistry, University of Glasgow, Glasgow G12 8QQ, UK and ISIS Facility, CCLRC Rutherford Appleton Laboratory, Chilton, Didcot, Oxon OX11 0QX, UK
C.C.Wilson@rl.ac.uk; C.C.Wilson@chem.gla.ac.uk*

1. ABSTRACT

The development and status of single crystal diffraction facilities at the ISIS spallation neutron source in the UK are reviewed, with particular reference to their applications in chemical crystallography and moving towards the study of larger structures. The achievements of the SXD instrument over the last few years are summarised, and details given of the recent upgrade of the instrument to encompass 11 area position-sensitive detectors, offering coverage of >50% of the available solid angle. The early impact of "SXD-11" is assessed, with reference to its anticipated limitations in terms of unit cell volume and crystal size. Plans for the recently funded ISIS Second Target Station (TS-2) are also discussed. TS-2 will be optimised for the production of cold neutrons, making it ideally suited to the study of larger structures. Developments of relevance to large molecule chemical and biological neutron crystallography will be summarised, including details of the planned high flux, large molecule crystallography instrument, LMX.

2. INTRODUCTION

Neutron diffraction is the method of choice for many crystallographic experiments. The nature of the scattering of neutrons by atomic species is such that the technique offers a description of all atoms in a structure at approximately the same level of precision. This is due to the fact that neutrons are scattered by the nucleus rather than the electrons in an atom, and hence the scattering power does not have the strong dependence on Z found for many other scattering techniques such as X-ray or electron diffraction.

These properties give neutron diffraction the following features compared with other techniques:

It is easier to sense light atoms, such as hydrogen, in the presence of heavier ones. For example, in the presence of relatively light carbon atoms, a hydrogen contributes only 1/36 (less than 0.03) of the X-ray scattering intensity from a carbon atom. The equivalent ratio for neutrons is around 0.32, meaning that hydrogen atoms are, roughly speaking, determined around 12 times more accurately with neutrons than X-rays in the presence of carbon atoms. This factor generally increases as the atomic number of the "heavy" atom increases, reaching 41 for H in the presence of oxygen (and almost 1100 for hydrogen in the presence of lead);

Neighbouring elements in the periodic table generally have substantially different scattering cross sections. For example manganese and iron have $Z=25$ and 26, respectively, giving a very small contrast for X-ray scattering while the respective neutron scattering lengths (-3.9 fm and 9.5 fm) are not only different in magnitude but also in sign, giving large contrast. For light elements in particular this is the only practical direct method of distinguishing neighbouring elements;

The dependence of the scattering on the nucleus allows isotopes of the same element to have substantially different scattering lengths for neutrons, thus allowing the technique of isotopic substitution to be used to yield structural and dynamical details. In the area of organic and biological molecular structures, the most relevant isotopic substitution is that of ^2H (deuterium, scattering length 6.67 fm) for ^1H (hydrogen, scattering length -3.74 fm). This also allows the use of contrast variation, where the scattering density of different parts of a molecule or of an $\text{H}_2\text{O}-\text{D}_2\text{O}$ mixture is altered. This method is extremely powerful and has been a key to many successful applications of the technique of neutron scattering in chemistry and biology;

The lack of a fall-off in scattering power as a function of scattering angle gives neutron diffraction and ability to study structures to very high resolution, although even for neutrons there will always be a fall-off in scattered intensity caused by thermal effects.

Among the other properties of the neutron which make it a probe of structure complementary to other techniques is the fact that neutrons interact weakly with matter and are therefore non-destructive, even to complex or delicate materials – this is particularly relevant in the study of biological materials. Correspondingly, neutrons are a bulk probe, allowing us to probe the interior of materials, not merely the surface layers probed by techniques such as X-rays, electron microscopy or optical methods. Neutrons also have a magnetic moment, allowing magnetic structure (the distribution of magnetic moments within a material) and magnetic dynamics (how these moments interact with each other) to be studied in a way not possible with other forms of radiation.

3. NEUTRON CRYSTALLOGRAPHY OF MOLECULAR MATERIALS

Neutron scattering has played a major role in developing an understanding of how structure affects the properties of crystalline materials, in areas of relevance to much of modern structural chemistry [2]. Areas accessible to single crystal and powder neutron diffraction include organic materials, pharmaceuticals, small biological macromolecules, zeolites, polymer electrolytes, battery materials, catalysts, superconductors, time-resolved and in situ studies, and chemical magnetism [3]. Neutron diffraction experiments are often carried out under extreme conditions of sample environment such as high and low temperature, under controlled atmospheres, high pressure and in chemical reaction cells. The combination of X-rays and neutrons is powerful in many studies, including the characterisation of host-guest interactions in, for example, zeolites, and in determination of charge distributions in crystal structures.

Specifically in molecular systems, neutron diffraction is essential for obtaining the most definitive answers to structural problems. Neutron diffraction is unparalleled in its ability to locate hydrogen atoms and refine their positions and thermal parameters. Hydrogen atoms (e.g. hydride ligands) can be located in organometallic complexes [4-10] far more reliably than by any other method. Much of the structural work on hydrogen bonded systems (e.g. amino acids, nucleic acid components, carbohydrates, cyclodextrins) has used neutron diffraction [11-22]. In addition, determination of the hydrogen anisotropic displacement parameters in short O...O hydrogen bonds allows, for example, the deduction of the shape of the potential well in which the atom sits [23-26]. Neutron single crystal diffraction has an important role in defining the patterns of “weak” intermolecular interactions in complex molecular and supramolecular structures, as these often crucially involve hydrogen atoms [27-29]. This leads directly to a strong impact in the expanding area of molecular and crystal engineering [1, 2]. Neutron diffraction also gives complementary information to X-ray diffraction for charge density studies [30-35]. In these X-N studies the neutron parameters fix the nuclear positions and the X-ray data determine the electron density involved in bonding and non-bonding interactions.

In addition to the major impact the technique has had in chemical crystallography, single crystal neutron diffraction has made a significant and important contribution in the determination of biologically important structures. There are several examples where single crystal studies of proteins have had a profound influence on our understanding of how the protein might function. An excellent summary of the application of single crystal neutron diffraction in the biological area has recently been given by Knott and Schoenborn [36]. They point out that in X-ray diffraction studies of biological molecules the location of hydrogen atoms is often at best inferred from stereochemical arguments which can be unreliable and misleading.

In the field of structural biology, the relation between structure and function has been established since the early days of protein structure determination. A full understanding of this relationship depends on an appreciation of the detailed molecular interactions involved. These interactions occur through mechanisms such as hydrogen bonding, charge transfer and other non-bonded interactions, and many of these are governed by the location of hydrogen atoms. Accurate neutron diffraction studies can define to high precision the geometry of an active site, and the role which this may play in important interactions, for example with drug molecules. Hydrogen atoms inevitably decorate much of the outer regions of both protein molecules and interacting small molecules. Many important protein functions can thus depend on the presence or absence of just one hydrogen atom and it is clearly important to locate these accurately.

It is this crucial aspect of the role of hydrogen atoms in biological function that has led to the continued pursuit of routine neutron protein crystallography through many years of effort and in spite of the intrinsic difficulty of the experiments. In addition to the obvious application of accurate hydrogen atom location [37-47], there are other areas where single crystal neutron diffraction has a unique contribution to make in this field. The ability of neutron scattering to distinguish clearly nitrogen from carbon and oxygen is important, for example in determining the orientation of histidines, and in resolving other conformational ambiguities [48]. The very large scattering length difference (“contrast”) between hydrogen and deuterium can be exploited to allow the determination of exchangeable hydrogen atoms [49], yielding information on protein dynamics and on solvent accessibility. In a traditionally powerful area of

application of neutron single crystal studies, analysis of thermal motions of hydrogen-containing groups in the structure can give information on the physics underlying the structure [50]. The ordered solvent structure around protein molecules has also been elucidated by high resolution neutron single crystal diffraction studies [51-53]. X-ray diffraction will provide information on the oxygen atoms, but only neutron studies will reveal the orientation of the water molecules by locating the hydrogens. The fact that typical protein crystals are more than 50% solvent emphasises the importance of such studies. Furthermore the predominance of water in real biological environments emphasises the importance of understanding protein-solvent interactions in this way.

3.1 The ISIS Spallation Neutron Source

This section concentrates here on the achievements and potential of single crystal diffraction at the ISIS pulsed spallation neutron source at Rutherford Appleton Laboratory in the UK. The characteristics of a pulsed spallation source are very different to those of a reactor neutron source. The production mechanism itself is a dynamic process, being based on an accelerator rather than a steady state reactor. The word “spallation” comes from a mining term meaning to chip, evoking visions of an impact mechanism for neutron production in such sources. This is more-or-less the case. Charged particles are accelerated to high velocities (and hence energies) in the accelerator before being fired at a heavy metal target. The consequent impacts induce nuclear processes which produce neutrons (typically tens of neutrons for each incident accelerated particle). As this method is less well known than steady-state fission (reactor) based neutron production, a more detailed account of the neutron production process at ISIS, the spallation neutron source at Rutherford Appleton Laboratory in Oxfordshire, UK follows.

The production of particles energetic enough to lead to efficient spallation involves three stages. First, an ion source produces H^- ions that are accelerated in a pre-injector column to 665 keV. In the linear accelerator, the second stage, the H^- ions pass through four accelerating radio frequency cavities to reach an energy of 70 MeV. At injection into the third acceleration stage, the synchrotron, the electrons are stripped from the H^- ions by a very thin (0.25 μm) alumina foil, producing a circulating beam of protons. The proton synchrotron, of 52 m diameter, accelerates 2.5×10^{13} protons per pulse to 800 MeV, before they are extracted and sent to the target station. This entire process is repeated 50 times a second. The spallation target is made from a heavy metal such as depleted uranium, tantalum or tungsten. The highly energetic protons produce neutrons by chipping nuclear fragments from the heavy metal nucleus. For example, for an 800 MeV proton beam some 15 neutrons are typically produced by each proton hitting a tantalum target. Importantly, in terms of potential future developments of spallation sources for enhanced neutron production (and of target-moderator assemblies - see below), this process is of low power (ISIS currently operates at 160 kW, compared with high flux reactor sources of many 10s of MW).

Around the target there is an array of small hydrogenous moderators to slow down the neutrons to thermal or close to thermal energies. There are three moderators at ISIS: one at ambient temperature (316 K, H_2O), one of liquid methane (100 K, CH_4) and the cold moderator of liquid hydrogen (20 K, H_2). To preserve the sharpness of the initial 0.4 μs neutron pulse, the ISIS moderators are small (typically $10 \times 10 \times 5 \text{ cm}^3$). The resultant under-moderation gives a rich epithermal component to the spectrum, with a high flux of high energy, short wavelength neutrons.

3.2 Time-of-flight Laue diffraction and SXD

The pulsed nature of a source such as ISIS makes it essential to exploit time-of-flight techniques on white neutron beams. For neutrons produced in a pulsed manner, using accelerator-based methods, the production time of the neutrons can be precisely defined as the moment when the proton beam hits the target. It is thus possible, by recording the arrival time of each neutron at the detector, to determine its wavelength providing the flight path is known. Each neutron detected is thus time-stamped, giving a direct determination of its velocity and hence its energy and wavelength. The use of white beams, sorted using the time-of-flight technique, allows fixed scattering geometries to be adopted which greatly simplifies the use of complex and extreme sample environments.

Time-of-flight Laue neutron diffraction remains a relatively novel technique for the determination of crystal structures.

The method exploits the time-sorted white beams available from a pulsed source, along with large area position-sensitive detectors, to allow the simultaneous measurement of fully-resolved three dimensional volumes in reciprocal space. By appropriate use of wavelength dependent corrections, the technique can easily be used in “standard” crystallography - structural refinement. The advantages of time-of-flight Laue diffraction in structure determination are that many Bragg reflections are collected simultaneously, allowing the instrumentation to be optimised fairly easily for each data collection. Time-of-flight Laue is the optimal white beam method, allowing the separation of Laue orders and also separating the diffraction pattern generally into three dimensions. This both avoids accidental reflection overlaps (frequently as much or more of a problem than the precise overlap of Laue orders) and stretches the “Laue

background” resulting from the incoherent scattering from the hydrogen content of the samples. Thus the whole pulse (all wavelengths) can be used with impunity.

In the period since the successful provision of an appropriate array of PSDs on the single crystal diffractometer SXD at ISIS (early-mid 1990s) [54-56], the instrument has established a strong programme in small molecule systems [57-79, **Figure 1**]. In particular the instrument has played a major role in the re-establishment of genuine variable temperature and more recently variable pressure approaches to single crystal neutron diffraction. SXD has been in the vanguard of moving neutron single crystal diffraction into regimes more suited to modern structural methods, for example towards one-day collection for average samples and allowing for fastest data collection times of only a few hours. SXD has over several years established an excellent reputation for innovative studies in a range of investigations of structural changes in molecular systems [80-93, **Figure 2**].

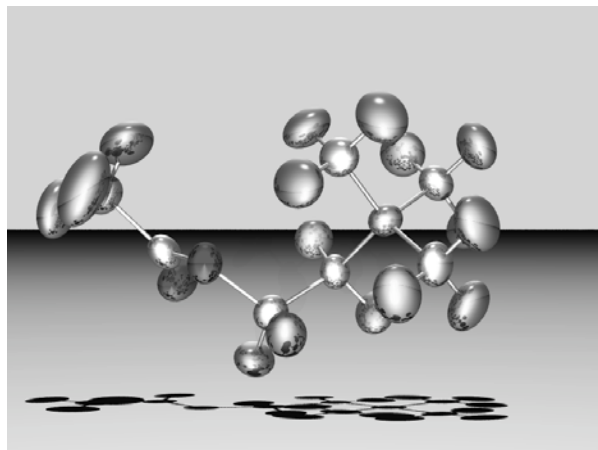


Figure 1. Typical SXD structure refinement of a small molecule system (the receptor molecule acetylcholine, studied as its bromine salt [60]), showing the fully anisotropic refinement of all atoms, including hydrogen, enabled by the use of neutron diffraction.

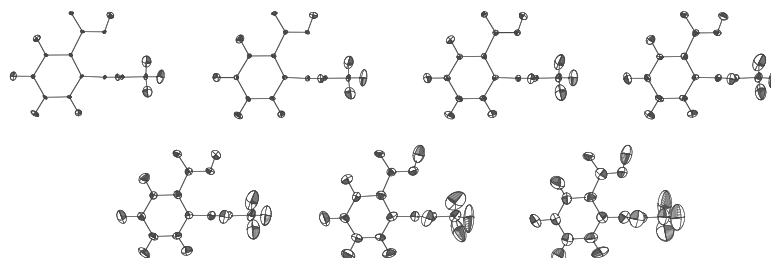


Figure 2. The use of SXD in “parametric” studies of molecular structures is illustrated in this view of the structural evolution of aspirin [88, 92].

SXD has recently been the subject of a major upgrade funded by the UK Engineering and Physical Sciences Research Council. The main features of the “SXD-11” upgrade project were the provision of an 11 position-sensitive detector array yielding 2π sr solid angle coverage **Figure 3**, along with enhanced beam tailoring characteristics and an initial benchmarking of the options for neutron beam focusing for smaller single crystal samples. The enhanced performance of the instrument has been reflected in excellent early performance in the new configuration [94-100; **Figure 4**]. The instrument remains, however, optimised for the study of smaller unit cell materials (up to 2000-3000 Å³).

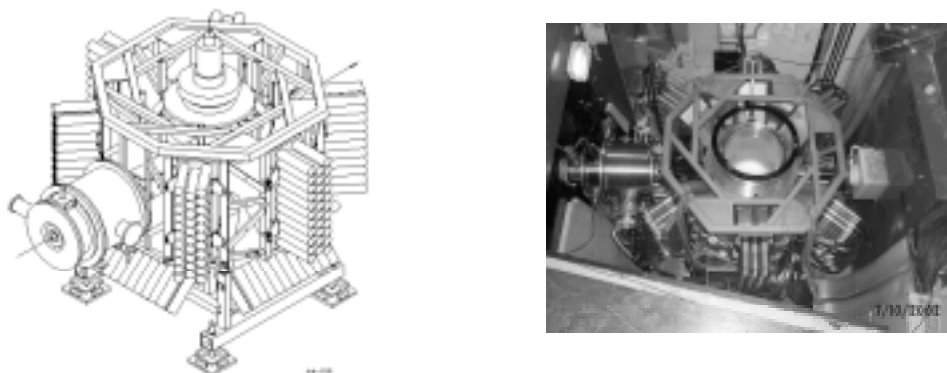


Figure 3. Schematic view (left) and picture (right) of the new SXD-11 instrument and its detector array.

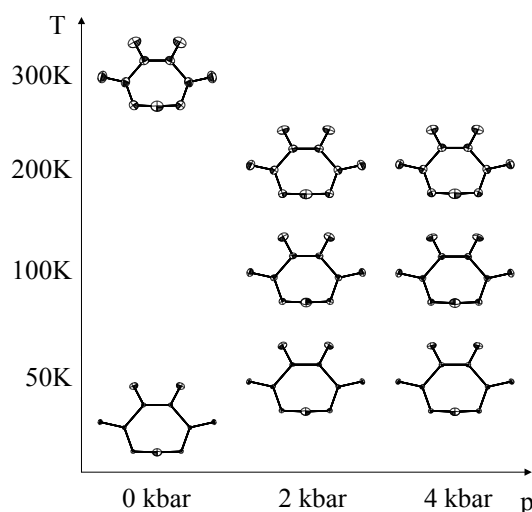


Figure 4. The effect of pressure and temperature on the hydrogen bond in the maleate ion in potassium hydrogen maleate studied on the upgraded SXD-11 instrument [96, 97]. The large sampling of p,T space made possible by the new instrument configuration is highly novel for neutron single crystal diffraction.

In moving beyond the current capabilities, in addition to many potential applications in chemistry, one area to be tackled by future developments is of particular interest in this Symposium, neutron crystallography of biological materials. As outlined above, the power of neutrons in determining solvent water structure, hydrogen bonding schemes and precise active site geometry in proteins is proven but applications to date, especially at pulsed neutron sources, have been limited due to the lack of appropriate instrumentation [101]. Much of large molecule organic and modest sized biological single crystal work should ideally be accessible in data collection times of around a week, even from the small single crystals which are likely to be available. Higher flux, improved dedicated instrumentation, more cold neutrons and more detectors are the keys to success in this area. Recent significant advances in addressing this area at other sources are covered elsewhere in this volume, here the potential at ISIS is discussed.

4. THE SECOND TARGET STATION AT ISIS (TS-2)

The ISIS Second Target Station [102], recently funded in the UK, will help to tackle this area. TS-2 will be optimised for specific cold neutron and high resolution studies at low repetition rate, by optimising the design of both the target and moderators for these applications. Substantial gains in performance of more than an order of magnitude over the original Target Station can be achieved in these areas. The Second Target Station enables optimisation to be made for the low power levels generated at the target, producing significant gains in cold neutron flux. The geometries of the moderators and target can also be optimised for cold neutron production. The removal of adsorbing ‘decoupling’ material

also provides a significant enhancement in cold neutron flux from so-called coupled moderators. This latter effect also naturally results in a broadening of the neutron pulse width that must be taken into account when designing instrumentation. The design of the Second Target Station will thus be optimised for applications which require a high cold neutron flux with a relaxed time structure and a broad wavelength band (for example, SANS, reflectometry, neutron spin echo, large unit cell diffraction), and for high resolution applications requiring a broad wavelength band (using appropriate 'decoupled' cryogenic moderators for meV spectroscopy and high resolution diffraction). All these techniques will experience significant gains from appropriate instrumentation on the Second Target Station.

The main features of the Second Target Station, of enhanced cold neutron flux, broad spectral range and high resolution, are particularly well matched to many of the emerging areas in its three target themes of Advanced Materials, Soft Condensed Matter and Bio-molecular Sciences.

5. LMX - LARGE MOLECULE CRYSTALLOGRAPHY AT ISIS TS-2

In the crystallographic context, the dramatically enhanced flux of cold neutrons offered by ISIS TS-2 means potentially more access to large structures, and to magnetism, as well as considerable potential for expanding our successful high resolution instrumentation. The instrument of relevance here, LMX, the large molecule crystallography diffractometer, will be optimised for high flux and has a two-fold purpose: to allow the study of large scale chemical and supramolecular structures, and to move single crystal diffraction at ISIS towards the study of the structure of smaller biological molecules. LMX will provide qualitatively different capability to the existing SXD, and provide strong complementarity with the LADI and VIVALDI diffractometers at the ILL over a wide range of materials. The basic design aims of the instrument will be to allow the study of large unit cell structures ($20\text{-}30,000 \text{ \AA}^3$) to good resolution ($d_{\text{min}} \sim 1\text{-}1.2 \text{ \AA}$), offer the potential to study larger unit cells at lower resolution, and routinely allow the use of relatively small samples of maximum dimension of order 1mm or less for these studies. An estimated flux gain of at least 40 over the current SXD in the wavelength range of interest to LMX provides the necessary capabilities in terms of performance and, together with retention of significant time-of-flight discrimination, ensures competitiveness with the best available instrumentation world-wide. LMX will also of course allow the study of substantially smaller single crystals of smaller unit cell materials, and it is anticipated that the instrument will enable the study of, for example, $\sim 0.05 \text{ mm}^3$ crystals of cell volume $\sim 2000 \text{ \AA}^3$.

LMX maps onto the major TS-2 themes of advanced materials and biomolecular sciences, and will help some of the exciting areas in chemistry and structural biology to be tackled which are currently not within the scope of existing ISIS instrumentation. There are several scientific areas that are likely to benefit from the high flux capabilities to be offered by LMX, and the common features of these areas can be summarised as follows: they produce problems where neutron diffraction can add significant value to the information offered by other techniques; the materials to be studied will often have larger unit cells; and/or available crystal size will be limited, and the problems are beyond the scope of the current ISIS instrument SXD which is optimised for higher resolution studies of smaller unit cell materials, along with fully-resolved reciprocal space surveying applications.

The outline science case developed for LMX focuses on six highlighted science areas in which the instrument will have a significant impact:

- i. Supramolecular chemistry, extended hydrogen bonded networks
- ii. Organometallic and co-ordination complexes and materials
- iii. Molecular magnets and single molecule magnets
- iv. Zeolites and other framework materials
- v. Biomolecular science and pharmaceuticals
- vi. Less-ordered systems and lower resolution studies, including fibre diffraction

Clearly (v) and (vi) are of particular relevance to the subject matter of this Symposium.

5.1 Towards LMX

With the previous SXD, and now with the developing user programme on the next generation SXD beginning, sufficient experience is now available in chemical crystallography on ISIS pulsed source single crystal instruments to allow sensible extrapolations and also to learn from this experience in detailing the design of new instrumentation. The ISIS Second Target Station, with its optimised flux of longer wavelength neutrons from the low power target, and its low repetition rate, allows us to produce an innovative solution for tackling the exciting areas of larger molecule crystallography. The proposed instrument, LMX, with its promise of yielding an effective count rate some 40 times

higher than the existing SXD for the materials of interest to this proposal, tackles two of the main disadvantages of the present SXD in relation to large molecule crystallography - the lack of time-averaged flux in current pulsed sources and the fact that the present SXD beamline is sited on the “hot” water moderator which produces a peak neutron flux at 1.14 Å with a very rapid fall off at longer wavelengths.

5.2 Detector array

Some of the instrument characteristics are obvious – for example, the requirement for large area detector coverage (as for SXD-11, see **Figure 3**). This is an emerging theme over most of the new generation of neutron single crystal instruments such as SXD-11, the quasi-Laue instruments LADI and VIVALDI at ILL and the upgrade in progress on the monochromatic D19 diffractometer at ILL. Clearly high pixel resolution detectors are highly desirable for this array, to allow for peak separation and integration. The alternative to higher resolution detectors (the upgraded SXD still operates with 3 mm pixel size which would not be adequate for LMX at the same secondary flight path, L_2) is to increase the secondary flight path to offer improved angular pixel resolution. This would lead to the requirement for more detectors and hence a more expensive detector array. The current LMX design thus has two detector options. With 3 mm resolution detectors, these would be situated at $L_2 \sim 500$ mm, which would require an array of 40-50 PSDs. However, for ~ 1.2 mm detector resolution this can be reduced to $L_2 \sim 200$ mm, as on the current SXD instrument, and only require an array of around 11 PSDs, a more cost-effective solution and one which is being actively explored in terms of the required detector development. In either case, LMX will have a massive pixel array of $\sim 4 \times 10^5$ pixels, with more than 10^3 time channels. Higher efficiency detectors than those currently used on SXD are also required; we aim for the provision of PSD detectors with efficiencies $> 50\%$ at 1.5 Å for LMX. The development of smaller pixel, higher efficiency PSDs is flagged as a high priority for TS-2.

5.3 Sample Orientation and Environment

The instrument itself can be designed rather simply, with a small “pseudo- χ - ϕ ” orienter being sufficient. In general the sample environment characteristics for this type of study will involve standard high and (more often) low temperatures, possibly atmosphere control including humidity and potentially modest high pressure capabilities. All of this is entirely compatible with the large, $> 2\pi$ sr solid angle, detector array envisaged for LMX.

5.4 Moderator Choice

Possibly the major issue on LMX is the choice of moderator. As outlined above, TS-2 offers both traditional and novel moderator types: relatively sharp pulses from the decoupled moderators, and broad pulses (with consequently more flux) from the coupled moderators. Since single crystal neutron diffraction from larger systems is fundamentally count rate-limited, flux is the over-riding concern in most of the problems to be tackled by LMX. The unpoisoned, decoupled moderator offers significant flux increases over SXD, but not sufficiently dramatic as to open up the qualitatively new areas being targeted. The coupled cold moderator offers the desired higher flux, and current estimates are that even with a 10 Hz repetition rate of TS-2, LMX will have a flux of at least 40 times SXD-11 over the wavelength ranges of primary interest (say 1.5-6 Å). Of course, there is a penalty to pay, and the price in this case is very broad pulses. This means that the peak profiles in the time-of-flight direction will be substantially degraded from those on the existing SXD **Figure 5**, implying a move towards a “Quasi-Laue” approach as adopted (in different ways) on the protein crystallography instrument PCS at LANSCE and at the ILL instruments LADI and VIVALDI. However, we note that significant time-of-flight discrimination will be retained on LMX, with many associated advantages.

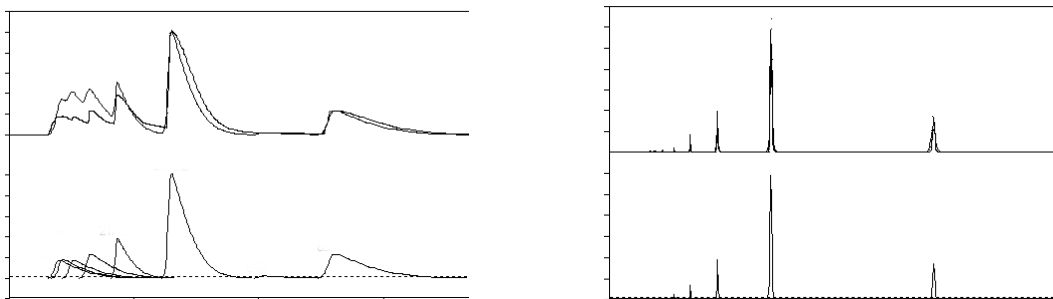


Figure 5. Schematic comparison of time-of-flight single crystal peaks from the current SXD (left) and the broadened peaks from the coupled moderator (right), for which advanced integration solutions will be developed for LMX.

5.5 Instrument length

The broader pulses resulting from choice of moderator are to some extent compensated for by increasing the instrument length (moderator-to-sample distance, L_1), which will lead to greater separation of peaks in the time-of-flight direction (proportional to the length). The chosen length for LMX is governed partly by this factor, but more so by the need to retain a wide band-width (wavelength range in a single data frame). The existing SXD operates on the 50 Hz target with L_1 of 8 m, and offers a wavelength band width of around 9 Å. (Not all of this wavelength range is necessarily useful for data collection, the equally important point is that frame-overlap thus only occurs for very long wavelength neutrons >9 Å). With LMX operating on the 10Hz TS-2, it follows that a similar wavelength band and related advantages will result for an instrument situated 40m from the moderator.

To illustrate the benefit a time-sliced Laue method offers in the design of an instrument such as LMX, we show in **Figure 6** the dramatic improvements offered by use of a time-of-flight Laue as opposed to a Laue method. The separation of peaks in three-dimensions in this way has significant advantages both in terms of required detector angular resolution and moderator-imposed peak shape. This means that an LMX instrument with 3 mm pixel resolution detectors at $L_2=500$ mm, or ~ 1.2 mm pixels at $L_2=200$ mm, will give adequate peak separation for the unit cells of interest even with the broad pulses from the coupled moderator.

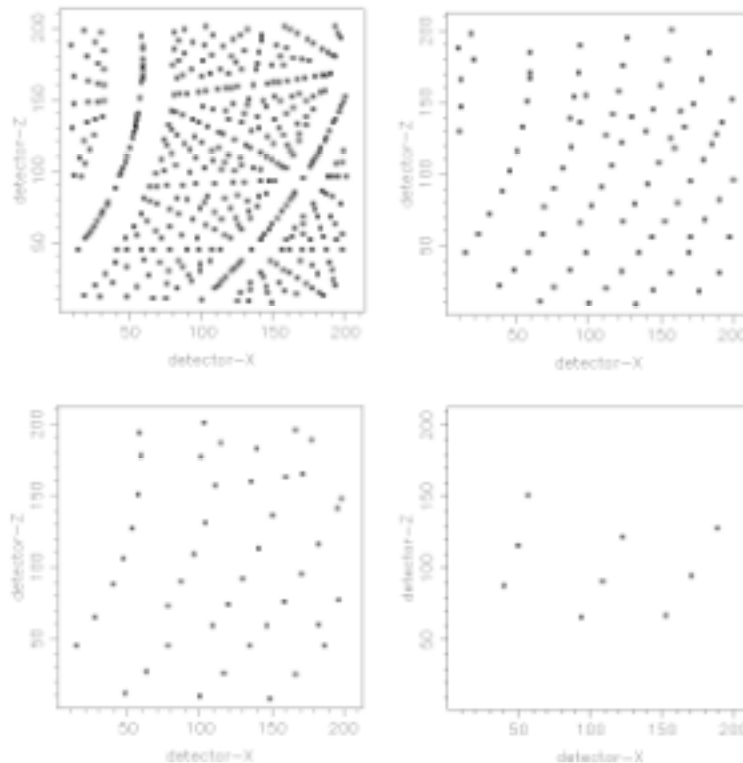


Figure 6. Illustration of the use of time-of-flight Laue diffraction on an instrument such as LMX. The top-left figure is a simulated Laue pattern for a single PSD from a typical orientation of a 27000\AA^3 unit cell, over the wavelength range to be used on LMX ($\sim 1.5\text{-}6\text{\AA}$). Substantial peak overlap would clearly result. However, the remaining three plots show the selectivity introduced by time-of-flight, by reducing to wavelength slices of $\sim 1.75\text{-}2.0$, $\sim 2.0\text{-}2.5$ and $\sim 2.5\text{-}3.0\text{\AA}$, allowing these peaks to be separated even at the relatively modest detector pixel resolution values proposed. The time-of-flight discrimination of LMX would be still more effective in peak separation of this nature.

5.6 Guides

To compensate for the potential $1/r^2$ flux loss from a longer instrument, high critical angle supermirror guides will be employed (these will be a standard feature of TS-2 instruments). An $m=3$ guide over most of the length of LMX will transport most of the neutrons towards the sample. However, it is clear that sample sizes on LMX will necessarily be small, and efficient exploitation of the beam will require higher brilliance than is usual for neutron beams. It is therefore proposed to use long, interchangeable, focusing supermirror sections to allow for tuning of the beam size to the problem under study.

5.7 Peak integration

The broad peak shapes will lead to similar data processing issues as for other broad pulse or Quasi-Laue instruments.

Advanced intensity extraction software is a major development need for LMX. However, full time-sampling of data in the acquisition electronics will be retained on LMX, allowing for a reduction in background levels under the Bragg peaks and allowing the experimenter the opportunity to select time binning to suit the problem under study.

6. CONCLUSIONS

Single crystal neutron diffraction studies of small molecular systems on the SXD instrument at the ISIS spallation source have been notably successful, and the time is right for an extension of this capability to larger unit cell systems and/or smaller crystals. In order to achieve this, more flux and larger detectors are required. The latter has been achieved and is in place with a recently installed radical new design of SXD instrument ("SXD-11") encompassing an array of 11 electronic position-sensitive area detectors. The former can be achieved by harnessing the high potential of the ISIS Second Target Station in providing a very high flux of colder neutrons from optimised cold moderators. The proposed LMX instrument will dramatically expand the horizons of this area at the ISIS source, allowing large chemical complexes, supramolecular materials and a range of biomolecules to be studied.

7. ACKNOWLEDGEMENTS

The author would like to thank colleagues on SXD (Dave Keen, Matthias Gutmann) and the LMX working group, particularly Lee Brammer. The SXD-11 upgrade project was funded by EPSRC under grant GR/M52243/01.

REFERENCES

- [1] C.C. Wilson (2000). *Single Crystal Neutron Diffraction from Molecular Materials*, World Scientific, Singapore, ISBN-981-02-3776-6.
- [2] C.C. Wilson (1999). In *Implications of Molecular and Materials Structure for New Technologies*, eds. J.A.K. Howard, F.H. Allen & G.P. Shields (1999), pp. 11-21, NATO Science Series E: Volume 360, Kluwer, Dordrecht, 1999. Modern neutron diffraction methods.
- [3] C.C. Wilson (1998). Contribution to the Royal Society of Chemistry Scientific Forward Look for Chemistry. Achievements and future prospects for neutrons in chemistry. At <http://www.rsc.org/pdf/forwardlook/neutrongrp.pdf>.
- [4] A.G. Orpen, D. Pippard, G.M. Sheldrick & K.D. Rouse (1978). *Acta Cryst.*, **B34**, 2466-2472.
- [5] R.C. Stevens, M.R. McLean, R. Bau & T.F. Koetzle (1989). *J. Amer. Chem. Soc.*, **111**, 3472-3473.
- [6] J.S. Ricci, T.F. Koetzle, M.T. Bautista, T.M. Hofstede, R.H. Morris & J.F. Sawyer (1989). *J. Amer. Chem. Soc.*, **111**, 8823-8827.
- [7] D.M. Heinekey, J.M. Millar, T.F. Koetzle, N.G. Payne & K.W. Zilm (1990). *J. Amer. Chem. Soc.*, **112**, 909-919.
- [8] L.S. van der Sluys, J. Eckert, O. Eisenstein, J.H. Hall, J.C. Huffman, S.A. Jackson, T.F. Koetzle, G.J. Kubas, P.J. Vergamini & K.G. Caulton (1990). *J. Amer. Chem. Soc.*, **112**, 4831-4841.
- [9] J.A.K. Howard, O. Johnson, T.F. Koetzle & J.L. Spencer (1987). *Inorg. Chem.*, **26**, 2930-2933.
- [10] C.Y. Wei, L. Garlaschelli, R. Bau & T.F. Koetzle (1981). *J. Organometall. Chem.*, **213**, 63-78.
- [11] G.A. Jeffrey, R.K. McMullan & S. Takagi (1977). *Acta Cryst.*, **B33**, 728-737.
- [12] M.S. Lehmann, J.J. Verbist, W.C. Hamilton & T.F. Koetzle (1973). *J. Chem. Soc., Perkin Trans. II*, 133-137.
- [13] S. Takagi & G.A. Jeffrey (1979). *Acta Cryst.*, **B35**, 902-906.
- [14] F. Takusagawa, T.F. Koetzle, T. Srikrishnan & R. Parthasarathy (1979). *Acta Cryst.*, **B35**, 1388-1394.
- [15] S. Takagi & G.A. Jeffrey (1979). *Acta Cryst.*, **B35**, 1482-1486.
- [16] A. Kvik, R. Thomas & T.F. Koetzle (1976). *Acta Cryst.*, **B32**, 224-231.

- [17] Mighell, A. Santoro, E. Prince & C. Reimann (1975). *Acta Cryst.*, **B31**, 2479-2482.
- [18] D.D. Jones, I. Bernal, M.N. Frey & T.F. Koetzle (1974). *Acta Cryst.*, **B30**, 1220-1227.
- [19] T.F. Koetzle, W.C. Hamilton & R. Parthasarathy (1972). *Acta Cryst.*, **B28**, 2083-2090.
- [20] C.H. Wei, B.E. Hingerty & W.R. Busing (1989). *Acta Cryst.*, **C45**, 26-30.
- [21] W. Depmeier & G. Heger (1978). *Acta Cryst.*, **B34**, 1698-1700.
- [22] J. Roziere & J.M. Williams (1978). *J. Chem. Phys.*, **68**, 2896-2901.
- [23] E.O. Schlemper, W.C. Hamilton & S.J. La Placa (1971). *J. Chem. Phys.*, **54**, 3990-4000.
- [24] E.C. Kostansek & W.R. Busing (1972). *Acta Cryst.*, **B28**, 2454-2459.
- [25] H. Küppers, F. Takusagawa & T.F. Koetzle (1985). *J. Chem. Phys.*, **82**, 5636-5647.
- [26] J. Roziere, C. Belin & M.S. Lehmann (1982). *J. Chem. Soc., Chem. Comm.*, 388-389.
- [27] J.A.K. Howard, C. Bilton, G.R. Desiraju & C.C. Wilson (1998). ISIS Annual Report 1998, pp 42-43. Designer Molecules.
- [28] F.H. Allen, J.A.K. Howard, V.J. Hoy, G.R. Desiraju, D.S. Reddy & C.C. Wilson (1996). *J. Amer. Chem. Soc.*, **118**, 4081-4084.
- [29] C. Bilton, J.A.K. Howard, N.N.L. Madhavi, A. Nangia, G.R. Desiraju, F.H. Allen & C.C. Wilson (1999). *Chem. Comm.*, 1675-1676.
- [30] X.M. He, S. Swaminathan, B.M. Craven & R.K. McMullan (1988). *Acta Cryst.*, **B44**, 271-281.
- [31] B.H. O'Connor & F.H. Moore (1973). *Acta Cryst.*, **B29**, 1903-1909.
- [32] R. Tellgren, J.O. Thomas & I. Olovsson (1977). *Acta Cryst.*, **B33**, 3500-3504.
- [33] J.O. Thomas, R. Tellgren & J. Almlöf (1975). *Acta Cryst.*, **B31**, 1946-1955.
- [34] B.M. Craven & R.K. McMullan (1979). *Acta Cryst.*, **B35**, 934-945.
- [35] P. Coppens & A. Vos (1971). *Acta Cryst.*, **B27**, 146-158.
- [36] R.B. Knott & B.P. Schoenborn (1996). In *Neutrons in Biology*, eds. B.P. Schoenborn & R.B. Knott, pp. 1-15, Plenum, New York.
- [37] G.A. Bentley, E.D. Duee, S.A. Mason & A.C.J. Nunes (1979). *Chim. Phys.*, 76, 817-821; G.A. Bentley, M. Delepierre, C.M. Dobson, R.E. Wedin, S.A. Mason & F.M.J. Poulsen (1983). *J. Mol. Biol.*, 170, 243-247; S.A. Mason, G.A. Bentley & G.J. McIntyre (1984). In *Neutrons in Biology*, ed. B.P. Schoenborn, pp. 323-334, Plenum, New York.
- [38] M.S. Lehmann & R.F.D. Stansfield (1989). *Biochemistry*, 28, 7028-7033.
- [39] M.M. Teeter & A.A. Kossiakoff (1984). In *Neutrons in Biology*, ed. B.P. Schoenborn, pp. 335-348, Plenum, New York.
- [40] F.M. Moore, B.T.M. Willis & D. Crowfoot-Hodgkin (1967). *Nature*, 214, 130-133.
- [41] H.F.J. Savage, P.F. Lindley, J.L. Finney & P.A. Timmins (1987). *Acta Cryst.*, **B43**, 280-295.
- [42] J.P. Bouquiere, J.L. Finney, M.S. Lehmann, P.F. Lindley & H.F.J. Savage (1993). *Acta Cryst.*, **B49**, 79-89.
- [43] B.P. Schoenborn (1969). *Nature*, 224, 143-146.
- [44] J.C. Hanson & B.P. Schoenborn (1981). *J. Mol. Biol.*, 153, 117-146.
- [45] S.E.V. Phillips & B.P. Schoenborn (1981). *Nature*, 292, 81-82.
- [46] A.A. Kossiakoff & S.A. Spencer (1981). *Biochemistry*, 20, 6462-6474.
- [47] A.A. Kossiakoff & S.A. Spencer (1980). *Nature*, 288, 414-416.
- [48] A. Wlodawer & L. Sjölin (1983). *Biochemistry*, 22, 2720-2728.
- [49] A.A. Kossiakoff (1983). *Nature*, 296, 713-721.
- [50] A.A. Kossiakoff & S. Shteyn (1984). *Nature*, 311, 582-583.
- [51] H.F.J. Savage (1986). *Biophys. J.*, 50, 947-965; H.F.J. Savage (1986). *Biophys. J.*, 50, 967-980.
- [52] S.E.V. Phillips & B.P. Schoenborn (1981). *Nature*, 292, 81-82.; N.V. Raghavan & B.P. Schoenborn

- (1984). In *Neutrons in Biology*, ed. B.P. Schoenborn, pp. 247-259, Plenum, New York; M.M. Teeter (1984). *Proc. Natl. Acad. Sci. USA*, 81, 6014-6018; H.F.J. Savage & A. Wlodawer (1986). *Methods Enzymol.*, 127, 162-183.
- [53] B.P. Schoenborn (1988). *J. Mol. Biol.*, 201, 741-749; X. Cheng & B.P. Schoenborn (1990). *Acta Cryst.*, B46, 195-208; A.A. Kossiakoff, M.D. Sintchak, J. Shpungin & L.G. Presta (1992). *Proteins: Struct., Funct. And Gen.*, 12, 223.
- [54] C.C. Wilson, in M.W. Johnson (Ed.), *Neutron Scattering Data Analysis*, 1990, p.145, IoP Conference Series, **107**, Adam Hilger, Bristol.
- [55] C.C. Wilson (1997). *J. Mol. Struct.*, **405**, 207.
- [56] D. A. Keen & C. C. Wilson (1996). Technical Report RAL-TR-**96-083**. Single crystal diffraction at ISIS. User guide for the SXD instrument.
- [57] F. H. Allen, J A K Howard, V. J. Hoy, G. R. Desiraju, D. S. Reddy and C. C. Wilson (1996) *J. Amer Chem Soc*, 118, 4081-4084
- [58] N. Shankland, A. J. Florence, P. J. Cox, D. B. Sheen, S. W. Love, N. S. Stewart and C. C. Wilson (1996) *Chem Comm* 1996 855
- [59] K. Wozniak, C. C. Wilson, K. S. Knight, W. Jones and E. Grech (1996) *Acta Cryst B*52, 691-696
- [60] N. Shankland, A. J. Florence and C. C. Wilson (1997) *Acta Cryst*, B53, 176-180
- [61] F. H. Allen, V. J. Hoy, J. A. K. Howard, V. R. Thalladi, G. R. Desiraju, C. C. Wilson and G. J. McIntyre (1997) *J Amer Chem Soc*, 119, 3477-3480
- [62] J. Ellena, A. E. Goeta, J. A. K. Howard, C. C. Wilson, J. C. Autino & G. Punte (1999). *Acta Cryst*, B55, 209-215
- [63] F. E. Mabbs, E. J. L. McInnes, M. Murrie, S. Parsons, G. M. Smith, C. C. Wilson & R. E. P. Winpenny (1999). *Chem Comm*, 643-644
- [64] H. Serrano-González, K. D. M. Harris, C. C. Wilson, A. E. Aliev, S. J. Kitchin, B. M. Kariuki, M. Bach-Vergés, C. Glidewell, E. J. MacLean & W. W. Kagunya (1999). *J. Phys Chem B*, 103, 6215-6223
- [65] P. R. Mallinson, K. Wozniak, C. C. Wilson, K. L. McCormack & D. S. Yufit (1999). *J. Amer Chem Soc*, 121, 4640-4646
- [66] C. Bilton, J. A. K. Howard, N. N. L. Madhavi, A. Nangia, G. R. Desiraju, F. H. Allen & C. C. Wilson (1999). *Chem Comm*, 1675-1676
- [67] V. I. Bakhmutov, J. A. K. Howard, D. A. Keen, L. G. Kuzmina, M. A. Leech, G. I. Nikonov, E. V. Vorontsov & C. C. Wilson (2000). *J. Chem Soc Dalton Trans*, 1631-1635.
- [68] G. C. Forbes, A. R. Kennedy, R. E. Mulvey, R. B. Rowlings, W. Clegg, S. T. Liddle & C. C. Wilson (2000). *Chem Comm*, 1759-1760
- [69] N. Shankland, A. J. Florence, C. C. Wilson & K. Shankland (2000). In "Applications of neutrons to soft condensed matter", ed. B J Gabrys, Chapter 2, pp. 27-59, Gordon & Breach, UK.
- [70] T Steiner, C. C. Wilson & I. Majerz (2000). *Chem Comm*, 1231-1232
- [71] A. E. Goeta, C. C. Wilson, J. C. Autino, J. Ellena & G. Punte (2000). *Chem Mater*, 12, 3342-3346
- [72] J. M. Cole, C. C. Wilson, J. A. K. Howard & F. R. Cruickshank (2000). *Acta Cryst*, B56, 1085-1093.
- [73] C. K. Broder, J. A. K. Howard, D. A. Keen, C. C. Wilson, F. H. Allen, R. K. R. Jetti, A. Nangia & G. Desiraju (2000). *Acta Cryst*, B56, 1080-1084
- [74] C. Bilton, J. A. K. Howard, N. N. L. Madhavi, A. Nangia, G. R. Desiraju, F. H. Allen & C. C. Wilson (2000). *Acta Cryst*, B56, 1071-1079.
- [75] M. A. Fox, A. E. Goeta, J. A. K. Howard, A. K. Hughes, D. A. Keen, A. L. Johnson, K. Wade & C. C. Wilson (2001). *Inorg Chem*, 40, 173-175.
- [76] S. F. Parker, C. C. Wilson, J. Tomkinson, D. A. Keen, K. Shankland, A. J. Ramirez-Cuesta, P. C. H. Mitchell, A. J. Florence & N. Shankland (2001). *J. Phys Chem A*, 105, 3064-3070.
- [77] C. Bilton, J. A. K. Howard, N. N. L. Madhavi, G. R. Desiraju, F. H. Allen & C. C. Wilson (2001). *Acta*

- Cryst, B57, 560-566.
- [78] K. Wozniak, P. R. Mallinson, C. C. Wilson, E. Hovestreydt & E. Grech (2002). *J Phys Chem A*, 106, 6897-6903.
- [79] P. R. Mallinson, G. T. Smith, C. C. Wilson, E. Grech & K. Wozniak (2003). *J. Amer. Chem. Soc.*, 125, 4259-4270.
- [80] C. S. Frampton, C. C. Wilson, N. Shankland and A. J. Florence (1997). *J Chem Soc Faraday Trans*, 93, 1875-1879
- [81] C. C. Wilson, N. Shankland and A. J. Florence (1996) *Chem Phys Letts*, 253, 103-107.
- [82] C. C. Wilson, N. Shankland and A. J. Florence (1996) *J Chem Soc Faraday Trans*, 92, 5051-5057
- [83] C. C. Wilson (1997) *J. Mol Struct*, 405, 207-217
- [84] C. C. Wilson (1997) *Chem Comm*, 1997, 1281-1282
- [85] C. C. Wilson (1997) *Chem Phys Letts*, 280, 531-534
- [86] C. C. Wilson (2000). *Z. Krist*, 215, 693-701.
- [87] C. C. Wilson & H. Nowell (2000). *New J Chem*, 24, 1063-1066.
- [88] C. C. Wilson (2001). *Chem Phys Letters*, 335, 57-63.
- [89] C. C. Wilson (2001). *Acta Cryst*, B57, 435-439.
- [90] C. C. Wilson, K. Shankland & N. Shankland (2001). *Z Krist*, 216, 303-306.
- [91] T. Steiner, I. Majerz & C. C. Wilson (2001). *Angew Chem Int Ed*, 40, 2651-2654.
- [92] C. C. Wilson (2002). *New J Chem*, 26, 1733-1739.
- [93] C. C. Wilson (2002). *Recent Res Devel Chem Phys*, 3, 119-147.
- [94] D. A. Keen, M. J. Gutmann and C. C. Wilson (2003). *J Appl Cryst*, submitted
- [95] C. C. Wilson & C. A. Morrison (2002). *Chem Phys Letters*, 362, 85-89.
- [96] M. J. Gutmann, D. A. Keen and C. C. Wilson (2003). *High Press Res*, in press
- [97] C. C. Wilson, L. H. Thomas and C. A. Morrison (2003). *Chem Phys Letters*, in press.
- [98] W. Q. Wang, L. N. Johnson, M. Ghosh, D. A. A. Myles and C. C. Wilson (2003). *Chem Phys Letters*, submitted
- [99] C. C. Wilson and L. H. Thomas (2003). *J Appl Cryst*, to be published
- [100] C. C. Wilson (2003). *Acc Chem Res*, in preparation
- [101] C.C. Wilson (1996). In *Neutrons in Biology*, eds. B.P. Schoenborn & R.B. Knott, pp. 35-55, Plenum, New York.
- [102] <http://www.isis.rl.ac.uk/targetstation2/>
- [103] L. Brammer, V. T. Forsyth, J. R. Helliwell, J. A. K. Howard, R. H. Jones, R. Winpenny and C. C. Wilson (2003). LMX - a Large Molecule Crystallography diffractometer for the ISIS Second Target Station, Beamline proposal, <http://www.isis.rl.ac.uk/targetstation/instruments/>

HYDROGEN AND HYDRATION IN PROTEIN STRUCTURAL CHEMISTRY

Nobuo Niimura,^{*1,2} Ichiro Tanaka,¹ Toshiyuki Chatake,¹ Kazuo Kurihara,¹
Mitsuru Maeda¹, Shigeki Arai¹

¹Neutron Science Research Center, Japan Atomic Energy Research Institute, 2-4 Shirane, Tokai-mura, Naka-gun, Ibaraki-ken, 319-1195, Japan; and ²Faculty of Technology, Ibaraki University, Naka-Narusawa, 4-12-1, Hitachi, Ibaraki-ken, 316-8511, Japan

** Author to which all correspondence and reprint requests should be sent.*

E-mail: niimura@kotai3.tokai.jaeri.go.jp

1. ABSTRACT

Neutron diffraction provides an experimental method of directly locating hydrogen atoms in proteins. High resolution neutron diffractometers dedicated to biological macromolecules (BIX-type diffractometer) have been constructed at the Japan Atomic Energy Research Institute (JAERI) and they have been used in the 1.5Å-resolution crystal structure analyses of several proteins. Very interesting topics relevant to hydrogen and hydration in proteins, which cannot be predicted stereochemically, such as hydrogen bonds, acidic hydrogen atom, hydrogen atoms in enzyme mechanisms and the identification of methyl hydrogen atoms and dynamical behaviors of hydration structures that include H positions have been extracted from these structural results. Preliminary hydrogen data base, which is now constructing, has been introduced. In addition, the crystallization of large single crystals based on phase diagrams and future prospect of neutron protein crystallography have been introduced and will be described in this paper.

2. INTRODUCTION

The three dimensional structure determinations of biological macromolecules such as proteins and nucleic acids by X-ray crystallography has improved our understanding of many of the mysteries involved in life processes. At the same time, these results have clearly suggested that hydrogen and water molecules around proteins and nucleic acids play a very important role in many physiological functions. However, since it is very hard to determine the positions of hydrogen atoms in protein molecules using X-rays alone, a detailed discussion of protonation and hydration sites can only be speculated upon so far. In contrast, it is very well known that neutron diffraction provides an experimental method of directly locating hydrogen atoms, but unfortunately, to date, there are relatively a few examples of neutron crystallography in biology since it takes a considerable amount of time to collect a sufficient number of Bragg reflections.

The recent development of a neutron imaging plate (NIP) became a breakthrough event in neutron protein crystallography [1-3]. The first application of the NIP was a structure determination of tetragonal hen-egg-white lysozyme using a quasi-Laue diffractometer, LADI at the Institute Laue-Langevin (ILL) in Grenoble [4]. In the Japan Atomic Energy Research Institute (JAERI), we have constructed several high-resolution neutron diffractometers dedicated to biological macromolecules (BIX-type diffractometers), which use a monochromatized neutron beam and a NIP [5-8, +1].

In this paper, we review several interesting results relevant to hydrogen positions and hydration in proteins, obtained using BIX-type diffractometer. The general subject of neutron protein crystallography has been reviewed by several authors [9-15], and these articles are helpful in understanding the historical background of this area of research. In this review, special topics relevant to hydrogen and hydration in proteins will be discussed. The proteins that have been studied with BIX-3 include myoglobin (Mb) [16], wild type rubredoxin (Rb-w) [17], a mutant form of rubredoxin (Rb-m) [18], hen egg-white lysozyme (HEWL) at pH4.9 [19] and cubic porcine insulin [20]. The detailed experimental procedures and structural descriptions of these individual proteins have already been published as original papers.

3. BIX-TYPE DIFFRACTOMETER

We have constructed a neutron diffractometer dedicated for protein crystallography, and one of the important aspects of this work is the development of an improved monochromator. In order to obtain more intensity at the biomolecular sample, an elastically-bent perfect-silicon crystal (EBP-Si), adjusted by a piano wire tension device, has been developed

and found to be very effective [23-25]. The reflected intensity of the EBP-Si monochromator is increased as the EBP-Si is bent. The neutron beam must be focused at the sample position as large as the sample size, which is at most 3mm in maximum dimension for most protein crystals. The EBP-Si monochromator fulfils this requirement because the horizontally reflected beam can be efficiently focused on the sample crystal, while the vertically reflected beam does not diverge because of the perfect silicon crystal. In contrast, although pyrolytic graphite (PG) is commonly used as a monochromator, the reflected beam from a PG monochromator diverges because of its mosaicity and the absolute intensity of neutrons at the small protein crystal becomes small. Moreover, a PG monochromator produces a neutron beam which is contaminated by $1/2$ neutrons and this effect is not negligible in protein crystallography because wavelengths longer than 2\AA are commonly used for those experiments.

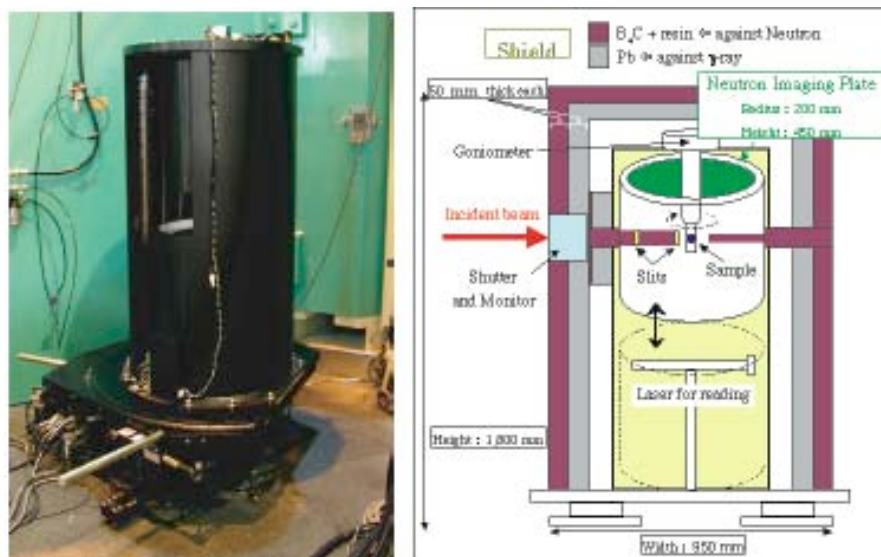


Figure 1. Photograph of BIX-3 without the detector shield (left) and a schematic view of the instrument (right).

The most characteristic and novel design of BIX-3 is the vertical arrangement of the main components of the diffractometer **Figure 1**. The vertical design simultaneously solves the low-flux problem by allowing the sample position to be closer to the monochromator, as well as the shielding problems by enabling a sufficiently small quasi-cylindrical detector shield to be built. Most importantly, the vertical arrangement dramatically decreases the overall size of the diffractometer. The goniometer with a sample crystal is set in an unconventional upside-down position, in order to permit access and allow rod rotation by the laser reader of the NIP. Because the recording of diffraction spots by the oscillation method may make the signal-to-noise ratio poor (as it is in the Laue method), we have decided to use a step-scanning method instead of an oscillation mode as our basic data collection procedure. After the data on the NIP are read for each exposure, the sample is rotated around the goniometer by a small angle (typically 0.3°), and then the erased NIP is returned to the measurement position again. This procedure is repeated several hundred times, with each exposure lasting approximately from half an hour to one hour for typical samples. A detailed description of the performance of BIX-3 has been given in reference 13.

Recently we have constructed a new neutron single crystal diffractometer (BIX-4) at 1G-B port of JRR-3M in JAERI [+1]. Since at 1G-B port another diffractometer for biology, BIX-3 and a high-resolution powder diffractometer (HRPD) coexist, the monochromator house needed to be reconstructed **Figure 2**. The main architecture of BIX-4 is based on that of BIX-3. BIX-4 uses an elastically-bent perfect-Si crystal monochromator and neutron imaging plates as BIX-3. In addition, several optimizations of the monochromator and modifications from previous BIX-3 are carried out. The final gain of the neutron intensity at the detector position is estimated to be 2.5 times larger than previous BIX-3. That higher performance increases the opportunities to apply neutron crystallography to biological macromolecules which give only weak reflections.

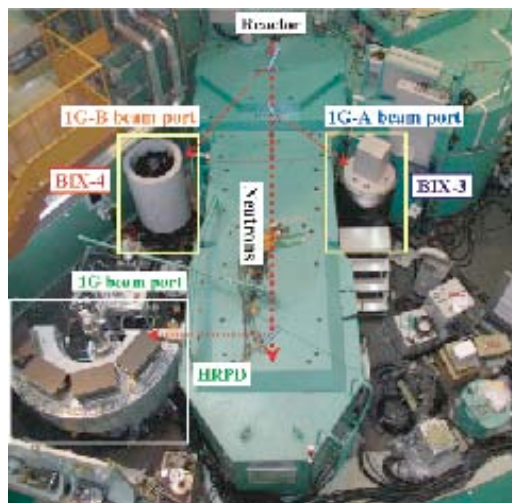


Figure 2. Top view around the neutron beam line shared with 1G, 1G-A and 1G-Bbeam in the reactor hall of JRR-3M. The dotted line indicate the path of neutron beam from the reactor as a guide for the eyes. From up-stream BIX-4, BIX-3 and HRPD are arranged, and they used different wavelengths, 2.6 Å, 2.9 Å and 1.8 Å, respectively.

4. NEUTRON IS COMPLEMENTARY TO X-RAY

Table 1 shows the neutron scattering lengths and X-ray atomic scattering factors of some elements that constitute proteins. Distinctive features of neutrons are summarized as follows:

- 1) Since the neutron scattering lengths of hydrogen and deuterium are comparable to those of other elements, they are easily observed by neutrons, but X-ray atomic scattering factor of hydrogen is much less and it is hard to be observed by X-ray.
- 2) Since proton has no electrons, it can not be seen by X-ray, On the contrary it can be observed by neutron. In neutron diffractometry heavy water (D₂O) is used for the crystallization of proteins, and D⁺ exists in proteins instead of H⁺ and it is observed by neutron.

The neutron scattering lengths of hydrogen and deuterium are different and the mobile hydrogen is distinguished because it is replaced by deuterium.

atom	Neutron $b_{\text{coh}} (10^{-12} \text{ cm})$	X-ray $f_{\text{x-ray}} (10^{-12} \text{ cm})$
D ⁺	0.67	0
H	-0.37	0.28
D	0.67	0.28
C	0.67	1.69
N	0.94	1.97
O	0.58	2.25
S	0.29	4.48

4.1. Hydrogen position is refined.

Since the neutron scattering lengths of hydrogen and deuterium are comparable to those of other elements, in neutron protein crystallography they are not only identified but also their positions are refined like other elements, such as carbon, nitrogen and so on. Several examples are shown in **Figure 3**. **Figure 3(a)** shows a $2|F_o| - |F_c|$ nuclear density map of Phe48 of Rb-w at 1.5 Å resolution [17]. The neutron scattering length of hydrogen atoms is negative and their density contours in neutron Fourier maps are shown in red, while deuterium, carbon, nitrogen and oxygen atoms all have positive neutron scattering lengths, and their contours are shown in blue. In this map, the hydrogen atoms bonded to carbon atoms are clearly visible. **Figure 3(b)** shows a similar nuclear density map for Tyr12 of Rb-w, also at 1.5 Å

resolution [17]. In a neutron diffraction experiments, hydrogen atoms produce a large amount of incoherent scattering, which results in an undesirably high level of background radiation. This effect can be partially overcome either by growing crystals from, or by soaking the crystals in, D₂O solutions. This treatment leads to the replacement by deuterium of some of the hydrogen atoms bonded to nitrogen and oxygen (exchangeable hydrogens), as well as the hydrogen atoms of the solvent molecules in the crystal, without modification of the overall structure of the macromolecule. In **Figure 3(b)**, the contours of the hydrogen atom of the O-H bond in Tyr12 are shown in blue and thus it can be concluded that it has been replaced by a deuterium atom. Figure 3(c) shows the $2|F_o|-|F_c|$ nuclear density of Trp36 of Rb-w at 1.5 Å resolution [17], and it is clearly seen that the N-H bond of the indole ring, which is shown in blue, has become an N-D bond.

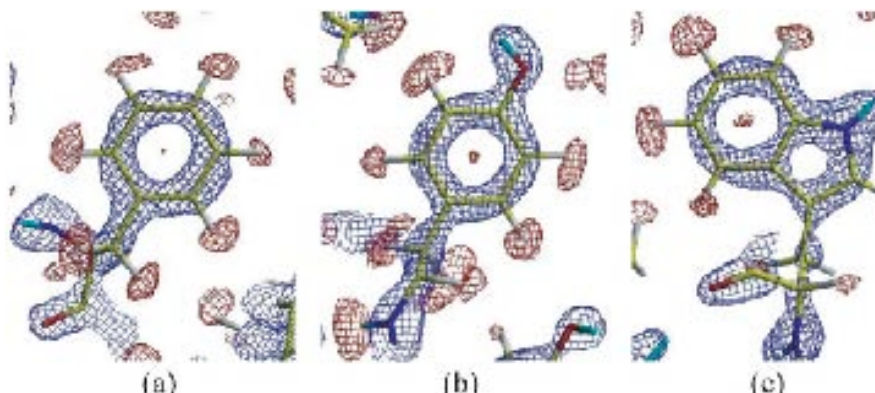


Figure 3. $2|F_o|-|F_c|$ nuclear density maps around (a) Phe48, (b) Tyr12, (c) Trp36; blue contours are positive, while red contours are negative.

4.2. Hydrogen (proton) which cannot be predicted stereochemically.

The positions of H atoms covalently bonded to carbon atoms can be calculated stereochemically based on the coordinates of carbon and nitrogen atoms determined by high resolution X-ray crystal structure analysis. However, the positions of some hydrogen atoms covalently bonded to carbon atoms are difficult to be calculated stereochemically, and the positions of hydrogen atoms bonded to oxygen, nitrogen and sulfur atoms are impossible to be identified and refined. On the contrary, neutron can identify and refine their positions. Moreover, we would like to stress that those These hydrogen atoms are summarized in Table 2.

Some hydrogen or deuterium atoms which are determined from our neutron diffraction studies are exemplified as follows:

Functional group	Chemical structure	Residues	Detection of Hydrogen positions	
			X-ray Analysis	Stereochemically
Aromatic ring	f-H, f-D	Phe, Tyr, Trp, His	Possible	Possible
Alkyl group (except methyl)	-CH-, -CH ₂ -	All residues	Possible	Possible
Peptide group and -ND group	-ND-	All residues except His	Possible	Possible
Methyl group	-CH ₃	Ala, Ile, Leu, Met, Thr, Val	Hard	Hard
Protonated amino group	-ND ₃	N-terminus, Lys	Hard	Hard
Hydroxyl group	-OD	Ser, Thr, Tyr	Impossible	Impossible
Protonated carboxyl group	-COOD	C-terminus, Asp, Glu	Impossible	Impossible
Amino group	-ND ₂	Arg, Asn, Gln	Impossible	Impossible
Sulfhydryl group	-SD	Cys	Impossible	Impossible

Methyl hydrogen atoms. The methyl hydrogens can sometimes be significantly off their predicted positions because of free rotation around C-C bonds. Consequently, if their precise positions are required they should be determined by neutron diffraction experiments. **Figure 4** shows examples of some methyl hydrogen atoms in Rd-w determined from our neutron diffraction data [17].

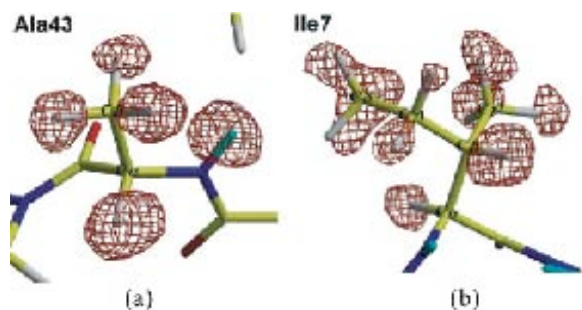


Figure 4. $|F_o|-|F_c|$ omit map of the hydrogen atoms around the residues Ala43 (a), Ile7 (b);

Hydrogen atoms of amino group. In X-ray protein crystallography sometimes it is very difficult to distinguish nitrogen and oxygen atoms in Asn and Gln, but in neutron protein crystallography such a difficulty never occurs because deuterium atoms of amino group (-ND₂) are identified very easily. **Figure 5** shows the 2Fo-Fc Fourier map of Asn 21 in Rb (m).

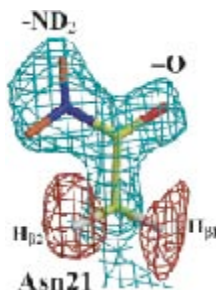


Figure 5. The 2Fo-Fc Fourier map of Asn 21 in Rb (m).

Hydrogen atoms of histidine. The protonation and deprotonation states of the two nitrogen atoms (N_p , N_t) in the imidazole ring of histidine are often very important pieces of information that need to be known in order to fully understand the function of certain enzymes, as well as the metal complexation behavior of certain proteins. This information can be obtained from neutron diffraction. The neutron diffraction analysis of cubic porcine insulin has been carried out [20]. The protein is a hetero-dimer, composed of an A-chain and a B-chain. **Figures 6(a)** and **(b)** show the $2|F_o|-|F_c|$ nuclear density maps of the His5 and His10 residues, respectively, of the B-chain of cubic porcine insulin at 1.6 Å resolution. For His5 of the B-chain, N_p is protonated and N_t is deprotonated. In contrast, for His10, both N_p and N_t are protonated. This means that His5 is electronically neutral while His10 is positively charged.

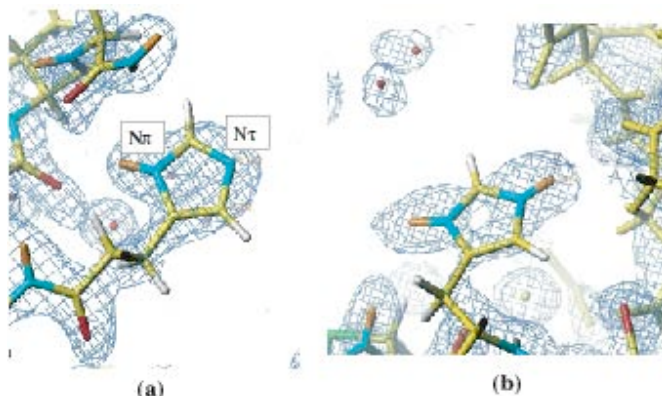


Figure 6. $2|F_o|-|F_c|$ nuclear density map of (a) His5 in B-chain and (b) His10 in B-chain of cubic porcine insulin.

As mentioned earlier, polar hydrogen atoms, like those of N-H and O-H bonds, can be exchanged by deuterium if the protein crystal is soaked in a D₂O buffer. In contrast, hydrogen atoms bonded to carbon are normally not exchangeable. An exception is the hydrogen atom bonded to the C_{ε1} carbon atom of histidine. The C_{ε1}-H of imidazole group is the most acidic C-H bond found in amino acids [29]. Therefore this hydrogen atom is in principle exchangeable, depending on its environment. We found direct experimental evidence for this in metmyoglobin, and **Figure 7** shows the nuclear density map for His97 in this protein [16].

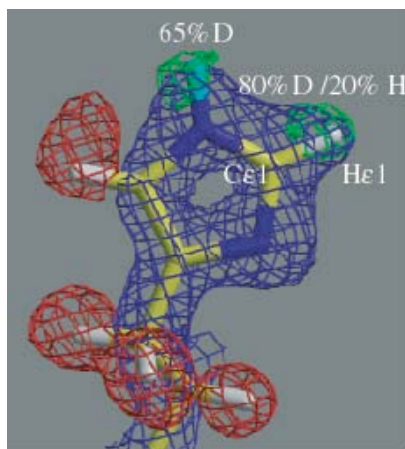


Figure 7. Histidine 97 in myoglobin. Nuclear density maps: blue: $2|F_o|-|F_c|$ map (positive); green: $|F_o|-|F_c|$ omit map (positive); red: $|F_o|-|F_c|$ omit map (negative). All H(D)-atoms were omitted for the calculation of the F_c and j_c for the omit-map.

The H_{ε1}-atom clearly shows positive neutron density contours near C_{ε1}, indicating an exchange of H atoms of the C-H bond to deuterium. An occupancy refinement yields the ratio 80% D/ 20% H. The nitrogen atom N_{ε2}-atom is also deuterated (occupancy: 65% D). The alternative conformation, obtained by rotating the imidazole ring by 180° around the C_β-C_γ axis, cannot explain this finding since the H_{α2}-atom shows a full hydrogen occupancy (red contours in **Figure 7**). His97 is located on the so-called proximal side of the heme plane (the ligand binding position is on the other site of the heme plane, the so-called distal side). To our knowledge, this is the first time neutron diffraction has been used to verify the acidic character of the H_{ε1} atom of His97 in myoglobin. In the case of hen-egg-white lysozyme, a similar conclusion was reported recently [30].

Hhydrogen atoms in enzyme function. In the proposed mechanism of the reaction of lysozyme with oligosaccharides, consideration was given to the fact that enzyme activity is maximal at pH 5 and is less active at pH 7. It is postulated that at pH 5, the carboxylate group of Glu35 is protonated, and it is this proton that is transferred to the oxygen atom on the bound substrate (sugar) during the hydrolysis process. During the reaction, another acidic residue Asp52, remains in its dissociated state [32]. In order to elucidate the role of hydrogen atoms in this reaction, neutron diffraction experiments of hen egg-white lysozyme, crystals of which have been grown at different pH's, [specifically, 4.9 [19] and 7.0 [4]], have been carried out. The detailed procedures of these neutron structure analyses have been already reported [4,19]. The results are shown in **Figures 8(a) and (b)**. **Figure 8(a)** shows the $2|F_o|-|F_c|$ nuclear density map around the carboxylate group of Glu35 at pH=4.9, while **Figure 8(b)** shows the same region at pH=7.0. In **Figure 8(a)**, as indicated by an arrow, neutron density was observed to extend from the position of the O atom of the carboxyl group labeled E35O_{ε1}, suggesting that this carboxyl oxygen atom is protonated atom. On the other hand, in **Figure 8(b)**, it is seen that around this oxygen (E35O_{ε1}) there is a water molecule at pH 7.0, but no indication of hydrogen (deuterium) atoms. The fact that this catalytic site is deprotonated explains why lysozyme has significantly reduced activity at pH7.0. These results indicate that a water molecule around the carboxyloxygen atom at pH=7.0 is kicked out as a result of the protonation of this oxygen atom at pH=4.9, and suggests that it is in fact this enzymatically-active proton which is subsequently transferred to the oxygen atom of the substrate (sugar) during the hydrolysis process.

Mason *et al* has already carried out the neutron diffraction study of lysozyme at pH4.2 using a triclinic crystal and the protonated carboxylate group of Glu35 has been reported [39].

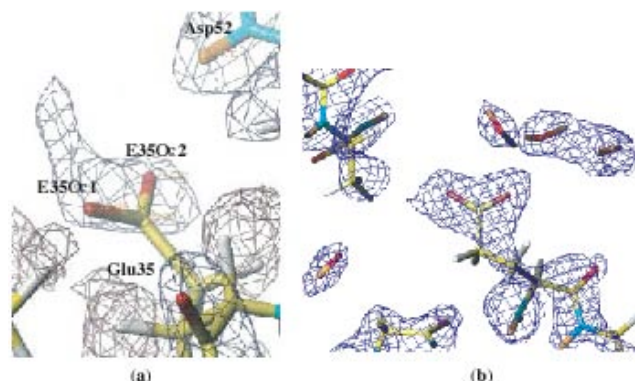


Figure 8. $2|F_o|-|F_c|$ nuclear density map around the carboxylate group of Glu35 at pH=4.9 (a), and Figure 15(b) at pH=7.0.

4.4. H bonds

Hydrogen bonds play important roles in countless biological processes. The interaction energy of the hydrogen bond is intermediate between those involving covalent and Van der Waals forces. Hydrogen bonds are directional and form several kinds of networks in biological macromolecules. However, since it is not easy to determine the positions of all the hydrogen atoms in protein molecules using X-rays or NMR alone, detailed discussions of hydrogen bonds have often been limited thus far, because of the absence of positional information of H atoms.

In order to fully discuss a hydrogen bond, X-H---Y, (in which X and Y are the hydrogen donor and acceptor, respectively), information about the hydrogen position is essential. Along with other investigators, Baker and Hubbard have extensively discussed H-bonds in globular proteins, using hydrogen atom positions predicted from atomic coordinates derived from high-resolution protein X-ray data [21]. Hydrogen atoms were added to the various protein models at their calculated positions, but only those that could be unambiguously defined by the protein geometry. As a matter of fact, no hydrogens were placed on amino or hydroxyl groups, such as those in Ser, Thr, Tyr or Lys side chains. In the conclusion, those authors stressed the necessity of high-resolution neutron diffraction studies.

Our high-resolution neutron results meet their suggestion. **Figure 9** shows one example, taken from our study of a Rb-m. In this diagram, the H-bonds, X-H(D)---Y have been plotted with the H(D) atom at the origin, the X-H(D) bond defining the horizontal axis, and the Y atom distributed in the (x,y) plane [18]. The resulting figure is consistent with the concept of the weak and strong H-bonds as proposed by Desiraju and Steiner [22].

$$\begin{aligned} \text{Strong H-bonds: } & 1.5\text{\AA} < d[\text{H}---\text{Y}] < 2.2\text{\AA}, \quad 130^\circ < \text{angle}[\text{X}-\text{H}---\text{Y}] < 180^\circ \\ \text{Weak H-bonds: } & 2.2\text{\AA} < d[\text{H}---\text{Y}] < 3.0\text{\AA}, \quad 90^\circ < \text{angle}[\text{X}-\text{H}---\text{Y}] < 180^\circ \end{aligned}$$

In **Figure 9**, strong and weak H-bonds are indicated by orange and blue areas, respectively. It can be seen that high-resolution neutron protein crystallography has allowed us to examine H-bonds in more detail, and that numerous “weak H-bonds” in a protein structure can be identified with this method.

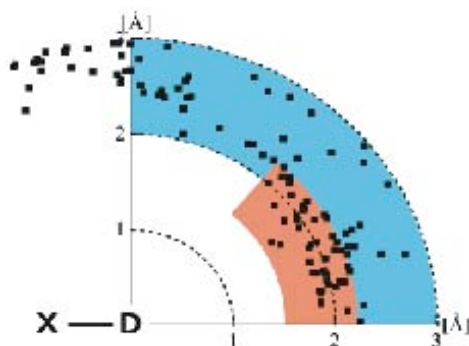


Figure 9. The distribution of Y atoms in X-H(D)---Y hydrogen bonds, with the position of the H(D) atom fixed at the origin. The component of H(D)---Y along the X-H(D) direction is plotted along the horizontal axis, and the component of H(D)---Y perpendicular to X-H(D) is plotted in the vertical direction. The region of strong hydrogen bonds is indicated by the orange area, while weak hydrogen bonds are shown in the blue area.

Bifurcated Hydrogen Bonds. In our studies of several small proteins, all the hydrogen bonds between the C=O and N-H groups in the helices of the proteins we studied have been surveyed including their hydrogen atom positions. **Figure 10** shows one example of how a conventional hydrogen bond in an α -helix of myoglobin is seen in a neutron diffraction experiment. The hydrogen positions as well as carbon, nitrogen and oxygen positions have been refined. This figure clearly indicates that the location of the experimental H positions with neutron data is usually unambiguous. However, we have found several exceptions to the conventional picture of H-bonds in α -helices.

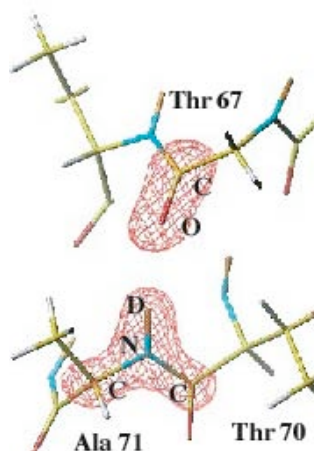


Figure 10. Hydrogen bond in an α -helix. $|F_o| - |F_c|$ omit nuclear density map (red) contoured. The marked atoms were omitted for the calculation of F_c for the omit-map.

When we surveyed the hydrogen bonds in the α -helices individually, we found that there were several bifurcated hydrogen bonds, one of which (from myoglobin) is illustrated in **Figure 11**. The occurrence of bifurcated hydrogen bonds in the α -helices of proteins has been proposed earlier, based on an analysis of calculated hydrogen atom positions from atomic coordinates derived from high-resolution X-ray data [21, 23]. However, it is somewhat risky to discuss the detailed structure of bifurcated hydrogen bonds based solely on those predictions. In high-resolution neutron protein crystallography, the H atoms of the polypeptide backbone can be identified and refined, as shown in **Figure 11**. In the case of Mb, we performed a positional refinement with loosened restraints for the planarity of the peptide plane: in other words, the O-C-N-H group was allowed to deviate from a planar trans-configuration. The result is that the O-C-N-H torsion angle showed deviations up to 15° from planarity with an average value equal to 179.2° and a standard deviation of 6.3° . These values are in good agreement with those from ultra-high-resolution X-ray structure determinations [24, 25].

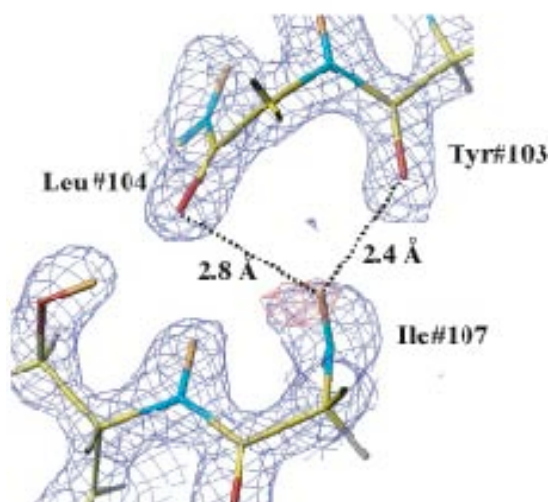


Figure 11. $2|F_o| - |F_c|$ nuclear density map (blue) contoured and $|F_o| - |F_c|$ omit nuclear density map (red). The amid hydrogen atom of residue 107 was omitted for the calculation of F_c for the omit-map.

4.5 Hydration

How a hydration molecule is observed experimentally. The hydration structure of Myoglobin has been studied by Schoenborn *et al* and the hydration layer structure such as radial distribution function of water around protein atoms have been obtained. [40-42] On the contrary, in our study the hydration structure of individual water molecules has been present [31]. **Figure 12** displays one region of the hydration structure around Mb, and shows that all of the hydration water molecules are complexly isolated. It is also remarkable that a sulfate group can be clearly distinguished in this map. In some cases, hydrogen (deuterium) atoms in water molecules can be clearly identified in triangular (boomerang) shaped peaks and the formation of the hydrogen bonds between two water molecules can be recognized as well. At the same time it is interesting to note that near the two triangular-shaped contours, a spherically shaped water molecule can be found. (**Figure 12**). Moreover, water molecules with other shapes, such as ellipsoidal (stick-shaped) ones, have been found in other places. The interpretation of these shapes will be discussed in the following section

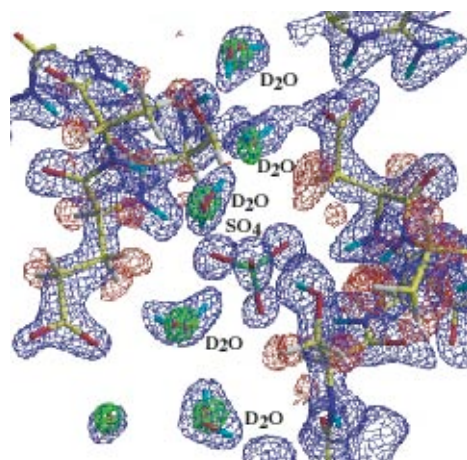


Figure 12. Protein-protein contact region in the case of myoglobin. $2|F_o|-|F_c|$ nuclear density map contoured at positive in blue and negative in red. The $2|F_o|-|F_c|$ X-ray electron density map for the water molecules is shown in green. The triangular shaped neutron contours correspond to D_2O molecules.

Classification of hydration. We have categorized observed water molecules into the following classes based on their appearance in Fourier maps: (i) triangular shape, (ii) ellipsoidal stick shape, and (iii) spherical shape, and moreover the second category, ellipsoidal stick shapes can be further sub-classified as (iia) short and (iib) long. We found that this classification conveniently reflects the degree of disorder and/or dynamic behavior of a water molecule. A typical example of the (i) triangular shape is shown in **Figure 13(a)**-1,2, in which the green and red contours indicate $2|F_o|-|F_c|$ maps calculated from neutron and X-ray data, respectively. The oxygen positions observed by X-ray and neutron scattering coincide within experimental error. In this case, the two deuterium atoms and the oxygen atom of the water molecule are H-bonded to nearby (O/N) and deuterium atoms, respectively. Thus, it can be seen that the orientation of this water molecule is well-defined. In fact, triangular shaped contours correspond to the most highly-ordered water molecules in our maps. A typical example of (iia) a short ellipsoidal stick shape is shown in **Figure 13(b)**-1,2. The oxygen position observed by X-rays is located at one end of the neutron Fourier peak, and only one deuterium atom could be observed. The observed D and O atoms are H-bonded to neighboring O/N and D atoms respectively, but the other deuterium atom was not identified because of the molecular rotation (or packing disorder) around the fixed O-D bond. Thus, we interpret short ellipsoidal stick shaped peaks to represent water molecules rotationally disordered around an O-D bond. A typical example of the (iib) long ellipsoidal stick-shaped peak is shown in **Figure 13(c)**. The O position observed by X-rays (but not by neutrons) is located in the middle of the neutron Fourier peak, and the two D atoms are clearly observed in the neutron map. The entire appearance is that of an elongated stick. In this case, the two D atoms are H-bonded to neighboring O and/or N atoms, but the O atoms of the D_2O molecule cannot be identified because of the molecular rotation or packing disorder around the D-D axis. Finally, a typical example of (iii) the spherical-shaped peak is shown in **Figure 13(d)**-1,2. Only the center of gravity of this type of water molecule can be defined because its orientation is totally disordered. A spherical peak in a neutron Fourier map always means that the whole water molecule is freely rotating, even if X-ray results (which only show the O atom) reveal no hint of this disorder.

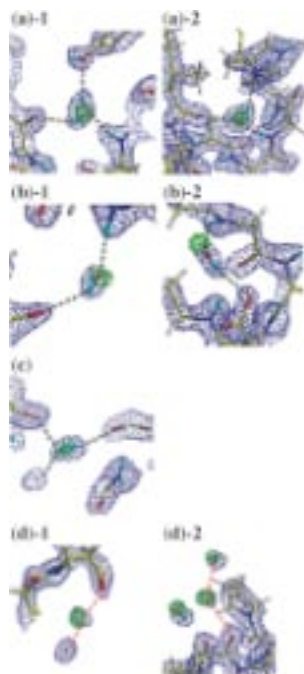


Figure 13. $2|F_o| - |F_c|$ nuclear density maps of water molecules of hydration for myoglobin and the rubredoxin mutant observed by neutron protein crystallography. Examples shown are those of those of: (a) triangular shape, (b) short ellipsoidal shape, (c) long ellipsoidal shape and (d) spherical shape. In these maps, the blue contours correspond to neutron peaks, while the green contours correspond to oxygen peaks from X-ray data. Observed (located) atoms from the neutron data are shown as stick diagrams, with the following color coding scheme: C (yellow), N (dark blue/violet), O (red), D (light blue/cyan), H (white). Note that in Figure 13(a) all atoms of the central D_2O molecule are visible (cyan/red/cyan), whereas in the other diagrams only some of the solvent atoms have been located: O, D (Figure 13(b)), two D (Figure 13(c)) and O only (Figure 13(d)).

Although the above classification has been carried out based on the appearance of peaks in Fourier maps, we found that the shapes are strongly correlated with the existence of hydrogen bonds, which fix the positions of atoms of water molecules. Most of the triangular-shaped water molecules are fixed at three atoms (D, O, D), while ellipsoidal ones are fixed at two atoms (D, D or D, O). In contrast, some spherical shaped water molecules are not fixed by any observed H-bonds. The average number of “anchor points” of triangular, ellipsoidal and spherical-shaped water molecules are 2.3, 1.3 and 0.3, respectively. In the three proteins, Mb, Rb-w and Rb-m, the average populations of triangular, ellipsoidal and spherical shapes are 29 %, 16 % and 55 %, respectively [30].

Dynamic behavior of hydration The dynamic behavior of water molecules becomes clearer when the B -factors obtained by neutron and X-ray are plotted against each other as shown in **Figure 14**, in which the B -factors obtained from the neutron analysis are the averaged values from three atoms (D, O and D), while those from the X-ray analysis are those of the O atoms only. The B -factors of oxygen atoms obtained by X-rays are in the range from 13 \AA^2 to 45 \AA^2 . It is observed that the small, intermediate and large B -factors from the X-ray analysis correspond to water molecules having the triangular, ellipsoidal and spherical shapes, respectively. The spherical peak in the neutron Fourier map always means that the whole water molecule is freely rotating, even though the X-ray results (which show only the O atom) reveal no hint of this disorder.

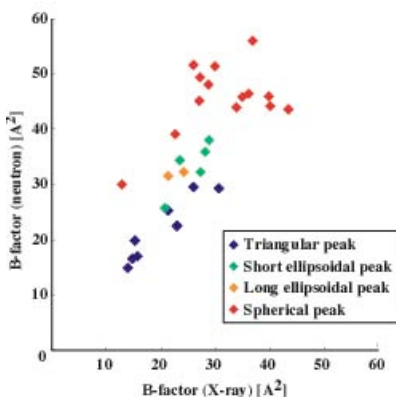


Figure 14. Correlation between the B -factors of hydration water molecules obtained from neutron and X-ray scattering data for the rubredoxin mutant. Neutron B -factors were obtained using the average scattering lengths of D, O and D atoms from every water molecule, regardless of shape; while in the case of X-ray B -factors, only those from O atoms were included.

5. CRYSTALLIZATION

One fundamental problem in neutron crystallography is the difficulty in obtaining large single crystals. It is really true that neutron protein crystallography necessitates the use of large protein crystals, the volume of which should be larger than 1 mm^3 currently. Usually such a large single crystal is difficult to grow. However, we have found that one rational way to find the proper conditions to grow large single crystals is to establish the complete crystallization phase diagram, which includes determining the solubility curve [38]. Generally speaking, a large single crystal can be grown under supersaturated conditions close to the solubility boundary. As a matter of fact, the large single crystals of cubic porcine insulin, human lysozyme and a DNA oligomer that we have used in our studies have been grown using this method. The phase diagrams of the DNA oligomer [38] and cubic porcine insulin [20] which have been determined by our group are shown in **Figure 15 (a),(b)**. The corresponding crystals which are obtained on the basis of these phase diagrams are shown in **Figure 16 (a),(b)**, respectively. This method is applicable not only to grow large single crystals which are large, but also crystals of a high quality, which is essential for high resolution crystallographic studies.

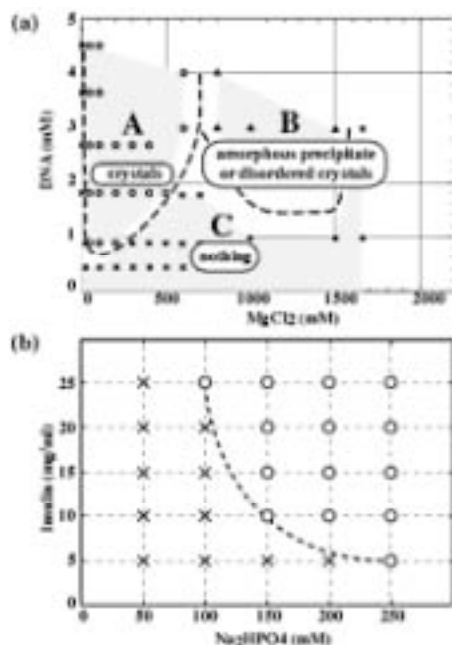


Figure 15. The experimentally determined phase diagram. (a) The solubility of the DNA decamer d(CCATTAATGG) vs MgCl_2 concentration. The broken lines show the boundary between regions: a circle, a triangle and a cross in the phase diagram correspond to the presence of crystals, amorphous precipitate and clear solutions (i.e., no crystals), respectively. Solutions were kept in an incubator at 6°C for 20 days with an MPD concentration of 30 % (v/v) and pH of 7.0 (buffer solution of 0.1 M sodium cacodylate). (b) The solubility of the cubic porcine insulin vs Na_2HPO_4 concentration. A circle and a cross mean the presence and absence of cubic porcine insulin crystals in the crystallization. Solutions were kept in an incubator at 25°C for 7 days with 0.01M $\text{Na}_3\text{-EDTA}$ buffer solution.

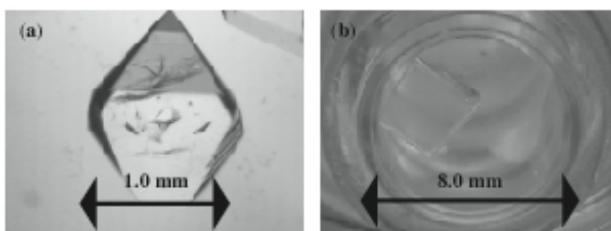


Figure 16. The large crystals of the DNA decamer (a) and cubic procine insulin (b) obtained on the basis of the phase diagrams in Figures 17 (a) and 17(b), respectively.

6. HYDROGEN DATA BASE

The construction of data base of 'hydrogen and hydration in proteins' is now under way. The positional coordinates of all the hydrogen atoms and hydration water molecules determined by neutron protein crystallography are stored according to the usual PDB format. The main function of the hydrogen hydration data base (HHDB) is to extract the structural information relevant to hydrogen atoms, such as stereochemical atomic configuration in the vicinity of a selected hydrogen atom, the search of all the H-bonds between main chains, the main chain and the side chain, and side chains and the statistical classification of H-bonds. During the analysis of H-bonds by the use of HHDB, very unfamiliar types of H-bonds have been discovered as shown in **Figure 17**. **Figure 17(a)** shows that the nitrogen atom of amide (Lys 78) in main chain is an acceptor of H atoms of the neighbor amide (Lys 79) (the H bond length H---N is 2.18Å, and **Figure 17(b)** shows that the H-bond is formed between the amide (Lys 2) N-H and O=C in Lys 2 (the H-bond length H---O is 2.50Å).

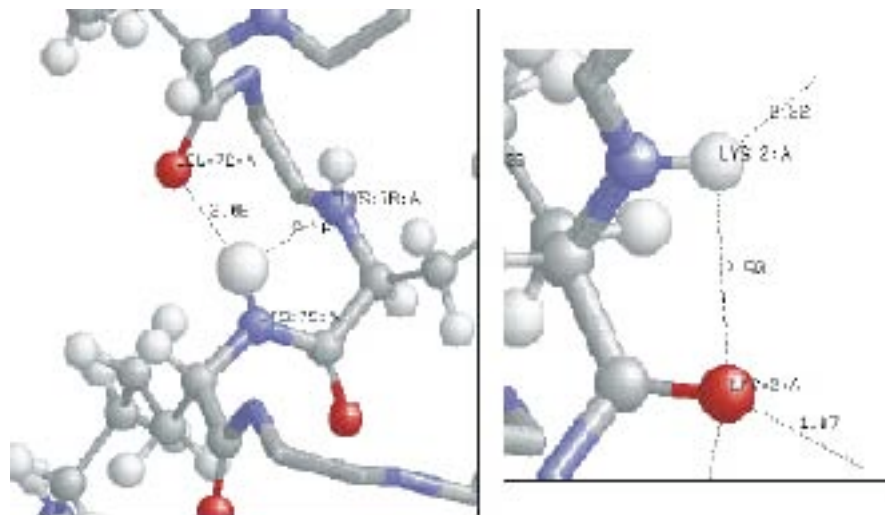


Figure 17. Very unfamiliar types of H-bonds of (a) myoglobin and (b) Rb-m.

7. FUTURE PROSPECT

The neutron protein crystallography experiment is now still time-consuming experiment. For example, when a single crystal of 1mm^3 in volume, the unit cell of the lattice of which is less than 100\AA , is available, it takes 3 or 4 weeks to collect 1.5\AA resolution data set at present. If the neutron intensity at the sample position increases 100 times higher than now, the above mentioned restriction (the size of a single crystal, unit cell size of the lattice constant, and the data collection time) of the neutron protein crystallography becomes looser.

J-PARC project in Japan (1MW spallation neutron source) and SNS in USA (2MW neutron source), which are now under construction, meet the above requirement. In J-PARC project, the construction of the neutron diffractometer for protein crystallography (so called BIX-P1) is scheduled, where the neutron intensity at the sample position becomes 50-100 times higher than the current BIX-type diffractometer.

8. CONCLUSION

Several conclusions are summarized as follows:

1. The presence of positional information of H atoms provides detailed discussions of hydrogen bonds, such as bifurcated H-bonds and strong and weak H-bonds.
2. The protonation and deprotonation states of the two nitrogen atoms in the imidazole ring of histidine are clearly presented.
3. Hydrogen atom positions, which cannot be predicted stereochemically, can be given.
4. The hydration structures are categorized based on their appearance in Fourier maps, and these reflect the dynamic behavior of water molecules.
5. The role of hydrogen atoms in enzyme function and thermostability is exemplified by hen egg-white lysozyme and rubredoxin, respectively.

9. ACKNOWLEDGMENT

This study is carried out as a part of a “Development of New Structural Biology Including Hydrogen and Hydration” Project, funded by the Organized Research Combination System (ORCS) and promoted by the Ministry of Education, Culture, Sports, Science and Technology of Japan.

10. REFERENCES

- [1] N. Niimura, Y. Karasawa, I. Tanaka, J. Miyahara, K. Takahashi, H. Saito, S. Koizumi and M. Hidaka, *Nucl. Instrum. Methods*. **A349** (1994), 521-525.
- [2] Y.K. Haga, S. Kumazawa and N. Niimura, *J. Appl. Cryst.* **32** (1999), 878-882.
- [3] Y.K. Haga, K. Neriishi, K. Takahashi and N. Niimura, *Nucl. Instrum. Methods Phys. Res.* **A487** (2002), 504-510.
- [4] N. Niimura, Y. Minezaki, T. Nonaka, J-C. Castanga, F. Cipriani, P. Hoghoj, M.S. Lehmann and Wilkinson, *Nat Struct Biol.* **4** (1997), 909-914.
- [5] N. Niimura, I. Tanaka, Y. Minezaki, Y. Karasawa, I. Tanaka, K. Miki, M. Sato, M. Hidaka, Minakawa and Y. Morii, *Physica* **B213-214** (1995), 786-789.
- [6] S. Fujiwara, Y. Karasawa, I. Tanaka, Y. Minezaki, Y. Yonezawa and N. Niimura, *Physica* **B241-243** (1998), 207-209.
- [7] I. Tanaka, K. Kurihara, T. Chatake, and N. Niimura, *J. Appl. Cryst.* **35** (2002), 34-40.
- [8] I. Tanaka, K. Kurihara, Y. Haga, Y. Minezaki, S. Fujiwara, S. Kumazawa, and N. Niimura, *J. Phys. & Chem. Solids* **60** (1999), 1623-1626.
- [9] N. Niimura, *Curr. Opin. Struct. Biol.* **9** (1999), 602-608.
- [10] J. R. Helliwell, *Nat Struct Biol.* **4** (1997), 874-876.
- [11] N. V. Raghavan and A. Woldawer, *Methods Exp. Phys., Part C* **23** (1987), 335-365.
- [12] B.P. Schoenborn, *Methods Enzymol.* **114** (1985), 510-529
- [13] A.A. Kossiakoff, *Annu. Rev. Biochem.* **54** (1985), 1195-1227.
- [14] I. Tsyba, and R. Bau, *Chemtracts.* **15** (2002), 233-257
- [15] N. Niimura, T. Chatake, A. Ostermann, K. Kurihara, and I. Tanaka, *Z. Kristallogr.* **218** (2003), 96-107.
- [16] A. Ostermann, I. Tanaka, N. Engler, N. Niimura and F.E. Parak, *Biohpys. Chem.* **95** (2002), 183-193.
- [17] K. Kurihara, I. Tanaka, M.W.W. Adams, F.E. Jenney Jr., N. Moiseeva, R. Bau and N. Niimura, *J. Phys. Soc. Jpn. Suppl. A*, **70** (2001), 400-402.
- [18] T. Chatake, K. Kurihara, I. Tanaka, M.W.W. Adams, F.E. Jenney Jr., I. Tsyba, R. Bau and N. Niimura,

- Applied Physics* **A75** (2002), 1-3
- [19] M. Maeda, S. Fujiwara, Y. Yonezawa and N. Niimura, *J. Phys. Soc. Jpn. Suppl. A*, **70** (2001), 403-405
- [20] M. Maeda, T. Chatake, A. Ostermann, I. Tanaka and N. Niimura, To be submitted.
- [21] E.N. Baker, and R.E. Hubbard, *Prog. Biophys. molec. Biol.* **44** (1984), 97-179.
- [22] G.R. Desiraju, and T. Steiner, *The weak hydrogen bond* (Oxford University Press, N.Y., 1999)
- [23] R. Preissner, U. Egner and W. Saenger, *FEBS letters* **288** (1991), 192-196
- [24] S. Longhi, M. Czjzek, V. Lamzin, A. Nicolas and C. Cambillau, *J. Mol. Biol.* **268** (1997), 779-799.
- [25] T. Sandalova, G. Schneider, H. Kack and Y. Lindqvist, *Acta Crystallogr.* **D55** (1999), 610-624.
- [26] K. Chiba-Kamosida, T. Matsui, I. Tanaka and N. Niimura, to be submitted.
- [27] P.R. Blake, J.B. Park, Z.H. Zhou, D.R. Hare, M.W.W. Adams and M.F. Summers, *Protein Sci.* **1** (1992), 508-21.
- [28] P.R. Blake, M.W. Day, B.T. Hsu, L. Joshua-Tor, J.B. Park, D.R. Hare, M.W. Adams, D.C. Rees and M.F. Summers, *Protein Sci.* **1** (1992), 1522-1525.
- [29] H. Matsuo, M. Oe, F. Sakiyama and K. Narita, *J. Biochem.* **72** (1972), 1057-1060.
- [30] C. Bon, M.S. Lehmann and C. Wilkinson, *Acta Crystallogr.* **D55** (1999), 978-987.
- [31] T. Chatake, A. Ostermann, K. Kurihara, F.G. Parak and N. Niimura, *Proteins*, to be published.
- [32] D.C., Phillips, *Sci. Am.* **215** (1966), 75-80.
- [33] G. Fiala and K.O. Arch. Stetter, *Microbiol.* **145** (1986), 56-61.
- [34] I. Mathieu, J. Meyer and J.M. Moulis, *Biochem. J.* **285** (1992), 255-262
- [35] P.R. Blake, J.B. Park, F.O. Bryant, S. Aono, J. K. Magnuson, E. Eccleston, J. B. Howard, M.F. Summers and M.W.W. Adams, *Biochemistry* **30** (1991), 10885-10895.
- [36] R. Bau, D.C. Rees, D.M. Kurtz, R.A. Scott, H.S. Huang, M.W.W. Adams and M. K. Eidsness, *J. Biol. Inorg. Chem* **3** (1998), 484-493.
- [37] Z. Dauter, K. S. Wilson, L.39C. Sieker, J. M. Moulis and J. Meyer, *Proc. Natl. Acad. Sci U. S. A.* **93** (1996), 8836-8840
- [38] S. Arai, , T. Chatake, , Y. Minezaki and N. Niimura, *Acta Cryst.* **D58** (2002), 151-153
- [39] Mason, Sax, Bentley, A. Graham and Garry J. McIntyre, *DeuteriumExchangein Lysozyme at 1.4A resolution. Neutrons in Biology*, (Plenum Press, New York and London, 1984), p323-334
- [40] W. Gu and B.P. Schoenborn, *Proteins* **22** (1995), 20-26
- [41] W. Gu, A.E. Garcia and B.P. Schoenborn, *Basic Life Science* **64** (1996), 289-298.
- [42] B.V. Daniels, B.P. Schoenborn and Z.R. Korszun, *Basic Life Science* **64** (1996), 325-331
- [+1] K. Kurihar, I. Tanaka, M.R. Muslih, A. Ostermann and N. Niimura, *J. Sync.* (2003) To be published.

Development of Neutron Structural Biology at BNL and LANL

Benno P Schoenborn

Biosciences Division, Los Alamos National Laboratory

PO Box 1663, Los Alamos NM 87545 USA

1. ABSTRACT

In the nearly 35 years since the first neutron diffraction data were measured from crystals of myoglobin, the field has been characterized by intermittent activity. Despite the uncertainties of instrumentation, many unscheduled lengthy reactor downtimes, as well as the constraints of crystal size and low flux, fundamental discoveries about enzyme mechanisms, biological complex structures, protein hydration and hydrogen atom position have been, and continue to be made using neutron diffraction. The promise of neutrons has not changed since the first crystal diffraction data were collected. Today, with the developments of beam lines at spallation neutron sources, increasingly sensitive detectors, and the use of the Laue method for data collection, the field of neutrons in structural biology has renewed vitality. The history and recent developments in this field at BNL and LANL will be described.

2. INTRODUCTION

The first mention of using neutron scattering to investigate hydrogen (H) bonding in proteins was made during a tea time discussion with H. Watson, U. Arndt, J. Kendrew, C. Nobbs and B. Schoenborn at the MRC Laboratory in Cambridge England in the spring of 1965. I had just finished the binding study of Xe to myoglobin (Mb) and was trying to calculate the binding energies. There were 32 atoms in van der Waals bonding distance to Xe and most were H atoms. The location of H atoms was based on structural assumptions and was only approximate, and clearly a map depicting actual H atom location was needed. We discussed a number of options but only neutron diffraction was a distant possibility. Discussions with neutron scattering experts at the Atomic Energy Research Establishment (Harwell, UK) were rather disappointing and I shelved the idea for the time being. During a seminar on the binding of the anaesthetic Xe to proteins at the Biochemistry Department in Berkeley, I mentioned the neutron approach and Prof. Koshland suggested I try to obtain some beam time on the High Flux Beam Reactor (HFBR) at the Brookhaven National Laboratory (Upton, USA). On Koshland's recommendation and with W. Hirs' help I obtained a position at BNL and took another leave of absence from UCSF on what many considered a wild goose chase. I learned very quickly that big crystals were needed which was fortunately quite easy for sperm whale Mb.

In mid 1968 I obtained a few days of beam time at Walter Hamilton's single crystal diffractometer. It was a monochromatic four circle instrument with a single detector with one of the first computer controlled systems made by BNL using a Scientific Data Systems (SDS) computer. After a few hours of playing with the automation we found the first reflection (**Figure 1**), which turned out to be the 6-0-3. The crystal was soaked in D₂O to reduce background scattering from the incoherent H atom scatter. Even with the large 25 cubic mm crystal with a ω -2 θ step scan of 0.1 degree, with a 2 degree reflection scan width, and with a step time of 1 minute it would take an enormous amount of time to collect even a 2.8Å map. Over the next year I was able to collect however 4800 reflections and produced a Fourier map that demonstrated that neutron protein crystallography was indeed possible and that H atom locations can be determined easily with a 2Å resolution map [1].

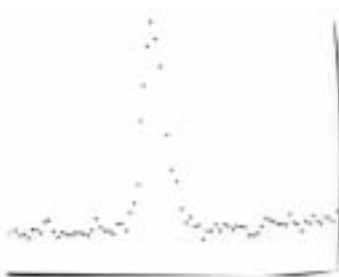


Figure 1. The first reflection (6-0-3) collected from a single crystal of myoglobin using a single crystal diffractometer on the High Flux Beam Reactor (HFBR) at the Brookhaven National Laboratory (BNL). The vertical axis is the scattered intensity and the horizontal axis is the scanning angle.

Max Perutz (**Figure 2**) was also interested in neutron maps to decipher the structures of deoxy- and oxy-hemoglobins in order to elucidate the structural basis of the large observed transition mechanism. Unfortunately those two hemoglobin derivatives in crystal form did not last long enough for the lengthy neutron data collection and even with the large crystals provided, we were not able to collect enough data to provide sufficiently accurate H/D information.

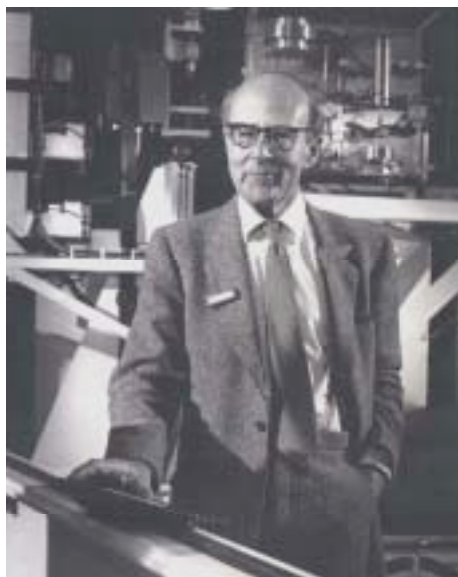


Figure 2. Max Perutz at the Brookhaven National Laboratory (BNL).

3. EXPANDING THE USE OF NEUTRONS IN STRUCTURAL BIOLOGY

It was soon realized that the different scattering length of D(+6.65) and H(-3.71) can be beneficially used to enhance contrast and even used like a heavy atom, at least for low resolution structures. The first experiment using H vs D was done on frog sciatic nerves in collaboration with D. Casper. After soaking the excised nerve in D₂O and mounting it we observed a very large peak of about 80% of the collimated incident beam. At first we looked for a leak in the shielding and collimation since we were working very close to the incident beam. We found nothing wrong and eventually we realized that we were observing a very intense 2-0-0 reflection. This was due to the membrane bilayer structure that approximated a positive scattering layer (D₂O) next to a negative scattering layer (nCH₂) of about equal thickness. This led to the development of multilayer monochromators [2,3,4,5] (Patent) now widely used.

The use of H₂O/D₂O exchange and specific deuteration were soon used by a number of scientists to elucidate membrane structures [6,7,8,9,10,11,12]. The low angle scattering analysis technique using H/D exchange was soon used to look at a number of large biological structures [13,14,15,16,17], and also used to study the structure of filamentous bacteria oriented in an 8 Tesla magnetic field [20]. A novel use of H/D exchange was proposed and pursued by Engelman and Moore to elucidate the structure of ribosomes [18,19].

The development of a dedicated small angle neutron scattering (SANS) station (**Figure 3**) for structural biology on the HFBR at BNL (Figure 4) improved the availability of neutrons for structural biology research in the US [21]. With the completion of the cold source, the utility of that instrument was greatly enhanced. The SANS instrument was soon followed by the establishment of a dedicated protein crystallography station, and a small angle diffraction station primarily for the study of membranes and fibers. Some of these developments were transferred by John Norvell from BNL to the National Institute of Standards and Technology (NIST) and were subsequently further developed by Alexander Wlodawer and provided the foundation of their present effort in small angle scattering and membrane diffraction.



Figure 3. The Small Angle Neutron Scattering (SANS) instrument H9B on the High Flux Beam Reactor (HFBR) at the Brookhaven National Laboratory (BNL).

Many of the early developments in structural biology using neutron scattering were presented at a Brookhaven Symposium on Neutrons in Biology in 1975 [22]. This symposium was held at the time when the new reactor at the Institute Laue-Langevin (ILL) (Grenoble) started to have an impact. The sophisticated instruments, such as the SANS instrument D11 located on a cold source, immediately generated superb data that enabled the analysis of chromatin [23,24], and protein complexes [25,26]. The development of structural biology at the ILL was due in part to the establishment of the EMBL outstation by Sir John Kendrew under the able scientific leadership of Andrew Miller.

With BNL and ILL as two major centers of activity, the world-wide interest in neutrons and structural biology grew substantially and many of the highlights were presented at the second Neutrons in Biology Conference held in 1981 [27].



Figure 4. High Flux Beam Reactor (HFBR) at the Brookhaven National Laboratory (BNL).

3.1 Neutron Protein Crystallography

Although we used high resolution neutron diffraction to reveal H atom positions (both on the protein and the solvent) [28] and, because of different scattering interactions, we were also able to distinguish nitrogen from carbon or oxygen. This was used to resolve ambiguities in X-ray crystallographic studies particularly the orientation of histidines, for example. To reduce background scattering during data collection and enhance the localization of exchangeable H atoms, we exchanged the H₂O solvent in most single crystals with D₂O. This led us immediately to the realization that H₂O/D₂O exchange could (i) provide some information on protein dynamics, and (ii) enhance protein/solvent contrast in diffraction and small angle neutron scattering (SANS) experiments.

Data collection from protein single crystals had a slow start and only with the development of 2D position sensitive detectors were we able to collect sufficient data to look at least a few macromolecules [29,30,31,32,33,34,35]. To enable us to obtain good peak integration we had to develop new tools to extract the often weak peaks from background [36]. A first step in data analysis was the correction of detector counting rate variations due to imperfection in the back plane and wire thickness as well as the radial decrease of the anode potential. This was achieved by a look-up table created through a uniform illumination of the detector. To obtain good peak to background ratios particularly for the weak reflections, the reflection integration scheme used involved the pre-calculation of peak shapes from the known diffraction parameters $\Delta\lambda$, crystal mosaic, detector resolution and diffraction angle [36]. These pre-calculated peak shapes were then refined using strong observed reflections and were then used as masks to extract the reflections and delineate background (Figure 5). A 3 or 5 element filter system developed by Kossiakoff, was used to scan the 2D detector array and was effective in finding large peaks for crystal orientation and unit cell parameter refinement. Unfortunately however, this technique often overestimated weak reflections by picking uneven features in the background. Promising trial data integration runs using a modified version of MADNESS for data integration took place just before the permanent shutdown of the HFBR.

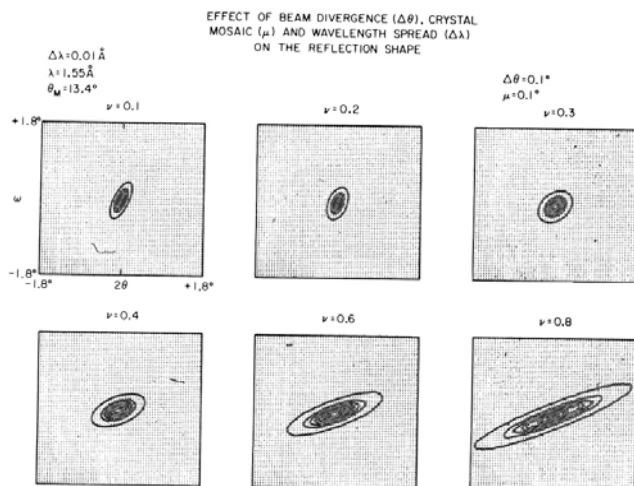


Figure 5. The effect of neutron beam divergence, crystal mosaicity, and wavelength spread on the shape of a reflection.

Protein refinement started with known phases from X-ray studies and used classical refinement approaches like real space techniques [32,38] that were later supplanted by rigorous least squares programs like PROLSQ; and molecular graphics programs like 'O'. The use of D₂O solvent with an hydrogenous protein requires special treatment of the solvent structure if accurate surface water molecules are to be determined. Another improvement in neutron structure refinement involved the better determination of restraints for H and D bonds [39].

The detailed analysis of water in Mb solved a long-standing controversy between magnetic resonance studies that observed only a few bound water molecules and X-ray structures that found close to 100 bound water molecules [40]. The neutron map clearly showed that only three water molecules were bound by three D bonds and therefore were irrotationally bound to Mb and only those water molecules would show up in a magnetic resonance studies. All the other water molecules have some freedom to tumble and exchange with the O atom more or less in the same location as observable in X-ray and neutron maps. The neutron maps clearly depicted water molecules with three, two and one D bonds. Such water bonding was further confirmed by molecular dynamics calculation [41].

The many H atoms covalently bound to carbon atoms in proteins contribute significantly to background scattering even

for crystals soaked in D₂O mother liquor. Complete per deuteration of a protein would greatly improve the peak to background ratio (**Figure 6**) and subsequently produce more accurate structures as demonstrated by a study of per deuterated Mb [42,43].

These developments have been rewarded with a number of crystallographic studies of macromolecules including myoglobin [31,32,44], trypsin [45,46,47], crambin [48,49] and later with cyclosporin [34,50], plastocyanin [51], concanavalin [Gilboa & Yariv, unpublished] and fatty acid binding protein [Sacchetini & Scapin, unpublished].

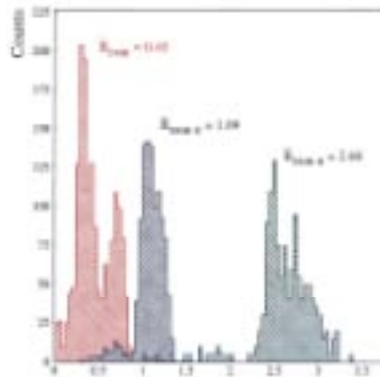


Figure 6. Background comparison of perdeuterated (B average = .45); soaked (B average = 1.09); and H Myoglobin (B average = 2.6); the horizontal axis is the background count and the vertical axis the number of reflections

Protein dynamics. Proteins are not static objects and any description of structure incorporates some element of dynamics. The structure determined by X-ray diffraction techniques will include the thermal motion (and possible disorder) of the individual non-hydrogen atoms, and a neutron diffraction analysis will provide similar information with additional data on the H atoms. Depending on the resolution of the data, the thermal motion of H atoms will be included in the refinement.

For trypsin this information was used to resolve an uncertainty on the rotation of terminal methyl groups. Spectroscopic studies had established that methyl groups exhibit rapid rotation but provided little information on preferred orientations. It was found from a high resolution neutron diffraction structure that 85% of the ordered methyl groups were within 20 degrees of the staggered conformation. This suggested that their rotation is quantised in 120 degree steps about a position of highest stability [52].

Dynamics in other time domains are explored by the distribution of exchanged H atoms throughout the protein structure. This distribution is a result of the exchange mechanism(s) on a scale dictated by the solvent-exchange time (from weeks to years). Clearly solvent accessibility plays a dominant role in the mechanism. For example, the amide H atoms located on exposed turns of alpha-helical segments are readily exchanged [53], however, access to some H atoms involve cooperative motions including local breathing and global unfolding [45,54].

Protein solvent structure. The layers of solvent that surrounded a protein molecule mediate its functional conformation as well as its biochemical characteristics. We obtained useful information on this interface region from high resolution neutron diffraction studies since water constitutes approximately 40-60% of the volume in typical protein crystals. Water molecules that are H/D bonded to the protein surface can be directly visualized as integral components of the structure [31,48,55,56]. Of course the oxygen atoms of well ordered water molecules are assigned in X-ray structures.

The localization of water molecules is usually correlated with the surface characteristics of the protein. Ordered water molecules have been located in hydrophilic regions, and small water clusters have been observed quasi-randomly distributed over the protein surface. We developed a formalism that modeled the solvent as a series of shells with spatial and physical characteristics [57,58,59]. Progressing outward from the protein surface, each shell was constructed of pseudoatoms arranged on a three-dimensional grid. Each pseudoatom was assigned coordinates and a global factor that represented the degree of order (or liquidity) within the shell. The solvent density was then refined by a minimization technique comparing observed low angle reflections with the calculated density. This resulted in a best solvent density and a smearing (temperature) factor B (**Figure 7**). This approach greatly improved subsequent least squares calculations. Such calculations clearly showed the higher water density close to polar groups compared to non polar regions. It has been shown in studies of myoglobins and plastocyanin that such a solvent refinement enhances surface characteristics

and even adjusts side chain locations. It was subsequently shown that such an approach is equally valid for X-ray data refinement [60,61].

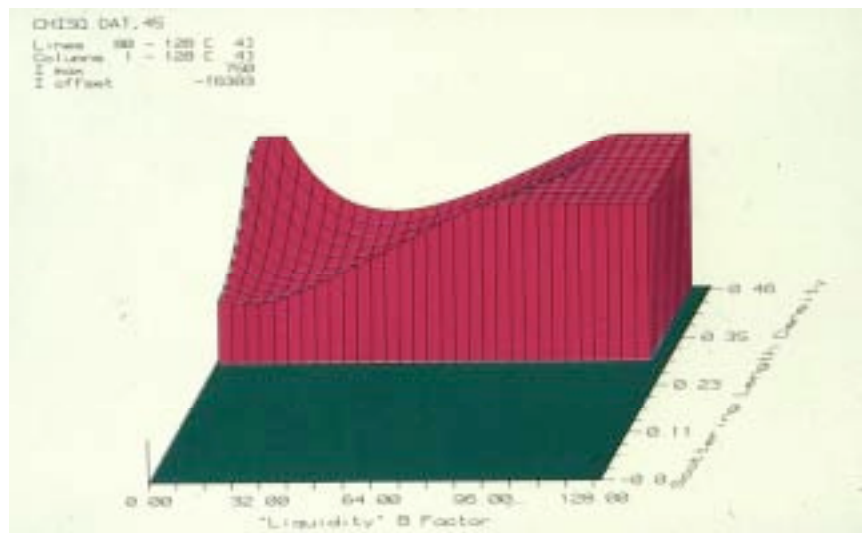


Figure 7. Graphical representation of the scattering length density and liquidity factor for a myoglobin crystal in a 40% D₂O solvent.

The refined solvent structure reveals a wealth of chemical information about the molecule, including the geometry of H bonding, states of protonation of histidines (**Figure 8**), and the location and geometry of water molecules at the surface of the protein (**Figure 9**). An X-ray and a neutron data set of a carbon-monoxymyoglobin crystal were used for such solvent structure studies [43].

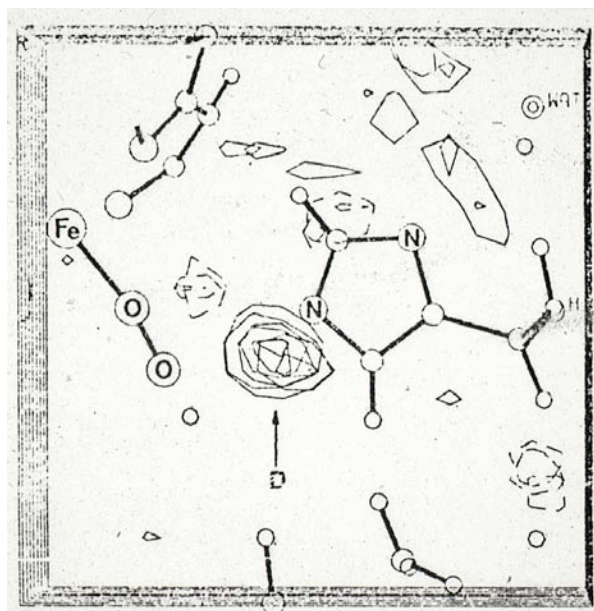


Figure 8. $|F_o| - |F_c|$ neutron difference map in a slab centered on the plane of the imidazole 7E ring in oxy-myoglobin. The refined model is superimposed, showing His 7E, FeO₂ and part of the heme. The strong positive peak indicates the presence of deuterium bonded to N_ε.

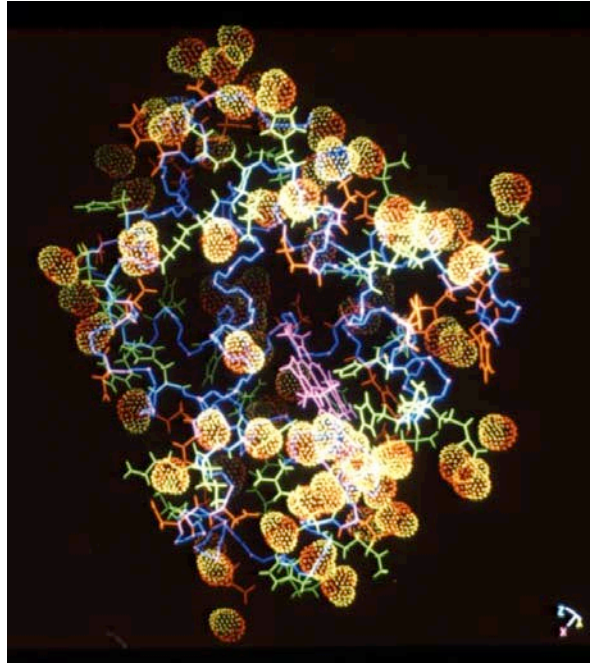


Figure 9. The myoglobin structure with water molecules as determined by neutron diffraction studies. Water is shown as dotted clouds on the surface of the protein.

Advantages of protein deuteration. Besides causing high background due to its incoherent scattering, the negative coherent scattering of H atoms tends to cancel out the positive contribution from other atoms in a neutron density map. Therefore a fully deuterated sample would yield better diffraction data with stronger density in the H atom positions. On this basis a sperm whale myoglobin gene modified to include part of the λ cII protein gene was cloned into the T7 expression system [42]. Milligram quantities of fully deuterated holo-Mb were obtained and used for crystallization. The synthetic sperm whale Mb crystallized in the $P2_1$ space group isomorphous with the native protein crystal. A complete X-ray diffraction dataset at 1.5\AA was collected first and followed by a 2\AA neutron diffraction analysis [43]. This analysis produced much better data and a vastly improved Fourier map compared to the hydrogenous Mb structure [43]. The decrease in background scattering alone makes it worthwhile to perdeuterate proteins for neutron diffraction studies (**Figure 10**).

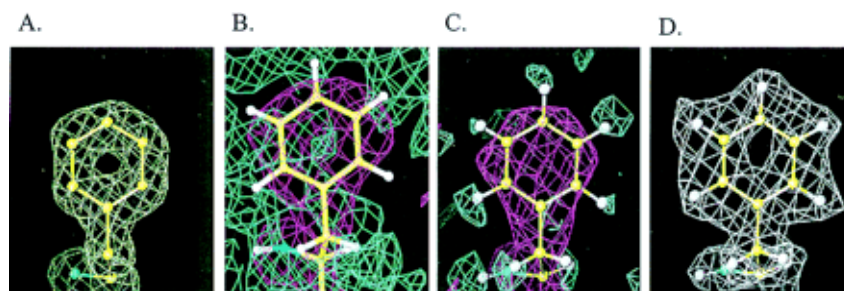


Figure 10. Deuterium (hydrogen) atoms can be located directly as positive peaks in $2F_o-F_c$ maps as illustrated by residue Phe-43 in oxymyoglobin. (A) The $2F_o-F_c$ X-ray map of fully deuterated Mb using 6.0 to 1.5\AA data, contoured at $+1.0\sigma$ ($0.84\text{ e}/\text{\AA}^3$). (B) A $2F_o-F_c$ neutron map on unlabeled Mb calculated to 2.0\AA resolution, with the pink map contoured at 1.0σ and the blue map contoured at -1.0σ . (C) An F_c neutron map generated by using equivalent experimental reflections in 6.0 to 2.0\AA calculated from the current protein model except that D was replaced with H. The pink map is contoured at $+1.0\sigma$, the blue map is contoured at 2.0σ . (D) The $2F_o-F_c$ neutron map of fully deuterated Mb using 6.0 to 2.0\AA data, contoured at $+1.0\sigma$ ($1.03\text{ fermi}/\text{\AA}^3$).

3.3 Small Angle Neutron Scattering

Early experiments with Mb and hemoglobin in solutions of various H₂O and D₂O mixtures showed that solvent contrast adjustment could be used to depict the hydration shell by analyzing the observed radii of gyration as a function of protein/solvent contrast (**Figure 11**). Stuhrmann [25,62] subsequently used these observations to develop the detailed analysis of proteins in solution resulting in the now commonly used Stuhrmann plot to analyze small angle scattering data. Such small angle solution scattering data were also frequently used to determine molecular weights using known proteins as calibration points [14] or using water to calibrate the intensity of the scattering curve [63]. These scattering analyses have led to a better understanding of the tertiary structure of proteins and protein complexes in solution, as well as the protein/solvent interface.

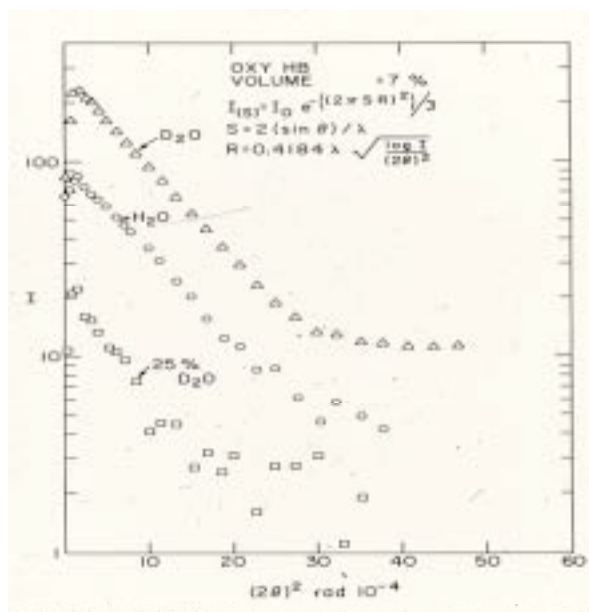


Figure 11. Intensity versus scattering angle for solutions of oxy-hemoglobin as a function of solvent contrast.

Engelman and Moore [64] proposed a notable extension of contrast enhancement in the analysis of large protein complexes (**Figure 12**). Incorporation of pairs of selectively deuterated proteins in the ribosome of *E. coli* caused the vector connecting the pair to make an enhanced contribution to the SANS pattern such that we could determine the length and orientation from measurements of ribosomes in solution (**Figure 13**). Selective deuteration of different pairs made it possible to build up sufficient spatial information that by triangulation the molecular arrangement in the ribosome could be determined. This ultimately led to the structural arrangement of the 21 proteins in the 30S subunit of the ribosome [19] (**Figure 14**) and the proteins in the 50S subunit [65] with data collected at the ILL. These were Herculean tasks that integrated specific deuteration of protein subunits with advanced neutron scattering techniques (**Figure 15**).

Another study of major significance is the continuation of the chromatin structure investigation – the complex between DNA and histones of chromosomes [67,68].

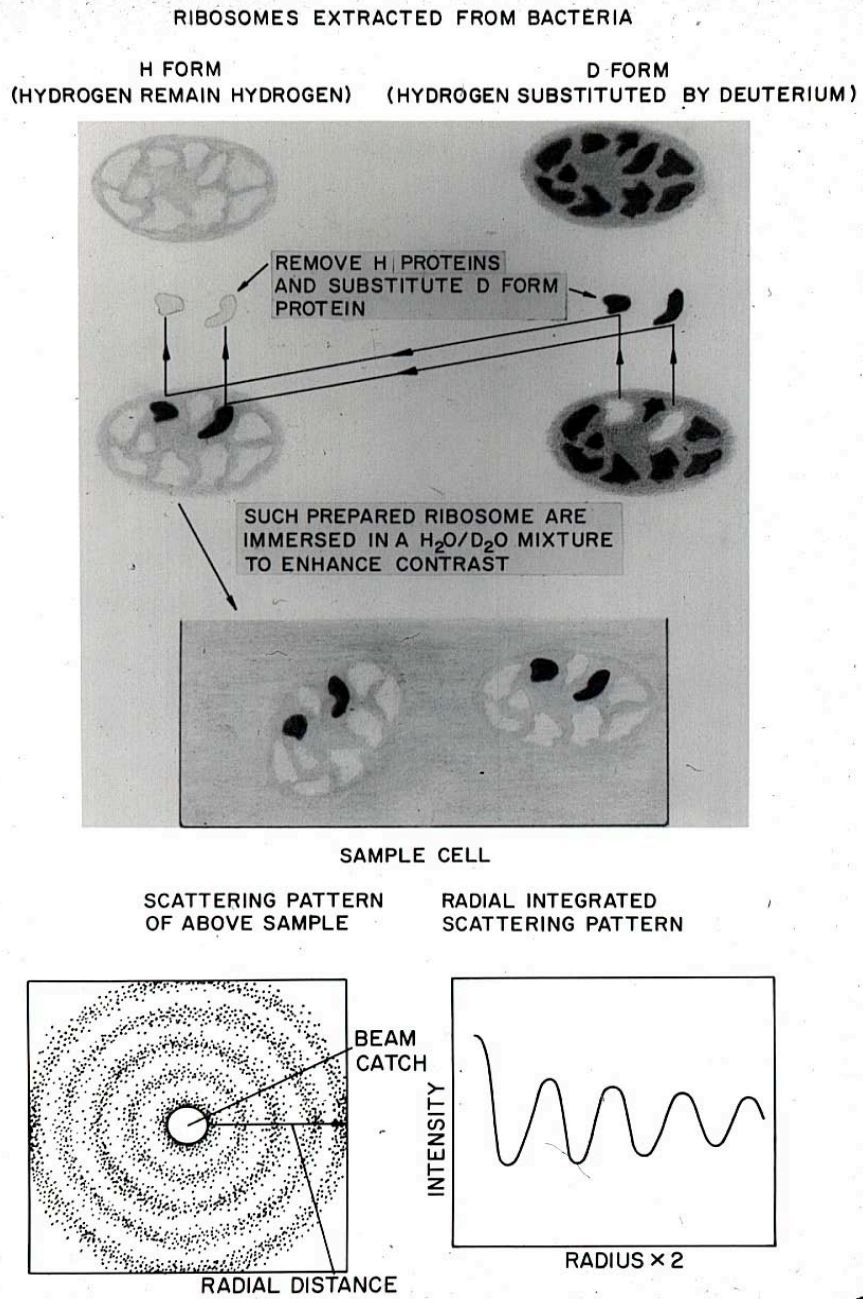


Figure 12. Outline of the strategy for determining the three dimensional arrangement of the proteins in the 30S ribosomal subunit of *E. coli*.

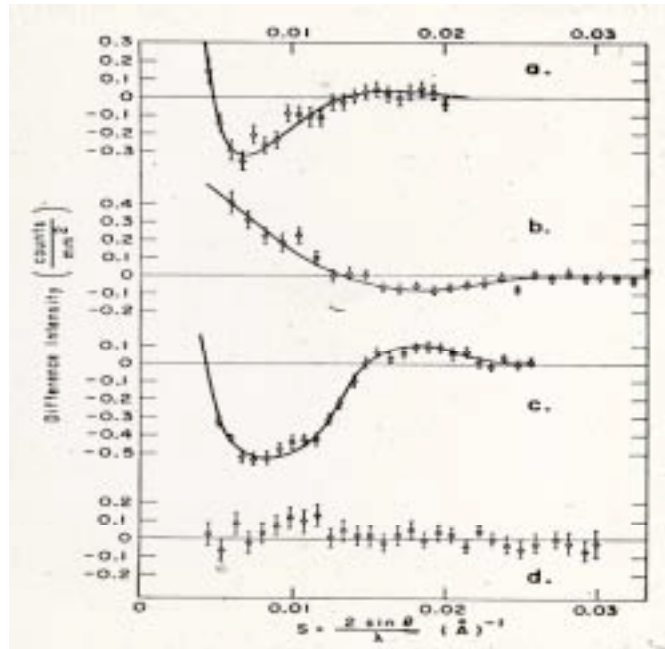


Figure 13. Protein-protein interference signals from the 30S ribosomal subunit of *E.coli*. Scattering profiles were determined on samples consisting either of equal parts of the doubly substituted and unsubstituted particles, or of equal parts of the two possible singly substituted preparations. These profiles were then subtracted from each other to give the difference curves in the figure. Four samples are shown.

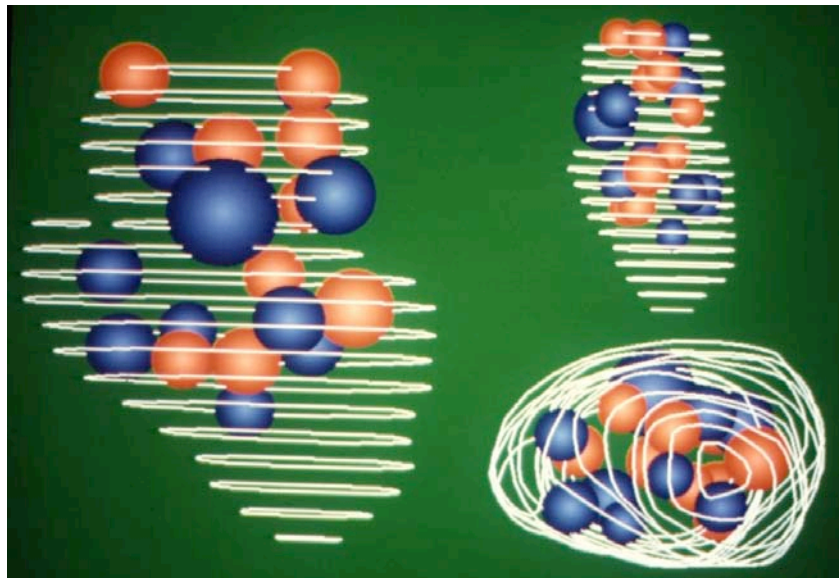


Figure 14. Three orthogonal views of the low resolution structure of the 30S ribosomal subunit of *E.coli*.



Figure 15. Don Engelman preparing an experiment on a makeshift 'small angle station', the detector is moved by a crowbar.

3.4 Membrane and Fiber Diffraction The concept of contrast enhancement was also employed to study membrane structures. Contrast enhancement, particularly specific deuteration, became a powerful tool in the one-dimensional diffraction analysis of membrane structures [6,7,69,70,71,72].

For example, the membrane-bound enzyme, Na/K-ATPase, regulates Na⁺ and K⁺ concentrations and energy metabolism, and was also implicated in regulation of the transport of H⁺, Ca⁺⁺, glucose, and amino acids, as well as being the receptor for the cardiac glycosides. The ultimate goal of this work was to determine the low resolution structure. The first step towards deriving significant structural information by way of diffraction experiments on membrane proteins in lipid bilayers was to develop a method for preparing oriented membrane multilayers that would diffract to about 1/10Å. Well ordered multilayers of Na/K-ATPase membrane sheets were prepared by ultracentrifugation, partial dehydration, followed by orientation in an intense (8 Tesla) magnetic field [73].

Contrast matching techniques also played a major role in the study of oriented but non-crystalline systems such as retinal rods (**Figure 16**) [9,70], lipid bilayers (Figure 17) [74,75,76], bacteriorhodopsin [8,77], and muscle [78,79].

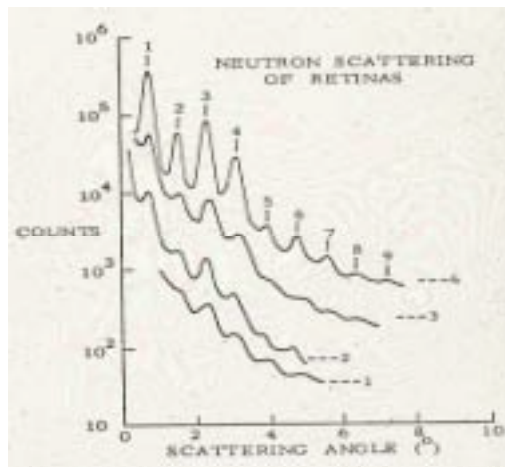


Figure 16. Neutron scattering profiles of intact retinas from *Rana catesbiana* frogs equilibrated in D₂O Ringer's solution. Patterns (1), (2) and (3) show successive enhancement of Bragg diffraction achieved by improvements in dissection technique, specimen stability, and sample cell design. Pattern (4) was obtained with only two retinas in the beam and a two-dimensional position sensitive detector.

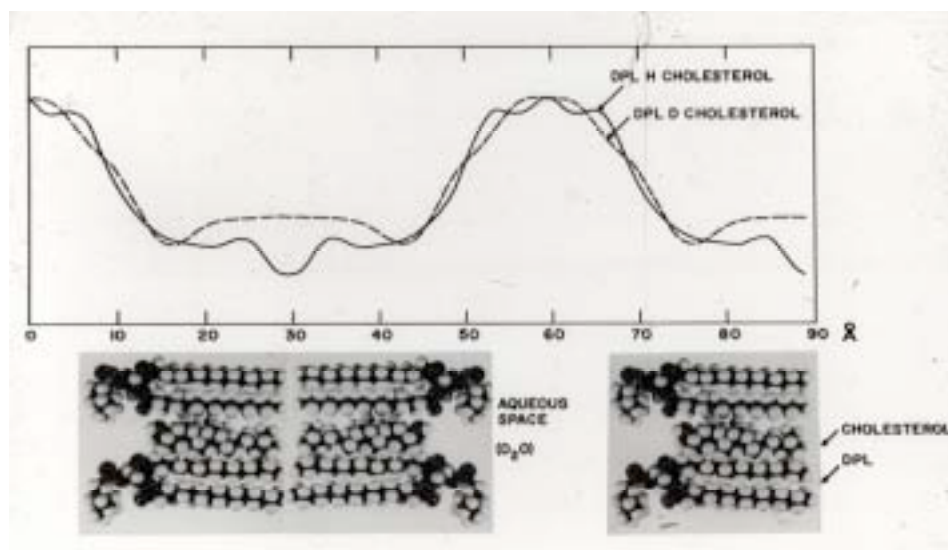


Figure 17. The measured neutron scattering density as a function of distance through reconstituted membranes of dipalmitoyl lecithin with and without cholesterol.

4. INSTRUMENTATION DEVELOPMENT

4.1 Devices

In order to offset the inherent limitations of neutron source intensity, we recognized that major developments in neutron scattering instrumentation were required if the techniques were to make a significant impact on the field of structural biology. The early uses of neutron scattering and diffraction for the analysis of biological structures were paralleled by extensive development of equipment including the multilayer monochromator and advanced position sensitive detectors (PSDs).

Multilayer monochromator. As mentioned previously, the concept of the multilayer monochromator originated from studies on highly oriented membrane systems. We translated this observed phenomenon into layers of two dissimilar metals (usually Ni and Ti) deposited on a float glass substrate. Over the next decade or so we carried out many experiments to perfect the technology and to understand the science of stacks of thin (~50-250Å) metal layers. As it turned out, multilayer monochromators are extraordinarily efficient neutron wavelength selection devices with high reflectivity (up to 98%), tunable wavelength (λ) and bandwidth ($\Delta\lambda/\lambda$), and negligible harmonic contamination (λ/n). By adjusting the d-spacing of the repeating layers, we could select λ and $\Delta\lambda/\lambda$ by Bragg diffraction of an incident neutron beam of known divergence.

This became particularly important in protein crystallography, for example, where the use of neutron beams with larger $\Delta\lambda$ is one way to increase flux [5,80]. Clearly to maximize the amount of radiation a crystal can diffract, $\Delta\lambda$, beam divergence and the crystal's mosaicity have to be matched. Most monochromators produce a nearly monochromatic beam with a $\Delta\lambda$ much less than the crystal can 'accept' - typically about 0.1Å. With the use of appropriate multilayer monochromators, $\Delta\lambda$ can be tailored to match the crystal's mosaicity and preliminary trials at the HFBR showed that gains of 3× in diffraction intensity were easily achieved [5].

As we improved the technology and our understanding, we were able to prepare very efficient multilayers with a d-spacing of ~50Å which enabled the selection of shorter λ . In addition, it was shown that multilayers made of suitable materials could be used as very efficient neutron polarizers [81], and ultimately supermirrors were developed by introducing a continuous variation in d-spacing [82,83]. In a field focussed on maximizing the neutron flux at the sample position, the multilayer monochromator system has been used with considerable success [4,84,85,86,87,88].

Position sensitive detectors. In our first efforts to achieve a PSD we simply replaced the single detector with a five-detector system using a white beam with individual monochromators [89]. However, this was soon replaced with an in-house built linear PSD using a graphite coated anode. Unfortunately this device proved quite unstable and the Instrumentation Division at BNL developed a 30cm long linear ^3He PSD detector. This started a long-term and very productive relationship with the Instrumentation Division. Initially we were faced with a number of choices for the technology of large efficient PSDs, however, we considered the gas detector - specifically the proportional gas detector

– would provide the best option for the types of systems envisaged. The major challenges included the detection efficiency and spatial resolution, especially given the large sizes we were planning. We started with small active areas, 18cm by 18cm (**Figure 18**), however we were soon contemplating a 50cm by 50cm, high efficiency detector for the SANS instrument.

Major improvements in both SANS research and in protein crystallography were achieved by use of efficient PSDs with good resolution and positional stability [21,90,91,92,93,94]. The sophisticated detector technology can now produce detectors of incredible performance, such as the detector built for the spallation neutron station at LANSCE (**Figure 19**). This detector is cylindrical and covers 120 degrees with a radius of 70cm. The neutron sensitive area is contiguous with 8 separate readout systems to achieve a total counting rate of more than 10^6 n/sec.

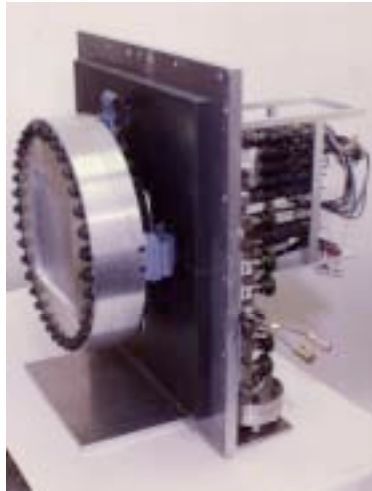


Figure 18. A 20cm × 20cm position sensitive detector built by the Instrumentation Division at BNL for a protein crystallography diffractometer.



Figure 19. The large position sensitive detector built by the Instrumentation Division at BNL for the protein crystallography station at LANSCE.

4.2 A Protein Crystallography Station at a Spallation Source

To enhance neutron beam intensity, the quasi Laue technique [5] is particularly well suited for protein crystallography

at reactor sources, and can be tailored to spallation neutron sources. Classical spallation neutron techniques use fully decoupled moderators producing neutron beams that travel along beam pipes as a function of their velocity with short wavelength neutrons arriving at a target station first, followed by the longer wavelength neutrons. Note that the velocity of a neutron is inversely related to its wavelength ($v = 3956/\lambda$ m/s). Spallation neutron beams at a given time are nearly monochromatic and over the pulse time produce a contiguous wavelength band typically in the range from 0.5 to 6 Å. The delta function (per time slice) like characteristics of such fully decoupled moderators can be broadened by using partially decoupled moderators giving a finite $\Delta\lambda$ but with a 4 fold flux increase [95].

The Protein Crystallography Station built at the Los Alamos Neutron Science Center (LANSCE) (**Figure 20**) uses such a decoupled moderator [96]. The moderated neutrons are extracted down a beam-pipe. From the moderator, neutrons travel a total flight path length of 28m down a vacuum pipe with collimation inserts that taper the neutrons to produce a beam with 0.1 degree divergence (matched to the average crystal's mosaicity). This 28m source-to-target length allows observation of neutrons between 0.7 and 6 Å with a $\Delta\lambda$ of about 0.1 Å. A chopper system removes unwanted high- and low-energy neutrons to protect the sample and detector from fast neutrons and gamma radiation produced during the initial proton pulse. A κ -circle goniometer allows for crystal orientations. A complete data set can consist of many thousands of reflections and typically requires between 12-30 crystal settings depending on the symmetry of the crystal. A large cylindrical PSD fabricated by the Instrumentation Division at BNL collects as many of the spots as possible at each crystal setting without having to re-position the detector (**Figure 21**). The whole data collection process involves a number of dedicated computer systems to decode the position of diffracted neutrons, time stamp the neutron's arrival time and ultimately integrate and store the reflections [97]. Initial experiments surpassed our expectations and preliminary results for rubredoxin and D-xylose isomerase are described elsewhere in these transactions.

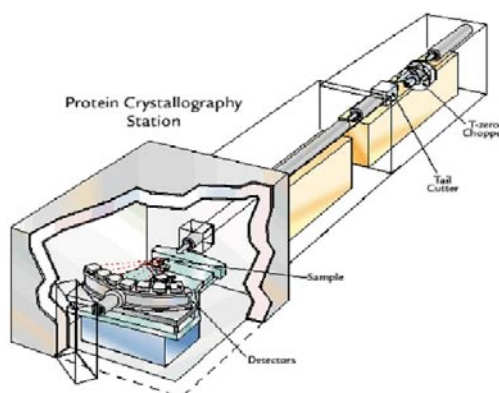


Figure 20. The Protein Crystallography Station at LANSCE.

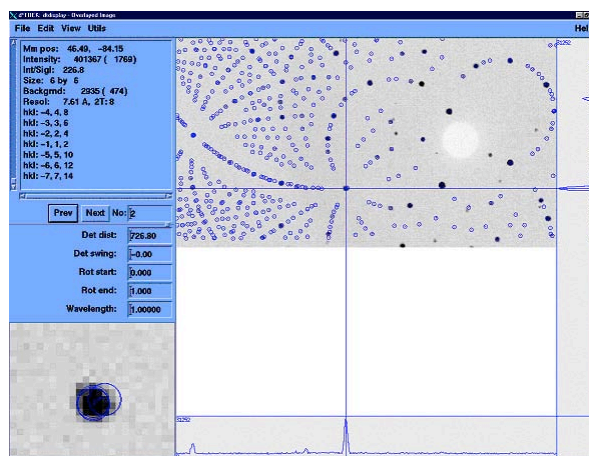


Figure 21. A Laue projection of data collected at one crystal setting from D-xylose isomerase. A total of 181,797 reflections were recorded, over 23 crystal settings (Courtesy of Gerry Bunick and Leif Hanson, ORNL).

5. SUMMARY

The foundations of modern structural biology were laid in the 1960's by studies such as those of myoglobin and hemoglobin by John Kendrew and Max Perutz. These pioneering efforts gave us the first insight into the complex relationship between structure and function of proteins, and raised a myriad of questions about detailed molecular interactions involving basic structural motifs such as hydrogen bonding, charge transfer, and non-bonding (van der Waals) interactions. It was clear that the detailed analysis of these interactions would require neutron scattering techniques since imaging H atoms by X-ray protein crystallography is problematic. The 1970's and 1980's were periods of initial major developments – the techniques are now mature and are poised to make a significant contribution to structural biology particularly with the advent of new and more powerful spallation neutron sources.

6. ACKNOWLEDGMENTS

The author would like to acknowledge the many students and colleagues that made the described work possible. Particularly I thank Robert Knott for helping with the editing of this paper, and Xinmin Li for help with the figures. I thank Paul Langan and Gayle Greene for major contributions in the development and fabrication of the Protein Crystallography station at LANL.

7. REFERENCES

- [1] B.P. Schoenborn, H.C. Watson and J.C. Kendrew, *Nature* **207** (1965), 28.
- [2] B.P. Schoenborn, D.L.D. Caspar and P.F. Kammerer, *J. Appl. Cryst.* **7** (1974), 508.
- [3] A.M. Saxena and B.P. Schoenborn, *Acta Cryst.* **833** (1977), 805.
- [4] J.W. Lynn, J.K. Kjems, L. Passell, A.M. Saxena and B.P. Schoenborn, *J. Appl. Cryst.* **9** (1976), 454.
- [5] B.P. Schoenborn, *SPIE* **1738** (1992), 192.
- [6] G. Zaccai, J.K. Blasie and B.P. Schoenborn, *Proc. Nat. Acad. Sci. USA* **72** (1975), 376.
- [7] B.P. Schoenborn, *Biochim. Biophys. Acta* **457** (1976), 41.
- [8] G.I. King, W. Stoeckenius, H.L. Crespi and B.P. Schoenborn, *J. Mol. Biol.* **130** (1979), 395.
- [9] M. Yeager, B.P. Schoenborn, D. Engelman, P. Moore and L.J. Stryer, *Mol. Biol.* **137** (1980), 315.
- [10] G. King, P. Mowery, W. Stoeckenius, H. Crespi and B.P. Schoenborn, *Proc. Natl. Acad. Sci. USA* **77** (1980), 4726.
- [11] G.L. King and B.P. Schoenborn, *Methods Enzymol.* **88** (1982), 241.
- [12] B.P. Schoenborn, V. Ramakrishnan and D. Schneider, *Physica* **137B** (1986), 214.
- [13] D.S. Wise, A. Karlin and B.P. Schoenborn, *Biophys. J.* **28** (1979), 473.
- [14] D.S. Wise, B.P. Schoenborn and A.J. Karlin, *Biol. Chem.* **256** (1981), 4124.
- [15] J.M. Pachence, I. S. Edelman and B.P. Schoenborn, *J. Biol. Chem.* **262** (1987), 702.
- [16] J. Schefer, R. McDaniel and B.P. Schoenborn, *J. Phys. Chem.* **92** (1988), 729.
- [17] Y. Ito, M. Harada, S. Ohta, Y. Kagawa, O. Aono, J. Schefer and B.P. Schoenborn, *J. Mol. Biol.* **213** (1990), 289.
- [18] P.B. Moore, D.M. Engelman and B.P. Schoenborn, *Proc. Natl. Acad. Sci. USA* **71** (1974), 172.
- [19] M. Capel, P. Moore, D. Engelman, D.K. Schneider, B.P. Schoenborn, M. Kjeldgaard, J. Langer, V.R. Ramakrishnan, I.-Y. Sillers and S. Yabuki, *Science* **238** (1987), 1403.
- [20] W. Stark, B.P. Schoenborn and L. Makowski, *Material Science Forum* **27/28** (1988), 137.
- [21] B.P. Schoenborn, J. Alberi, A.M. Saxena and J.J. Fisher, *J. Appl. Cryst.* **11** (1978), 455.
- [22] *Neutron Scattering for the Analysis of Biological Structures*, ed. B.P. Schoenborn, Brookhaven Symp. Biol. **27** (1976).
- [23] J.P. Baldwin, P.G. Boseley, E.M. Bradbury and K. Ibel, *Nature* **253** (1975), 245.
- [24] R.P. Hjelm, G.G. Kneale, P. Suau, J.P. Baldwin, E.M. Bradbury and K. Ibel, *Cell* **10** (1977), 139.
- [25] H.B. Stuhmann, *J. Appl. Cryst.* **7** (1974), 173.
- [26] G. Marguerie and H.B. Stuhmann, *J. Mol. Biol.* **102** (1976), 143.

- [27] *Neutrons in Biology*, ed. B.P. Schoenborn, (Plenum Press, New York, 1984).
- [28] R.B. Knott and B.P. Schoenborn, in: *Physical Chemistry of Food Processes*, eds. I.C. Baianu and H. Pessen (Van Nostrand Reinhold, New York, 1993), p 151.
- [29] B.P. Schoenborn, Cold Spring Harbor Symp. Quant. Biol. **36** (1971), 569.
- [30] B.P. Schoenborn and J.C. Hanson, ACS Symposium Series No. 127, *Water in Polymers*, ed. Stanley P. Rowland (1980), p 215.
- [31] S.E.V. Phillips and B.P. Schoenborn, Nature **292** (1981), 81.
- [32] J.C. Hanson and B.P. Schoenborn, J. Mol. Biol. **153** (1981), 117.
- [33] R.E. Koepe and B.P. Schoenborn, Biophys. J. **45** (1985), 503.
- [34] R.B. Knott, J. Schefer and B.P. Schoenborn, Acta Cryst. **C46** (1990), 1528.
- [35] B.V. Daniels, B.P. Schoenborn and Z.R. Korszun, in: *Neutrons in Biology*, eds. B.P. Schoenborn and R.B. Knott (Plenum Press, New York, 1996), p 325.
- [36] B.P. Schoenborn, Acta Cryst. **A39** (1983), 315.
- [37] B.P. Schoenborn, in: *Neutrons in Biology*, ed. B.P. Schoenborn (Plenum Press, New York, 1984), p 261.
- [38] J.C. Norvell and B.P. Schoenborn, in: *Neutron Scattering for the Analysis of Biological Structures*, ed. B.P. Schoenborn, Brookhaven Symp. Biol. **27** (1976), II-12.
- [39] B.P. Schoenborn, J. Biol. Chem. **262** (1987), 702.
- [40] G. Otting, E. Liepinsh and K. Wuethrich, Science **254** (1991), 974.
- [41] W. Gu and B.P. Schoenborn, Proteins **22** (1995), 20.
- [42] F. Shu, V.R. Ramakrishnan and B.P. Schoenborn, in: *Neutrons in Biology*, eds. B.P. Schoenborn and R.B. Knott (Plenum Press, New York, 1996), p 309.
- [43] F. Shu, V.R. Ramakrishnan, B.P. Schoenborn, Proc. Natl. Acad. Sci. USA **97** (2000), 3872.
- [44] X. Cheng and B.P. Schoenborn, Acta Cryst. **B46** (1990), 195.
- [45] A.A. Kossiakoff and S. Shteyn, Nature **311** (1984), 582.
- [46] A.A. Kossiakoff and S.A. Spencer, Nature **288** (1980), 414.
- [47] A.A. Kossiakoff and S.A. Spencer, Biochem. **20** (1981), 6462.
- [48] M.M. Teeter, Proc. Natl. Acad. Sci. USA **81** (1984), 6014.
- [49] M.M. Teeter and A.A. Kossiakoff, in: *Neutrons in Biology*, ed. B.P. Schoenborn (Plenum Press, New York, 1984), p 335.
- [50] R.B. Knott, J. Schefer and B.P. Schoenborn, Material Science Forum **27/28** (1988), 147.
- [51] B. Church, *Ph.D. Thesis* (University of Sydney, 1992).
- [52] A.A. Kossiakoff, Nature **296** (1983), 713.
- [53] B.P. Schoenborn, in: *Structure and Function of Oxidation Reduction Enzymes*, eds. A. Akeson and A. Ehrenberg (Pergamon Press, Oxford, 1972), p 109.
- [54] S.A. Mason, G.A. Bentley and G.J. McIntyre, in: *Neutrons in Biology*, ed. B.P. Schoenborn (Plenum Press, New York, 1984), p 323.
- [55] N.V. Raghavan and B.P. Schoenborn, in: *Neutrons in Biology*, ed. B.P. Schoenborn (Plenum Press, New York, 1984), p 247.
- [56] H.F.J. Savage and A. Wlodawer, Methods Enzymol. **127** (1986), 162.
- [57] B.P. Schoenborn, J. Mol. Biol. **201** (1988), 741.
- [58] X. Cheng and B.P. Schoenborn, Acta Cryst. **A47** (1991), 314.
- [59] X. Cheng and B.P. Schoenborn, J. Mol. Biol. **220** (1991), 381.
- [60] J. Jiang and A.T. Brünger, J. Mol. Biol. **243** (1994), 100.
- [61] F. Shu, *Ph.D. Thesis* (SUNY Stonybrook, 1994).
- [62] H.B. Stuhmann, J. Mol. Biol. **77** (1973), 363.
- [63] B. Jacrot and G. Zaccai, Biopolymers **20** (1981), 2413.
- [64] D.M. Engelman and P.B. Moore, Proc. Natl. Acad. Sci. USA **69** (1972), 1997.
- [65] R.P. May, H.B. Stuhmann and K.H. Nierhaus, in: *Neutrons in Biology*, eds. B.P. Schoenborn and R.B.

- Knott (Plenum Press, New York, 1984), p 25.
- [66] D.M. Engelman, P.B. Moore and B.P. Schoenborn, in: *Neutron Scattering for the Analysis of Biological Structures*, ed. B.P. Schoenborn, Brookhaven Symp. Biol. **27** (1976), IV-20.
- [67] V. Graziano, S.E. Gerchman, D.K. Schneider and V.R. Ramakrishnan, in: *Neutrons in Biology*, ed. B.P. Schoenborn and R.B. Knott (Plenum Press, New York, 1996), p 127.
- [68] V.R. Ramakrishnan, J.T. French, V. Graziano, P.L. Lee and R.M. Sweet, *Nature* **362** (1993), 219.
- [69] B.P. Schoenborn, A.C. Nunes and R. Nathans, *Berichte Bunsengesellschaft für Physical Chemistry* **74** (1970), 1202.
- [70] M. Yeager, in: *Neutron Scattering for the Analysis of Biological Structures*, ed. B.P. Schoenborn, Brookhaven Symp. Biol. **27** (1976), III-3.
- [71] J.K. Blaise, B.P. Schoenborn and G. Zaccari, in: *Neutron Scattering for the Analysis of Biological Structures*, ed. B.P. Schoenborn, Brookhaven Symp. Biol. **27** (1976), III-58.
- [72] R.B. Knott and B.P. Schoenborn, *Methods Enzymol.* **127** (1986), 217.
- [73] J.M. Pachence, R.B. Knott, I.S. Edelman, B.P. Schoenborn and B.A. Wallace, *Annals NY Acad. Sci.* **435** (1984), 566.
- [74] S.H. White and M.C. Werner, in: *Neutrons in Biology*, eds. B.P. Schoenborn and R.B. Knott (Plenum Press, New York, 1996), p 203.
- [75] S.H. White, G.I. King and J.E. Cain, *Nature* **290** (1981), 161.
- [76] G.I. King, N.-M. Chao and S.H. White, in: *Neutrons in Biology*, ed. B.P. Schoenborn (Plenum Press, New York, 1984), p159.
- [77] G.I. King and B.P. Schoenborn, *Methods Enzymol.* **88** (1985), 241.
- [78] P.M.G. Curmi, D.B. Stone, D.K. Schneider and R.A. Mendelson, *Adv. Biophys.* **27** (1991), 131.
- [79] P.M.G. Curmi, D.K. Schneider, J.A. Spudich and R.A. Mendelson, *J. Mol. Biol.* **203** (1988), 781.
- [80] P. Langan, B.P. Schoenborn and L.L. Daemon, in *Neutron Optics*, eds. James L. Wood and Ian Anderson, *Proceedings of SPIE* **4509** (2001), 66.
- [81] C.F. Majkrzak, L. Passell and A.M. Saxena, *AIP Conf. Proc.* **89** (1981), 131.
- [82] F. Mezei, *Commun. Phys.* **1** (1976), 81.
- [83] T. Ebisawa, N. Achiwa, S. Yamada, T. Akiyoshi and S. Okamoto, *J. Nucl. Sci. Tech. Japan* **16** (1979), 646.
- [84] A.M. Saxena and B.P. Schoenborn, in: *Neutron Scattering for the Analysis of Biological Structures*, ed. B.P. Schoenborn, Brookhaven Symp. Biol. **27** (1976), VII-30.
- [85] A.M. Saxena and B.P. Schoenborn, *Acta Cryst.* **A33** (1977), 813.
- [86] A.M. Saxena and B.P. Schoenborn, *Material Science Forum* **27/28** (1988), 313.
- [87] A.M. Saxena and C.F. Majkrzak, in: *Neutrons in Biology*, ed. B.P. Schoenborn (Plenum Press, New York, 1984), p 143.
- [88] R.B. Knott, in: *Neutrons in Biology*, eds. B.P. Schoenborn and R.B. Knott (Plenum Press, New York, 1996), p 69.
- [89] B.P. Schoenborn, and A.C. Nunes, *Ann. Rev. Biophys. Bioengineer.* **1** (1972), 529.
- [90] J. Alberi, in: *Neutron Scattering for the Analysis of Biological Structures*, ed. B.P. Schoenborn, Brookhaven Symp. Biol. **27** (1976), VIII-24.
- [91] J.E. Cain, J.C. Norvell and B.P. Schoenborn, in: *Neutron Scattering for the Analysis of Biological Structures*, ed. B.P. Schoenborn, Brookhaven Symp. Biol. **27** (1976), VIII-43.
- [92] J. Fischer, V. Radeka and R.A. Boie, in: *Position-Sensitive Detection of Thermal Neutrons*, eds. P. Convert and J.B. Forsyth (Academic Press, New York, 1983), p 129.
- [93] V. Radeka, N.A. Schaknowski, G.C. Smith and B. Yu, in: *Neutrons in Biology*, eds. B.P. Schoenborn and R.B. Knott (Plenum Press, New York, 1996), p 57.
- [94] B.P. Schoenborn, in: *Position Sensitive Detection of Thermal Neutrons*, eds. P. Convert and J.B. Forsyth (Academic Press, New York, 1983), p 321.
- [95] B.P. Schoenborn, J.D. Court, A.C. Larson and P. Ferguson, *J. Neutron Research* **7** (1999), 89.
- [96] B.P. Schoenborn and P. Langan, *J. Synch. Rad.* (2003), (in press).

[97] P. Langan, G. Greene, X. Li and B.P Schoenborn, these Transactions.

NEUTRON “SMALL-ANGLE” CRYSTALLOGRAPHY: CONTRAST VARIATION IN SINGLE CRYSTALS OF BIOLOGICAL MACROMOLECULES.

P.A. Timmins
ILL, Grenoble, France

1. ABSTRACT

The contrast variation technique is best known through its application in neutron small-angle scattering. The concept was, however, first applied in the early days of X-ray protein crystallography when Bragg and Perutz [1] determined the molecular envelope of haemoglobin by soaking crystals in salt solutions in order to change the electron density and hence contrast of the solvent with respect to the protein.

By analogy contrast variation using H₂O/D₂O mixtures or molecule specific deuteration can be used to determine molecular envelopes in neutron crystallography. This is particularly useful when one component of a molecular complex is disordered in the crystal. Such is the case for example in many viruses where the protein coat may be perfectly ordered but due to symmetry mismatch the nucleic acid is disordered and invisible in standard high-resolution x-ray crystallographic studies. A similar effect is seen in crystals of membrane proteins where, although the protein itself is well ordered and its structure can be obtained at high resolution, the detergent used to solubilize the protein is fluid and disordered and hence invisible in X-ray maps.

In order to measure diffraction from small crystals of large unit cell proteins optimised instrumentation has been developed exploiting the ILL's high flux of long-wavelength neutrons. The phase problem can be solved in a manner similar to single isomorphous replacement exploiting the linear relationship between phase and contrast if the structure of one component in the crystal is known.

The structure determination of detergent/membrane-protein complexes is a particularly good example of the low-resolution crystallographic method illustrating the unique power of neutrons in identifying molecular interactions in crystals. A number of examples in which protein-protein, detergent-detergent and protein-detergent interactions have varying significance will be shown

2. INTRODUCTION

The overall shapes and location of different components within a biomolecular complex are often determined by neutron small angle scattering using the H/D contrast variation method (reviewed in [2]). The major drawback of solution scattering is that the particles in solution take up all possible orientations and a unique solution to the scattering problem does not exist. Modern modelling methods [3] go some way to removing this problem but still do not provide a unique solution. Moreover, the averaging in solution leads to rather weak scattering such that information extends often to a resolution of only about 20Å. There are however a number of cases in which such large macromolecular complexes form crystals which are not sufficiently ordered as to allow the whole structure to be determined at high resolution but are sufficiently ordered as to give shape and orientational information at a resolution ~10Å. Such studies are the subject of this review that extends and updates previous work [4,5,6].

3. LOW-RESOLUTION DIFFRACTION – WHAT USE IS IT?

The very existence of crystals of biological macromolecules diffracting to high resolution implies in the eyes of many investigators that a high (quasi-atomic) resolution structure of the whole macromolecule can be obtained. It has been shown, however, that this is often not the case. Striking examples come from virus crystals where the protein coat may be ordered at very high resolution whereas the nucleic acid in the interior is, according to X-ray electron density maps, invisible. A similar result is obtained from crystallographic studies of crystallized membrane proteins, where the protein itself is highly ordered but the protein bound detergent is essentially invisible apart from a very small number of single detergent molecules. Why should this be?

3.1 Virus Crystals

In the case of virus particles there is a rather special effect due to a symmetry mis-match. The crystal contacts are made exclusively through interactions between the coat proteins. These are arranged on the surface with exact icosahedral symmetry (532) and the 2- or 3-fold symmetry axes may or may not coincide with crystallographic symmetry axes. There are therefore at least 20 different but equivalent orientations of a single virus particle as far as the coat is concerned. The nucleic acid is however a single or, in some cases, a few strands of nucleic acid which cannot have any internal symmetry and can certainly not match the symmetry of the coat. The nucleic acid is therefore “unaware” of the coat symmetry and is most probably assumes a different, random orientation with respect to the crystal symmetry axes in each virus particle. An electron density or scattering length density map involving the nucleic acid is therefore averaged over all the orientations found in the crystal. If the nucleic acid has a unique rigid conformation within the virus particle we would therefore, at best, see an icosahedrally averaged density. In practise the conformation could be different from one particle to another or the nucleic acid could be mobile and the density would be a time-average over the different conformations.

3.2 Membrane Proteins

Membrane protein crystals constitute another class of complexes where the protein is generally highly ordered whereas the solubilising agent, detergent, which simulates in some ways the natural membrane is often invisible in electron density maps. In this case the lack of density is probably due to the fluidity of the detergent phase. Thus, although the phase is confined to a well-defined volume within that volume the molecules are mobile and thus a time and space-averaged picture shows no high-resolution density.

4. THE ADVANTAGES OF NEUTRONS

It may still be asked why X-ray diffraction does not show low-resolution density in these cases. In fact the whole concept of contrast variation originated from experiments by Bragg and Perutz [1] to try and determine the overall shape of haemoglobin using salt solutions to modify the electron density of the crystal solvent with respect to the protein. The natural contrast between protein and water is very low for X-rays; the electron density of RNase for example is $0.432\text{e}\text{\AA}^{-3}$ and for pure water $0.335\text{e}\text{\AA}^{-3}$. The addition of salt to water raises the electron density even closer to that of protein. Small molecules such as sucrose or indeed high salt concentrations may be used to vary the contrast but the chemical effects of such additives are often such as to destabilise the crystal or even the complex itself or alter the conformations of the component molecules. The exchange of deuterium for hydrogen is a much less perturbative change. In addition it is not trivial to collect low resolution X-ray diffraction data from crystals of biological macromolecules although a number of workers have built specialised beam-lines to do this (7,8). Thus in principle it is possible to determine a molecular envelope by X-rays but there remain severe restrictions of a practical nature. Recent experiments to improve contrast using Xenon as a contrast agent have been described [9] and their limitations have been discussed [9,10].

5. CONTRAST VARIATION

The arguments given above to explain the absence of high resolution structure indicate that there still exists structure at low resolution but that for X-rays this may be difficult to measure due in particular to lack of contrast. Manipulation of contrast in neutron scattering is particularly straightforward and has been heavily exploited for many years in neutron small angle scattering. The presence of a well-defined solvent (water) phase in crystals of macromolecular complexes means that the same principles may be applied in neutron crystallography – hence the term small-angle neutron crystallography. **Figure 1** shows the neutron scattering length density for a number of chemically distinct components of biological molecules. These are calculated from the atomic composition of average proteins, nucleic acids etc and do not vary greatly between for example different proteins. The values shown for detergents and lipids may vary considerably however depending particularly on the balance between hydrophilic head and hydrophobic tail.

At low resolution the scattering is due to the contrast between solvent and macromolecule, i.e. the difference in scattering length density. Thus for example proteins have a zero scattering length density difference with respect to water in a solution containing $\sim 40\% \text{D}_2\text{O}/60\% \text{H}_2\text{O}$. This concentration at which a particle has zero contrast is known as the *isopicnic point*. It should be noted that the concept of zero contrast applies only to the average scattering length density and hence only to scattering at $Q=0$. At all other Q -values there will be some contributions from internal scattering length density fluctuations within the molecule such that there are always some parts of the molecule that have a

positive or negative contrast. Hence the Bragg scattering is a minimum at the isopicnic point but is not zero. A striking point of **Figure 1** is that the scattering length densities of H₂O and D₂O encompass those of all other natural components of biological macromolecules. The only exception to this is the case of fully deuterated protein or nucleic acid which have a scattering length density greater than that of pure D₂O.

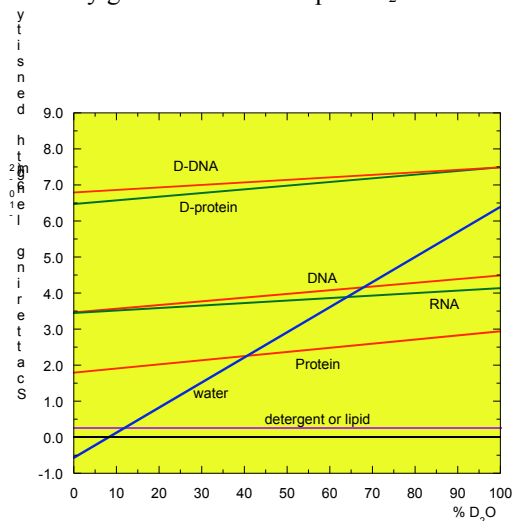


Figure 1. Neutron scattering length densities of biological macromolecules as a function of the deuterium content of the solvent water.

6. INSTRUMENTATION AND DATA REDUCTION

One of the difficulties encountered in low resolution protein crystallography is the problem of measuring data at very low resolution – including for example the first order of a 700Å unit cell. Modern synchrotron radiation with its highly collimated beams and advanced optics can overcome to a large extent such problems, at least on a purpose built instrument. The effect of contrast agents on the native structure due to specific binding or inhomogeneous diffusion is however less well understood. Hence cold neutrons and H/D contrast variation can be combined to measure neutron diffraction data in a rather simple way. A dedicated diffractometer was constructed at ILL some years ago as collaboration between ILL and EMBL. This instrument, DB21, is a four-circle diffractometer with multi-detector and is described in some detail in Roth et al. [11,12]. A schematic representation of the instrument is shown in **Figure 2**. The beam is monochromated by a potassium intercalated graphite crystal giving a neutron wavelength of 7.56 Å and a wavelength spread of ~2% (FWHM) or a pyrolytic graphite crystal giving a wavelength of 4.6Å. The beam is collimated using LiF pinholes and a graphite collimator after passing a series of graphite filters for eliminating 1/2, 1/3 and 1/4 contamination. The detector is of the Anger camera type allowing a resolution of 1.75 x 1.53 mm. Due to the g-sensitivity of this detector no cadmium is used in beam defining apertures that are instead made of LiF backed with B₄C. A single crystal of Bi removes in-beam g-radiation.

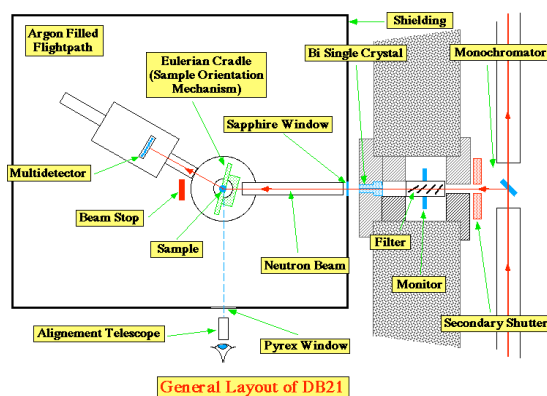


Figure. 2 Schematic representation of the DB21 instrument.

Data acquisition is by f - or w -scans. In low symmetry space groups reorientation of the crystal may be required to obtain a full data step due to the rather restricted reciprocal space coverage of the current detector. Determination of the crystal orientation may be difficult at low resolution and many of the standard auto-indexing algorithms have failed. A program based on the graphics package ‘O’ has been written to allow manual rotation of the known reciprocal cell into the reciprocal space diffraction pattern in order to determine the crystal orientation [13]. Data reduction is carried out using a modified version of XDS [14]. Another problem that arises is the scaling of data measured from crystals of different H₂O/D₂O content. This is done by using the parabolic relationship between intensities or the linear relationship between structure amplitudes in centric zones [15] as described in eqn 2 below. This of course requires consistent indexing which in certain enantiomorphic space groups may be a problem. For example in space group P312 it is impossible to distinguish between hkl and khl reflections. In high resolution data this problem can be resolved when the final structure is known but in the neutron low resolution case it is absolutely necessary to carry out a correct scaling. In practise it may be necessary to perform the scaling using all possible combinations of index and to select that having the best scaling for all reflections.

7. DATA ANALYSIS

7.1 The Crystallographic Phase Problem

The variation of the crystallographic structure factor as a function of contrast can be expressed as:

$$\vec{F}(h, X) = \vec{F}(h, 0) + X\vec{F}(h)_{HD} \quad \dots\dots\dots(1)$$

where h is the reciprocal lattice point
 X is the mole fraction of [D₂O]/[D₂O]+[H₂O] in the crystal
 $\vec{F}(h)_{HD}$ is the vector difference between the structure factor in H₂O and that in D₂O.

Multiplying by the complex conjugate we obtain the diffracted intensity:

$$I(h, X) = F(h, 0)^2 + 2X \cos \phi F(h, 0)F_{HD}(h) + X^2 F_{HD}^2(h) \quad \dots(2)$$

where ϕ is the phase angle between $\vec{F}(h, 0)$ and $\vec{F}(h)_{HD}$.

This relationship has several important consequences for low resolution crystallography including, as mentioned above, the possibility of scaling together data from different contrasts and the interpolation of missing data [16]. In terms of structure solution it is of fundamental importance as it means that the phase difference, ϕ between any two contrasts, of a reflection (h), may be determined except for the sign (\pm), if the amplitudes at 3 contrasts are known. Therefore if the structure is known at any one contrast then the phases at that contrast may be calculated and then determined at any other contrast except for knowledge of the sign. In the particular case of centrosymmetric reflections where $\phi = 0$ or π then there is of course no ambiguity and the phase may be calculated at any contrast [17].

In most studies carried out to date the structure of one component of the macromolecular complex has been determined by X-rays or could be modelled from other information. Hence structure factors calculated from the known part of the structure at a contrast where the other component is visible provide starting phases for the determination of the structure at any contrast. This is illustrated in **Figure 3**, which demonstrates the vector relationships between structure factors at four different contrasts. The two triangles bounded by F_0 , F_{HD} and F_D are the two possible relationships which can be constructed through knowledge of the structure factor amplitudes alone following eqn. 1, and corresponding to the two possible signs of ϕ . This particular figure illustrates the case of, for example, a protein/RNA complex where data would be measured at 40% D₂O where the protein is invisible, 70% D₂O where the RNA is invisible and two other contrasts, 0 and 100% D₂O. In this case we imagine that the protein structure is known and that the RNA structure is to be determined. We may therefore calculate the phase of the structure factor in 70% D₂O and thus determine the orientation of the phase triangle with just the ambiguity of sign corresponding to the two triangles shown. This is very closely analogous to the situation of single isomorphous replacement [18,19] in X-ray protein crystallography. Once this (ambiguous) phase has been determined then the ambiguity may be resolved and an approach to the true phase may be made using density modification based on constraints such as the invariability of the known part of the structure, solvent flattening or non-crystallographic symmetry averaging [20,21].

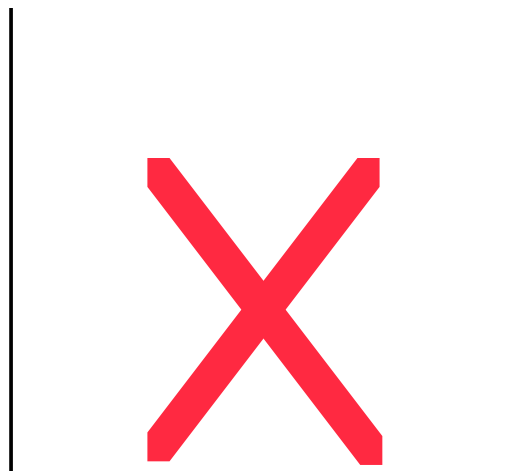


Figure 3. Vector diagram illustrating the relationship between structure amplitudes and phases at different contrasts. The two vector triangles are oriented arbitrarily with the F_{HD} vector parallel to the real axis.

8. A COMPARISON OF PROTEIN DETERGENT INTERACTIONS IN A NUMBER OF MEMBRANE PROTEIN CRYSTALS

Because of the very different scattering lengths of protein and detergent and in particular the very high contrast obtained between detergent and D_2O , complexes of protein and detergent make ideal objects for study by neutron contrast variation. X-ray crystallographic studies have to date succeeded in resolving the structure of a number of membrane proteins and in some cases individual tightly bound detergent or residual lipid molecules have been observed but in no case has this method been able to visualize the solubilizing belt of detergent. Using the known X-ray structure and neutron diffraction data measured at a number of H_2O/D_2O component contrasts it has been possible to calculate neutron scattering length density maps which show only the detergent. The methodology has been described in some detail by Roth et al., 1991 [20]. Briefly, starting phases are obtained from the X-ray crystallographic model and these phases are applied to the data measured at the match point of the protein. The contrast variation relationship (Eqn 2) allows the phases to be extended to other contrasts by a procedure rather like single isomorphous replacement. The phases are then improved by solvent flattening and density modification. The key factor here is the detergent content of the cell. The volume in which the protein is located is known from the X-ray structure but generally speaking the amount of detergent in the crystals is unknown. It is therefore necessary to estimate this and to perform solvent flattening and density modification as a function of the detergent content as a variable parameter.

9. REACTION CENTERS AND LIGHT HARVESTING COMPLEXES

The first membrane protein/detergent structures to be studied by low resolution neutron crystallography were the photosynthetic reaction centers of *Rhodospseudomonas viridis* [21] and *Rhodobacter sphaeroides* [20]. In the reaction center from *R. viridis* only one molecule of the detergent N,N' dimethyldodecylamine N-oxide (LDAO) could be visualized in the high resolution X-ray maps. The neutron diffraction results show the reaction center to be surrounded by a detergent belt some 25-30Å thick. This corresponds to roughly twice the length of an extended LDAO molecule. The aliphatic chain of the detergent molecule observed in the X-ray maps falls within the neutron density although its polar head is outside. The lack of density corresponding to the head may be due to its small size compared with the resolution of the data and to its rather low scattering density arising from disorder and hydration. As Roth et al. point out it should also be noted that in the case of the reaction center the detergent does not necessarily mimic the biological membrane as in the real membrane the reaction center is surrounded by and makes contact with several light harvesting molecules.

The photoreaction center from *R. sphaeroides* crystallizes in the presence of n-octyl-β-glucoside (b-OG) and the small amphiphile heptane-1,2,3-triol (HP). Michel [22] was the first to use small amphiphiles in membrane protein crystallization and suggested that they had the effect of reducing the size of detergent micelles and thereby facilitating crystallization of the membrane protein/detergent complex. This effect was confirmed in neutron small angle scattering experiments by Timmins et al. [23] which showed that HP was indeed included in micelles at least of LDAO and

Neutron “Small-Angle” Crystallography: Contrast variation in single crystals of biological macromolecules

decreased their radius of gyration. Gast et al [24] also showed by turbidity measurements that addition of 5% HP decreased by a factor of two the amount of LDAO bound to the reaction center of *R. viridis*. The most striking observation in the neutron diffraction results on the *R. sphaeroides* reaction center was that the detergent ring formed by the b-OG was almost identical in size and shape to that formed by the LDAO around the *R. viridis* reaction center. Given the similarity in total length of b-OG and LDAO it would appear that detergent size/geometry plays a key role in the crystallization of membrane proteins.

As mentioned above the reaction centres are usually found in the membrane closely associated with several copies of light harvesting proteins and therefore the protein-detergent interactions observed in the crystal may not always be representative of protein lipid interactions in the membrane. Recently a study has been published on the light harvesting complex LH2 from the photosynthetic purple bacterium *Rhodospseudomonas acidophila*, a nonameric complex with a central hole which *in vivo* contains membrane lipids [25]. The complex was crystallized from solutions containing b-OG and experiments were performed using both hydrogenated and tail deuterated detergent. As well as demonstrating the presence of a detergent ring as with other membrane proteins the experiments also showed the central hole to be occupied by two detergent/amphiphile micelles which must have displaced the original lipid during purification.

10. PORINS

Another class of membrane proteins to be studied were the outer membrane proteins known as porins. In contrast to the bacterial photosynthetic reaction centers these proteins form multi-stranded β -barrel structures which are deeply embedded in the membrane with relatively small protruding loops. The Ompf porin from *E. coli* was in fact, along with the photosynthetic reaction center from *R. viridis*, the first membrane protein to be crystallized in the early 1980s [26,27]. Due however to technical crystallographic problems its structure was not solved until 1994 when a trigonal form was crystallized and served as model for a molecular replacement solution [28]. The neutron crystallographic analysis of the tetragonal form [29] showed very clearly the detergent belt bound to the hydrophobic surface of the protein and suggested how the protein is anchored in the membrane. **Figure 4** shows how the detergent binding surface is clearly delimited by two lines of aromatic amino acids with tyrosine residues directed towards the headgroups and phenyl alanines towards the hydrophobic acyl chains. This had been surmised from the X-ray structure but the absence of any density in the electron density maps did not allow this to be demonstrated. Another important observation to come from the neutron diffraction analysis concerned the packing of the molecules in the crystal. The X-ray structure shows the Ompf trimers to pack as two interpenetrating lattices with no protein-protein contacts between molecules in the separate lattices. The question then arises as to how such a structure is stabilised. The answer was provided by the neutron data which showed the two lattices to come into contact through the detergent belts of adjacent molecules. The crystal is therefore stabilised by protein-protein, protein-detergent and detergent-detergent contacts.

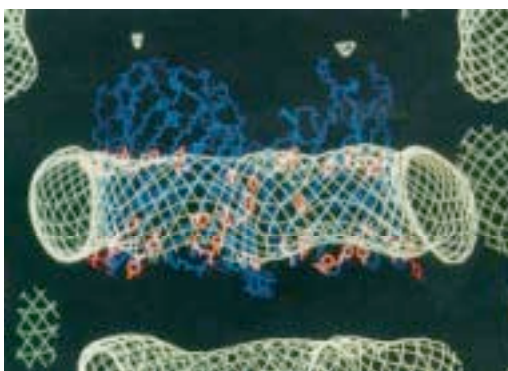


Figure 4. Detergent (green) binding in tetragonal crystals of Ompf. Note the binding surface delimited by aromatic residues (orange).

The trigonal form of Ompf is very different from this [30]. The Ompf trimers here form columns of molecules running in opposite directions with protein-protein contacts being responsible for the interactions within each column. The columns of molecules are then held together by fusion of the detergent rings surrounding the hydrophobic protein surfaces. No distinct detergent belts remain but protein trimers interact directly through hydrophobic interactions or mediated by patches of detergent (**Figure 5**). X-ray contrast variation using salt solutions has also been used to

investigate detergent binding in these crystals [9]. Although the detergent containing volumes determined by neutrons and X-rays partly overlap there are significant differences. This is due most probably to the xenon penetrating only the most hydrophobic parts of the detergent (the tails) as well as into the surface of the protein [9,10]

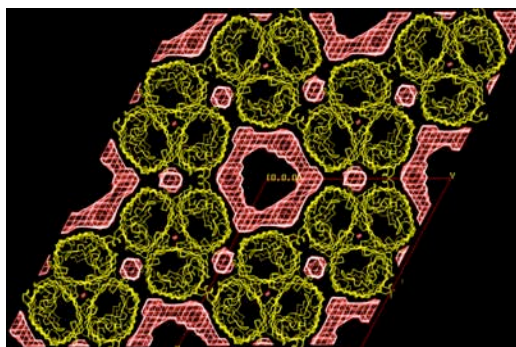


Figure 5. Neutron scattering density map showing the detergent (red) distribution in trigonal crystals of OmpF porin from *E. coli*. Note the hydrophobic protein-protein contacts.

Another outer membrane protein to have been studied is the outer membrane phospholipase A (OMPLA) from *E. coli*. The structure of this protein is a 12 stranded β -barrel and its active form is a dimer [31]. Here the neutron data showed a detergent structure distinct from any other of the known structures with a continuous detergent phase throughout the crystal, somewhat reminiscent of lipid cubic phases. An attempt was also made in this case to obtain the structure from x-ray diffraction of Xe soaked crystals but the results were not consistent with the neutron maps.

11. CONCLUSIONS

Neutron low resolution crystallography is a powerful technique for visualizing disordered regions in crystals of biomolecular complexes and in particular the localisation of detergent in crystals of membrane proteins. The technique of course relies on the availability of crystals but these do not necessarily have to be very large as required for high resolution crystallography – 0.1 mm^3 or less is sufficient. The membrane protein structures studied to date have demonstrated that not only are protein-protein interactions important in the formation of crystals but that in some cases protein-detergent and even detergent-detergent interactions can be crucial.

12. REFERENCES

- [1] W.L. Bragg and M.F. Perutz, *Acta Cryst.* **5** (1952), 277.
- [2] P.A. Timmins and J. Zaccai, *J. Eur. Biophys. J.* **15** (1988), 257.
- [3] D.I. Svergun, *Biophys. J.* **76** (1999), 2879.
- [4] P.A. Timmins, E. Pebay-Peyroula and W. Welte, *Biophys. Chem.* **53** (1994), 27.
- [5] P.A. Timmins, *Neutron News* **6** (1995), 13.
- [6] P.A. Timmins, E. Pebay-Peyroula, and W. Welte, in: *Neutrons in Biology*, Eds. B.P. Schoenborn and R.B. Knott, (Plenum Press, 1996).
- [7] W. Shepard, R. Kahn, M. Ramin and R. Fourme, *Acta Cryst* **D56** (2000), 1288-1303
- [8] H. Tsuruta, *Synchrotron Rad. News*, **13**, (2000) 10.

Neutron “Small-Angle” Crystallography: Contrast variation in single crystals of biological macromolecules

- [9] O. Sauer, M. Roth, T. Schirmer, G. Rummel, C. Kratky, *Acta Cryst* **D58** (2002) 60.
- [10] H.J. Snijder, P.A. Timmins, K.H. Kalk, and B.W. Dijkstra B., *J. Struct. Biol.* **141** (2003) 122.
- [11] M. Roth, A. Lewit-Bentley, *Acta Cryst*, **A38** (1982), 670.
- [12] M. Roth, A. Lewit-Bentley, G.A. Bentley, in: *Position sensitive detection of thermal neutrons. Based on the proceedings of the workshop on PSD of thermal neutrons, 11-12 Oct. 1982* eds. P. Convert, J.P. Forsyth (Academic Press, 1983)
- [13] S. Penel, and P. Legrand, *J. Appl. Cryst*, **30** (1997), 206.
- [14] Kabsch, W., *J. Appl. Cryst.* (1993) **26**, 795.
- [15] M. Roth, A. Lewit-Bentley, G.A. Bentley, *J. Appl. Cryst*, **17** (1984), 77.
- [16] M. Roth, *Acta Cryst.* **A42**, (1986), 230.
- [17] M. Roth, *Acta Cryst.* **A43**, (1987), 780.
- [18] T.L. Blundell, & Johnson, L. N. (1976). *Protein Crystallography*. London: Academic Press.
- [19] M. Roth, (1992) in: *Crystallographic Computing 5*, eds. Moras, D., Podjarny, A.D. and Thierry, J.C. (Oxford Univ. Press, Oxford, UK. 1992).
- [20] M. Roth, B. Arnoux, A. Ducruix, and F. Reiss-Husson, *Biochemistry*, **30** (1991) 9403.
- [21] M. Roth, A. Lewit-Bentley, H. Michel, J. Deisenhofer, R. Huber, D.Oesterhelt, *Nature*, **340** (1989) 659.
- [22] H. Michel, *J Mol Biol.*, **158** (1982) 567.
- [23] P. A. Timmins, Hauk, J., Wacker, T., and Welte, W., *FEBS Lett*, **280**, (1991) 115.
- [24] P. Gast, Hemelrijk and Hoff, A.J., *FEBS Lett.*, **337** (1994) 39.
- [25] S.M. Prince, T.D. Howard, D.A.A. Myles, C. Wilkinson, M.Z. Papiz, A.A. Freer, R.J. Cogdell, and N.W. Isaacs, *J. Mol. Biol.* **326** (2003) 307.
- [26] R.M. Garavito, Rosenbusch J.P. (1980) *J Cell Biol.* **86**(1):327.
- [27] R.M. Garavito, Jenkins JA, Neuhaus JM, Pugsley AP, Rosenbusch JP. *Ann Microbiol (Paris)*. (1982) **133A**, 37.
- [28] S.W. Cowan, Schirmer, T., Rummel, G., Steiert, M., Ghosh, R., Pauptit, R.A., Jansonius, J.N. and Rosenbusch, J.P., *Nature*, **358** (1992) 727

P.A. Timmins

- [29] E. Pebay-Peyroula, R.M. Garavito, J.P. Rosenbusch, M. Zulauf and P.A. Timmins, *Structure* **3** (1995) 1051.
- [30] S. Penel, E. Pebay-Peyroula, J. Rosenbusch, G. Rummel, T. Schirmer, and P.A. Timmins, *Biochimie* **80** (1998) 543.
- [31] H.J. Snijder, Ubarretxena-Belandia, I., Blaauw, M., Kalk, K.H., Verheij, H., Egmond, M.R., Dekker, N. and Dijkstra, B.W., *Nature*, **401** (1999) 717.

DESIGN AND EXPECTED PERFORMANCE OF A HIGH RESOLUTION MACROMOLECULAR NEUTRON DIFFRACTOMETER (MANDI) AT THE SPALLATION NEUTRON SOURCE

P. Thiyagarajan¹, A.J. Schultz¹, Ch. Rehm², J.P. Hodges^{2,3}, W.T. Lee² and A. Mesecar⁴

¹Intense Pulsed Neutron Source, Argonne National Laboratory, 9700 South Cass Ave, Argonne, IL, ²Spallation Neutron Source and ³Metals and Ceramics Division, Oak Ridge National Laboratory, Oak Ridge, TN, ⁴Department of Medicinal Chemistry and Pharmacognosy, University of Illinois at Chicago, Chicago, IL.

1. ABSTRACT

We have designed a dedicated best-in-class high throughput and high resolution time-of-flight single crystal macromolecular neutron diffractometer (MaNDi) at the SNS high power target station to fulfill the enormous interest shown by the macromolecular crystallography community. MaNDi has been designed to be able to collect a full hemisphere of Bragg data with a resolution of 1.5 Å on a macromolecular crystal with a lattice constant in the range of 150 Å ($Dd/d = 1\%$) in about a week. Design calculations show that the data rates at the MaNDi instrument will be over 50 times greater than those for the best existing facilities. The unprecedented high data rates and high resolution with MaNDi for neutron macromolecular crystallography will greatly advance the fields of structural biology and enzymology.

2. INTRODUCTION

Neutron macromolecular crystallography (NMC) can provide accurate information on the positions of the protons and water molecules at active sites of enzymes even at a moderate 2.0 Å resolution.¹⁻²² Although UHRMXC at third generation X-ray synchrotrons can locate the positions of protons in cases where highly ordered crystals are available, in many instances the structural information obtained for solvation shells and protonation states at critical sites of the enzymes continues to remain inadequate. Enzymologists, molecular biologists and protein crystallographers are seeking complementary techniques for accurate determination of the positions of the protons and water molecules at active sites of enzymes in order to elucidate the mechanistic details involved in their function.

NMC offers a number of unique advantages to structural biology. The large difference in the neutron scattering cross-sections of hydrogen and deuterium nuclei allows for the extraction of important structural information on exchangeable protons and bound water in macromolecules.^{6,10} Deuteration of macromolecules enhances visibility of hydrogen atoms and increases the data rates by a factor of 8 compared to the crystals of normal counterparts.¹⁴ Since long wavelength neutrons do not cause any radiation damage to macromolecular crystals, experiments can be readily carried out at room temperature. Time-of-flight neutron diffraction techniques at pulsed neutron sources increase the data rates and resolution by the usage of a large wavelength band separated into a large number of wavelength channels and a large detector solid angle coverage.

A survey of the literature indicates that the overall contribution of NMC has so far been limited. One major reason for the limited impact is the lack of beam time at instruments dedicated to macromolecular crystallography and intrinsic flux limitation at the current facilities. At present there are only 3 dedicated instruments that are recognized to be useful for high resolution single crystal neutron macromolecular crystallography: LADI at the Institut Laue-Langevin (ILL), Grenoble, France; BIX3 at the Japan Atomic Energy Research Institute (JAERI); and PCS at Los Alamos National Laboratory. While LADI and BIX3 have been operational for a few years, the time-of-flight diffractometer PCS at the LANSCE pulsed neutron source has become available only recently. Thus the field of NMC has been severely constrained by the lack of dedicated instruments. The advent of the Spallation Neutron Source (SNS) at Oak Ridge National Laboratory offers an excellent opportunity for the development of a powerful high resolution diffractometer that has a potential to narrow the gap in this area of research.

3. DESIGN OF MANDI

By employing well established analytical procedures and Monte Carlo simulations²³ the performance of MaNDi at both the coupled and decoupled liquid hydrogen moderators at the SNS has been investigated. Although a coupled hydrogen moderator, due to its long pulse widths, can provide higher neutron flux, calculations show that for the

high resolution applications in structural biology MaNDi requires a high resolution moderator such as the decoupled liquid hydrogen moderator at SNS that can provide high cold neutron flux in the wavelength region 1.5 to 5 Å and narrow pulse widths.

MaNDi has been designed with a 24.5 m flight path wherein a useful wavelength bandwidth of about 2.7 Å (without any frame overlap) will be available, given that the source frequency is 60 Hz at SNS. It will employ a set of 3 choppers at 7.2 m, 8.2 m, and 10.4 m downstream from the moderator, respectively, for the selection of wavelength bandwidth. State-of-the-art high index neutron supermirror guides will be used for the efficient beam transport leading to a flux gain at the sample position in the range of 2-10 when compared to that with no guide. A curved guide in the middle section will reduce the overall instrument background and will eliminate any potential radiation damage by γ rays and high energy neutrons from the target to the crystals of biological samples. The combination of a wide wavelength bandwidth and large solid angle detector coverage will provide unprecedented high through-put and resolution for MaNDi in comparison to the current facilities for NMC.

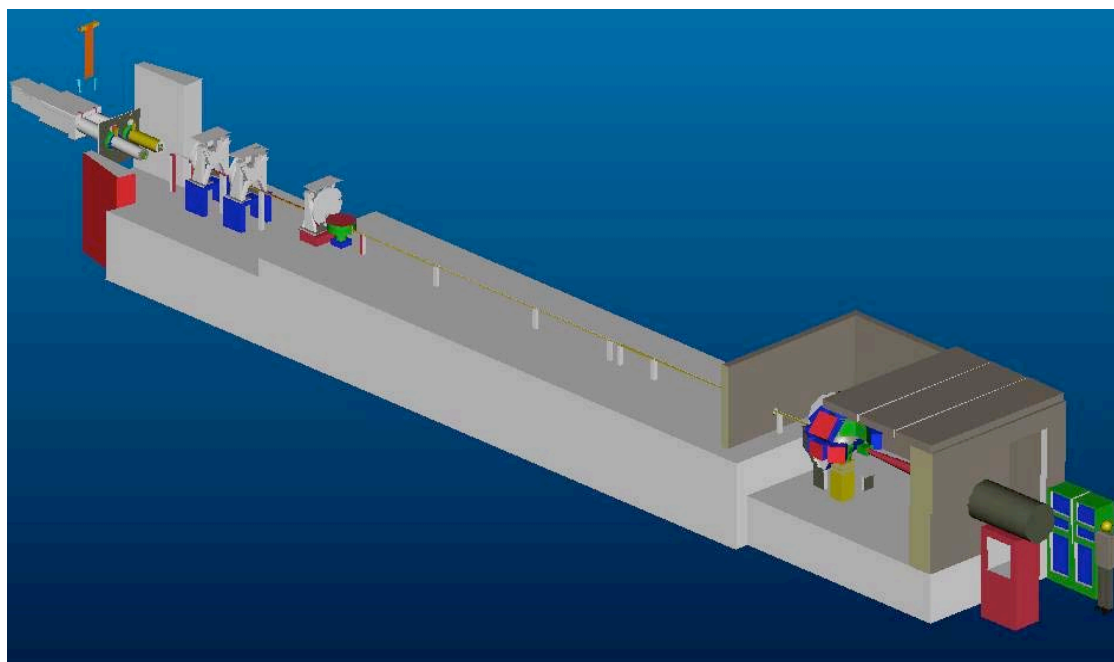


Figure 1. 3D conceptual model of *MaNDi*

3.1 Layout of *MaNDi*

The layout and the parameters of the *MaNDi* instrument determined from analytical calculations and Monte Carlo simulations are shown in **Figure 1** and Table 1, respectively.

3.2 Moderator Choice

Since high resolution structural biology requires high neutron flux a coupled hydrogen moderator²⁴ has been proposed by many for NMC applications. However, when high resolution data for crystals with unit cell size in the range of 150 Å are required our calculations show that it is important to consider both the flux and the resolution (pulse lengths of the emission time) of the moderator. The increased flux from the coupled moderator (8X that of the decoupled moderator) comes at the cost of a pulse width that is about 8 times larger than that of the decoupled moderator. Monte Carlo simulations show that if MaNDi views a coupled hydrogen moderator the long tails in the emission times (pulse width) will be detrimental to its resolution.

Table 1
Instrument parameters of MaNDi

Moderator	Moderator type	Top Upstream
	Material	Para-Hydrogen
	Decoupler	Cadmium
	Poison	Gadolinium
	Poison depth	27 mm
	Width	0.10 m
	Height	0.12 m
Curved Guide	Starting point	6 m downstream
	Width	1.5 cm
	Height	1.5 cm
	Length	12 m
	Supermirror coating	$m=3$
	Total turn angle	0.43°
	Radius of curvature	1599 m
	Line-of-sight lost	≈ 20 m
Straight Guide	Starting point	18 m downstream
	Width	1.5 cm
	Height	1.5 cm
	Length	Variable: Depends on resolution requirement
	Supermirror coating	$m=3$
Bandwidth Choppers	Positions	7.2 m, 8.2 m, 10.4 m
Moderator-to-sample distance		24 m
Wavelength range	$2.0 \text{ \AA} \leq \lambda \leq 4.69 \text{ \AA}$	$\Delta\lambda = 2.69 \text{ \AA}$
Wavelength resolution		$\approx 0.15\%$
Sample-to-detector distance		0.4 m
Detectors	Array of 2-D PSDs	1 mm resolution scintillation detectors

3.3 Effective Flux of the Decoupled Hydrogen Moderator

In order to make decisions on the optimal wavelength range for the diffraction experiments an effective flux is calculated by weighting the flux from the moderator for the reflectivity of neutrons.

The integrated intensities I_{hkl} are reduced to structure factor amplitudes $|F_{hkl}|$ based on the Laue formula:

$$I_{hkl} = \phi(\lambda) \frac{V_s}{V_c} \frac{|F_{hkl}|^2}{V_c} \frac{\lambda^4}{2 \sin^2 \theta} \quad (1)$$

where $f(l)$ is the incident neutron intensity per unit wavelength range at wavelength l ($\text{n}\cdot\text{cm}^{-2}\cdot\text{sec}^{-1}\cdot\text{\AA}^{-1}$), V_s is the sample volume, V_c is the crystal unit cell volume, F_{hkl} is the structure factor, and $2q$ is the Bragg angle. Terms for the detector efficiency, sample absorption and extinction have not been included.

Equation (1) can be rewritten as

$$I_{hkl} = \phi(\lambda) \frac{V_s}{V_c^2} |F_{hkl}|^2 \lambda^2 d_{hkl}^2 \quad (2)$$

This leads to an effective flux of

$$f_{\text{eff}}(l) = f(l) \cdot l^2 \quad (3)$$

In this case, one takes into account that for any hkl , the d -spacing is constant regardless of the angle. Then, the optimal wavelength for measuring all Bragg peaks is the same, but the optimal angle will be different for each hkl .

Multiplying the flux for the decoupled hydrogen moderator by l^2 at each wavelength gives the curve shown in **Figure 2**. It is clear from **Figure 2** that wavelengths in the range of 1.5 to 5.0 Å provide the highest effective flux.

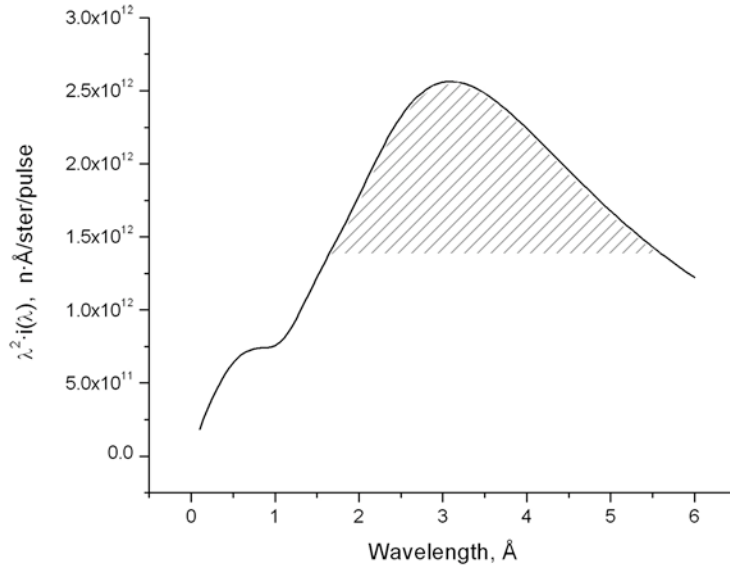


Figure 2. Plot of $\lambda^2 \cdot i(\lambda)$, $n \cdot \text{Å}/\text{ster}/\text{pulse}$, versus wavelength for the decoupled, poisoned hydrogen moderator.

In **Figure 3**, the wavelength dependence of the ratios of the total intensity from the coupled and decoupled moderators is plotted. This is the gain in total intensity provided by the coupled moderator. It is seen that for wavelengths of about 2.5 Å or greater a flux gain of 8X can be obtained with the coupled moderator. However, for wavelengths below 2.5 Å the gain decreases dramatically.

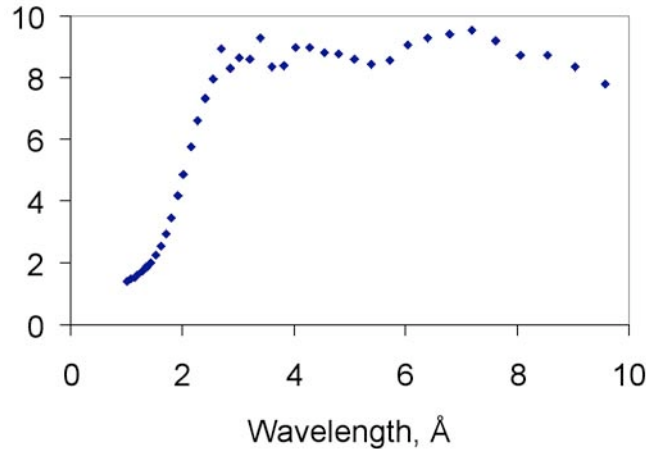


Figure 3. Intensity gain for the coupled hydrogen moderator obtained by calculated the ratio of the total intensities of the pulse at each wavelength of the coupled and decoupled moderators.

3.4 Resolution with Different Moderators

For a cubic unit cell with lattice constant a , it can be shown that to resolve two Bragg peaks at d_{\min} the condition in Equation (4) has to be fulfilled

$$R < \frac{d_{\min}}{a} \quad (4)$$

where the resolution R is based on a Gaussian distribution. For single crystal diffraction, it is not sufficient to resolve peaks, but to be able to integrate the intensity under the peak. Therefore, the peaks have to be fully separated such that the resolution requirement is^{25,26}

$$R < \frac{d_{\min}}{5a} \quad (5)$$

since from $-2.5s$ to $+2.5s$ about the mean contains almost 99% of a Gaussian peak. Hence

$$R_{FWHM} < \frac{d_{\min}}{2.12a} \quad (6)$$

It should be noted that 99% of the peak is not necessary. If this is relaxed to 90%, then the peak width becomes substantially smaller.

The pulse width time resolution contributes primarily to the resolution parallel to the diffraction vector, whereas the angular resolution primarily contributes to that in the perpendicular direction. From Jauch²⁷, the condition

$$\Delta t_{\text{pulse}}(FWHM) \leq 238.1L\left(\frac{d_{\min}^2}{a}\right)\sin\theta \quad (7)$$

must be met for peaks to be completely separated peaks in the direction of the reciprocal lattice vector at d_{\min} for a crystal with a unit cell axis length of a . In this equation, the units are: t , ms; L , m; d_{\min} and a , Å. For a Gaussian peak, the full width of $5s$ is then 2.12 times the $Dt_{\text{pulse}}(FWHM)$ obtained from equation (7).

3.5 Effective FWHM of the Pulses

Figure 4 shows the pulse shapes for 2.55 Å neutrons from the coupled and decoupled hydrogen moderators. For the coupled liquid hydrogen moderator, the intensity at the peak region of the pulse is only about 1.5 times greater than that from a decoupled liquid hydrogen moderator. However, the pulse width is over 8 times larger for the coupled moderator. Thus the pulse shapes are not Gaussian so that $2.13FWHM$ does not contain 99% of the peak. The values for the coupled and decoupled parahydrogen moderators are compared in Table 2. Since 99% can be considered as too difficult to achieve, we have adopted a goal of 90% of the total intensity, or 10% of the maximum, whichever is longer. It is seen from Table 2 that the eightfold gain in intensity with the coupled moderator results at the expense of nearly ten times larger pulse width for the decoupled moderator. The longer pulse widths at the coupled moderator, in addition to affecting the resolution parallel to the q-vector, will increase the background by about 8 times, thus affecting the signal to noise ratio of the diffraction peaks.

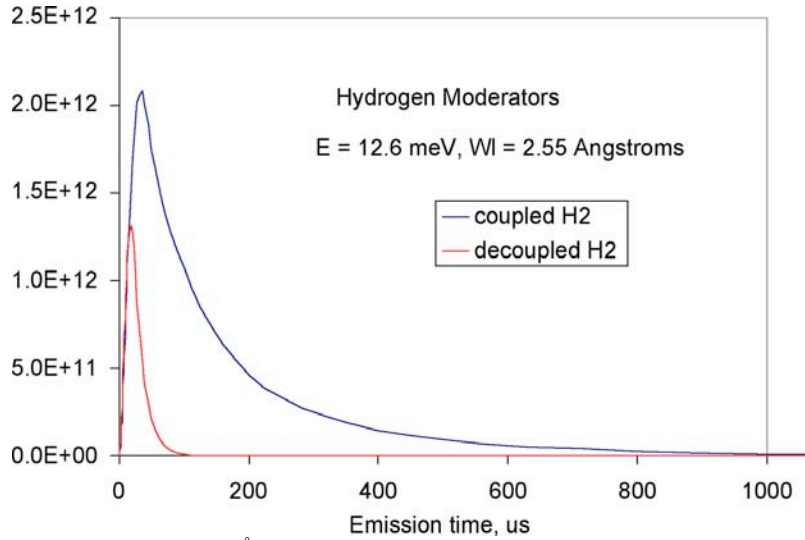


Figure 4. Emission time for neutrons with $\lambda = 2.55$ Å for the coupled and decoupled liquid hydrogen moderator at the HPTS at SNS.

Table 2
Comparison of coupled and decoupled H₂ moderators for the pulse corresponding to $l = 2.55 \text{ \AA}$

Parameter	Coupled H ₂	Decoupled H ₂	Ratio
Total intensity (n/ster/pulse/eV)	3.06×10^{14}	3.84×10^{13}	8.0
Gaussian FW = 2.13 FWHM (msec)	193	52	3.7
Simulated FW at 90% of total intensity (msec)	430	45	9.6
FW at 10% of max (msec)	335	58	5.8

Table 3 provides the maximum allowable pulse full widths derived from equation (7) for different wavelengths and corresponding Bragg angles to resolve peaks for a cubic system with $a = 150 \text{ \AA}$, $d_{\min} = 1.5 \text{ \AA}$, and $L = 24.5 \text{ m}$. Also shown are the full widths corresponding to 90% of the total intensity, or 10% of the maximum, whichever is longer, for the pulse from each moderator.

Table 3
Calculated maximum allowed pulse full widths [Eq. (7)] and the pulse full widths of the moderators for a 24.5 m instrument.

2q (deg)	λ (Å)	Equation (7) FW (µsec)	Coupled FW (µsec)	Decoupled FW (µsec)	FW Ratio	Intensity Ratio
30	0.776	49	33	17	1.9	1.1
60	1.500	94	300	27	11.1	2.2
90	2.121	132	400	44	9.1	5.8
120	2.598	162	430	58	7.4	8.0
150	2.898	181	445	66	6.7	8.3

The data in Table 3 leads to the following conclusions:

- The pulse width of the decoupled moderator is more than adequate at all scattering angles and wavelengths. Perhaps a partially coupled moderator or one with a greater poison depth could be useful, but such a moderator is not available at the SNS.
- The effective FWHM values for the coupled moderator are higher than the values in Equation (7) and hence a 24.5 m long instrument cannot take advantage of the higher flux with coupled moderator. One way to use the higher flux from the coupled moderator for NMC is by increasing the length of the flight path to 75 m [see Equation (7)].

Although such a long flight path instrument can be useful for NMC applications, there are several disadvantages.

- Resolution is still borderline as can be seen in **Figure 5**, where we have shown the peak shapes for a top hat function corresponding to a $d_{\min} = 1.5 \text{ \AA}$ for a cubic unit cell of 150 \AA . The peaks are well separated for a 24 m long instrument with a decoupled liquid hydrogen moderator, while there is a large peak overlap for a similar length instrument viewing a coupled moderator. Although the peak overlap has improved for a 75 m long instrument, it is still inferior to the decoupled moderator case.
- The gain factor will reduce to a factor of 2.67 as the usable wavelength bandwidth (DI) will reduce by a factor of 3 due to frame-overlap condition,

$$DI = 3955/f.L \quad (8)$$

where, L is the instrument flight path length and f, the source frequency that is 60 at SNS.

- Total guide efficiency for longer wavelengths at 75 m will be about 60% (based on MC simulations) and much less for shorter wavelengths. The gain factor will further reduce to 1.6 or less.
- There is a large additional cost associated with the construction of a 75 m long instrument.

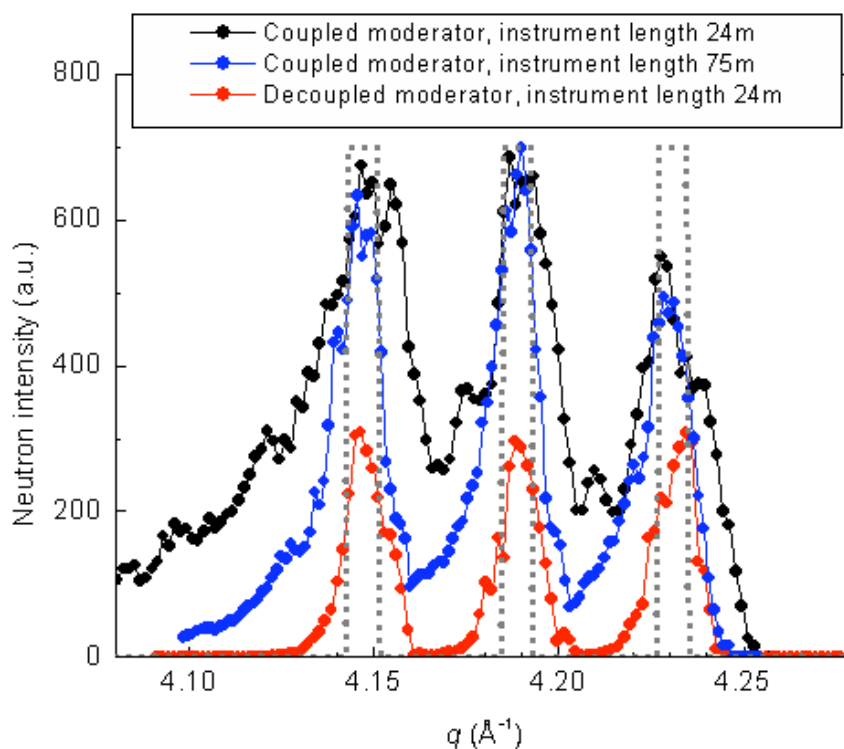


Figure 5. Peak shapes for a top hat function corresponding to a $d_{\min} = 1.5 \text{ \AA}$ for a cubic unit cell of 150 \AA . MC simulation results for 3 different instrument configurations of MaNDi.

3.6 Neutron Guide System

To efficiently transport cold neutrons from the moderator to the sample position, *MaNDi* will use high index curved and straight guides because of their following advantages:

- Neutron guides offer significant gain in flux when compared to natural collimation viewing the whole moderator.
- Curved guides in the middle section of the beam line make it possible to gently steer the neutron beam such that the sample is completely out of line-of-sight of the source.
- Small widths of the beam allow for the more efficient operation of bandwidth choppers for wavelength selection.

A curved guide provides two advantages: (1) It has a clear cut-off wavelength, i.e. it prevents leakage of high-energy neutrons through absorbing beam conditioning devices (chopper blades, slits etc.), and (2) It will make the operation of *MaNDi* easier from the safety point of view because it will allow only cold neutrons in the beam at the sample position.

Monte Carlo (MC) simulations using the *IDEAS* package were used to optimize the length, location, curvature, and type of supermirror coating of the neutron guide system, and the distance from the guide exit to the sample. *MaNDi*'s guide system starts at a distance of 6 m from the moderator, and consists of a 12-m-long curved guide followed by a straight guide (**Figure 6**) whose length can be selected based on the resolution requirement. The sample position is at 24 m and the distance between sample and detector will be in the order of 0.5 m. However, the sample-to-detector distance will be defined at a later stage giving due consideration to the spatial resolution of the detector, cost, DQ resolution, etc.

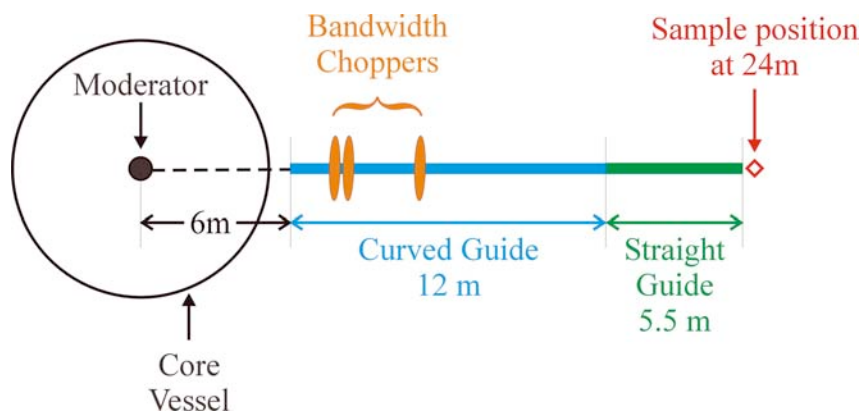


Figure 6. Schematic layout of the neutron guide system and choppers

Figure 7 shows the ratio of the intensity values at sample position with and without guides as a function of wavelength. It follows that substantial gain in flux can be achieved by using a guide system (supermirror coating $m=3$) when compared to the natural collimation. The gain in intensity is related to the increase in the angular divergence of the beam (e.g. for neutrons with $\lambda = 2 \text{ \AA}$ the FWHM beam divergence is $\approx 0.3^\circ$). However, the increase in divergence can be exploited to match the resolution requirements of a given experiment by using a variety of collimators at the sample position.

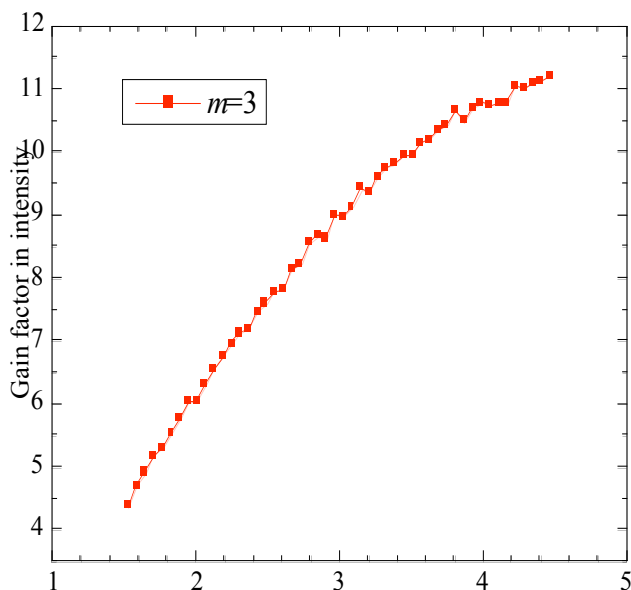


Figure 7. Gain in intensity when using a neutron guide relative to no guide

3.7 Beam Defining Optics

The beam divergence can be readily tuned by addition/removal of 0.5m long guide sections between the guide exit and the sample. In addition, beam defining optics such as Soller collimators, polycapillary focusing optics²⁸, tapered guides and pinhole collimators, will be designed for insertion between the guide exit and the sample to further optimize the beam divergence to experimental requirements.

3.8 Detectors

An array of state-of-the-art high efficiency position sensitive area detectors with a spatial resolution of 1 mm will be used to cover a wide solid angle around the sample. Recently developed scintillation detectors for time-of-flight single crystal neutron diffractometer SCD at IPNS can potentially be used on MaNDi. New detector technology being developed at IPNS will enable the use of tiled area detectors with minimal gaps.

4. PERFORMANCE

The performance of MaNDi has been calculated based on counting times necessary to obtain a complete data set for protein crystals with different unit cell sizes, by taking into consideration of the data precision, Debye-Waller factor, flux and incoherent background.

We calculated counting times based on an equation proposed by Jauch²⁷. Below is a plot of data collection times for MaNDi. Validation of this approach was achieved by using the published beam time data used for a few protein crystals of known volume from PCS, BIX3 and LADI.

For crystals of deuterated proteins with a volume of 0.125 mm^3 complete data set for a $d_{\min} = 2 \text{ \AA}$ can be obtained from MaNDi in a few days (**Figure 8**). Our calculations indicate that similar amount of beam time will be required to obtain data of similar precision for 1 mm^3 normal protein crystals.

The counting times for a $d_{\min} = 1.5 \text{ \AA}$ for the above systems will be an order of magnitude higher than that for $d_{\min} = 2.0 \text{ \AA}$. For instance, counting times for crystals with a 60 \AA unit cell will require about 7 days, while those with a 100 \AA unit cell will require about 30 days to obtain data of similar precision. Current instruments for NMC will require 10 to 50 times larger than the above times. Thus the performance of MaNDi will open up new avenues thus far not available for NMC.

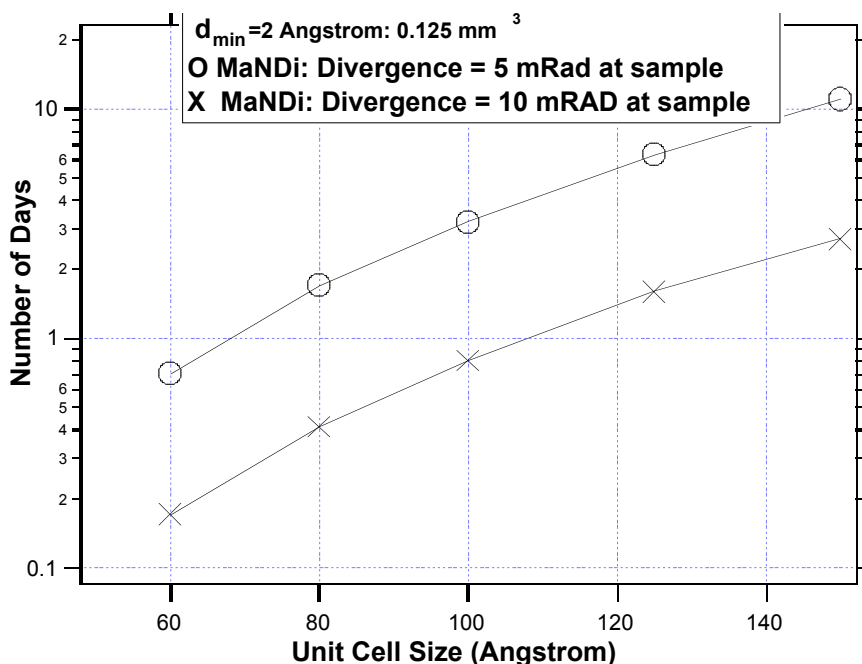


Figure 8. Data collection times for MaNDi for 0.125 mm^3 95% deuterated protein crystals with different unit cell dimensions.

5. ACKNOWLEDGEMENT

This work carried out at IPNS at Argonne National Laboratory was funded by the U.S. Department of Energy, BES-Materials Science, under Contract W-31-109-ENG-38. This work is supported by the Spallation Neutron Source Project (SNS). SNS is managed by UT-Battelle, LLC, under contract DE-AC05-00OR22725 for the U.S. Department of Energy. SNS is a partnership of six national laboratories: Argonne, Brookhaven, Jefferson, Lawrence Berkeley, Los Alamos, and Oak Ridge.

6. REFERENCES

- [1] Tsyba, I.; Bau, R. *Chemtracts - Inorganic Chemistry* **2002**, *15*, 233-257.
- [2] Schoenborn, B. P. *Nature* **1969**, *224*, 143-146.
- [3] Schoenborn, B. P. In *Neutrons in Biology*; Schoenborn, B. P., Ed.; Plenum Press: New York, 1984; Vol. 27, pp 261-281.
- [4] Schoenborn, B. P. *Methods Enzymol.* **1985**, *114*, 510.
- [5] Kossiakoff, A. A. *Annu. Rev. Biophys. Bioeng.* **1983**, *12*, 159.
- [6] Kossiakoff, A. A. *Basic Life Sci.* **1984**, *27*, 281.
- [7] Kossiakoff, A. A. *Annu. Rev. Biochem.* **1985**, *54*, 1195.
- [8] Wlodawer, A. *Prog. Biophys. Mol. Biol.* **1982**, *40*, 115.
- [9] Raghavan, N. V.; Wlodawer, A. *Methods Exp. Phys. Part C* **1987**, *23*, 335.
- [10] Timmins, P. A. *Physica B* **1995**, *213-214*, 26.
- [11] Helliwell, J. R. *Nature Struct. Biol.* **1997**, *11*, 874.
- [12] Niimura, N. *Current Opinion in Structural Biology* **1999**, *9*, 602-608.
- [13] Gutberlet, T.; Heinemann, U.; Steinera, M. *Acta Cryst. D* **2001**, *57*, 349-354.
- [14] Shu, F.; Ramakrishnan, V.; Schoenborn, B. P. *Basic Life Sci* **1996**, *64*, 309-323.
- [15] Coates, L.; Erskine, P. T.; Wood, S. P.; Myles, D. A.; Cooper, J. B. *Biochemistry* **2001**, *40*, 13149-13157.
- [16] Niimura, N.; Minezaki, Y.; Nonaka, T.; Castagna, J.-C.; Cipriani, F.; Hoghoj, P.; Lehmann, M. S.; Wilkinson, C. *Nat Struct Biol* **1997**, *4*, 909-914.
- [17] Ostermann, A.; Tanaka, I.; Engler, N.; Niimura, N.; Parak, F. G. *Biophys Chem* **2002**, *95*, 183-193.
- [18] Bon, C.; Lehmann, M. S.; Wilkinson, C. *Acta Cryst. D* **1999**, *55*, 978-987.
- [19] Wlodawer, A.; Hendrickson, W. A. *Acta Crystallogr.* **1982**, *A38*, 239-247.
- [20] Wlodawer, A.; Walter, J.; Huber, R.; Sjolin, L. J. *J. Mol. Biol.* **1984**, *180*, 301-329.
- [21] Borah, B.; Chen, C. W.; Egan, W.; Miller, M.; Wlodawer, A.; Cohen, J. S. *Biochemistry* **1985**, *24*, 2058.
- [22] Habash, J.; Raftery, J.; Nuttall, R.; Price, H. J.; Wilkinson, C.; Gilboa, A. J. K.; Helliwell, J. R. *Acta Cryst. D* **2000**, *56*, 541-550.
- [23] Lee, W.-T.; Wang, X.-L. *Neutron News* **2002**, *13*, 30-34.
- [24] Iverson, E. B.; Ferguson, P. D.; Gallmeier, F. X.; Popova, I. I. "Detailed SNS Neutronics Calculations for Scattering Instrument Design: SCT Configuration," Oak Ridge National Laboratory, 2002.
- [25] Jauch, W. In *ISIS Workshop*: Rapallo, Italy, 1986.
- [26] Jauch, W. *Transactions ACA* **1993**, *29*, 55-61.
- [27] Jauch, W. *J. Neutron Research* **1997**, *6*, 161-171.
- [28] Gibson, W. M.; Schultz, A. J.; Chen-Mayer, H. H.; Mildner, D. F. R.; Gnaupel-Herold, T.; Miller, M. E.; Prasad, H. J.; Youngman, R.; Carpenter, J. M. *J. Applied Cryst.* **2002**, *35*, 677-683.